NAVORD REPORT 1488 (Vol. 3)

HANDBOOK OF SUPERSONIC AERODYNAMICS

A BUREAU OF ORDNANCE PUBLICATION

NAVORD REPORT 1488 (Vol. 3)

HANDBOOK OF SUPERSONIC AERODYNAMICS

Compiled and edited under Bureau of Ordnance Contract NOrd 7386 by the Aerodynamics Handbook Staff of The Johns Hopkins University, Applied Physics Laboratory, Silver Spring, Maryland. The selection and technical review of the material appearing in this section of Volume 3 of the Handbook were functions of a Reviewing Committee appointed by the Director of the Laboratory. The membership of this Committee during the preparation of this section was as follows: Ione D. V. Faro, Lester L. Cronvich, and Robert N. Schwartz (Chairman).

For sale by the Superintendent of Documents, U. S. Government Printing Office
Washington 25, D. C. : Price $1.50

1 JUNE 1957 A BUREAU OF ORDNANCE PUBLICATION

HANDBOOK OF SUPERSONIC AERODYNAMICS

Volume 3

Section 6

Preface

A preface to the entire Handbook of Supersonic Aerodynamics appears in Volume 1 and includes a brief history of the project. As stated in Volume 1, "The primary criterion used in selecting material for the Handbook is its expected usefulness to designers of supersonic vehicles. Thus a collection of data directly useful in the design of supersonic vehicles, results of the more significant experiments, and outlines of basic theory are included ...."

The present edition of the Handbook, printed and distributed by the Bureau of Ordnance, is being published in separate sections as material becomes available. The Table of Contents of the entire work is given on page iii. It may be noted, the majority of sections of the Handbook are being prepared by individual authors for the Applied Physics Laboratory. Those sections are noted for which an early publication date is expected. The selection of material, editing, and technical review of the Handbook of Supersonic Aerodynamics continue to be carried out by an editor and a technical reviewing committee at the Applied Physics Laboratory.

Volume 3 of the Handbook of Supersonic Aerodynamics contains three closely related sections, "Two-Dimensional Airfoils" (Section 6), "Three-Dimensional Airfoils" (Section 7), and "Bodies of Revolution" (Section 8). A fourth related section on wing-body interference (Section 9) is placed in Volume 4 with sections on stability and control because of its importance to this later subject.

The staff of the Aerodynamics Handbook Project at the Applied Physics Laboratory gives grateful acknowledgment to the Aeromechanics Division of the Defense Research Laboratory of The University of Texas for the large amount of computational work carried out by them for the Sections 6 and 7 of the Handbook.

The numbering system of Volume 3 is essentially the same as that used in the last preceding volumes.

Agencies and individuals interested in the aeronautical sciences are invited to submit and to recommend material for inclusion in the Handbook; full credit will be given for all such material used. Regarding the selection of material and the preparation of the volumes in the Handbook Series, the Applied Physics Laboratory earnestly solicits constructive criticisms and suggestions. Correspondence relating to the editing of the Handbook should be directed to

Editor and Supervisor, Aerodynamics Handbook Project
Applied Physics Laboratory
The Johns Hopkins University
8621 Georgia Avenue
Silver Spring, Maryland

Communications concerning distribution of the Handbook should be directed to

Chief, Bureau of Ordnance
Department of the Navy
Washington 25, D. C.

TABLE OF CONTENTS OF THE

HANDBOOK OF SUPERSONIC AERODYNAMICS

NAVORD REPORT 1488 (Unclassified)

VOLUME 1

VOLUME 2

VOLUME 3

VOLUME 4

VOLUME 5

VOLUME 6

Volumes 1 and 2, and available sections of Volumes 3, 4 and 5, may be obtained by addressing the Superintendent of Documents, U. S. Government Printing Office, Washington 25, D. C.

SECTION 6 - TWO-DIMENSIONAL AIRFOILS

CONTENTS

(Figures are numbered so as to correspond to the subsection in which they are located.)

SECTION 6 - TWO-DIMENSIONAL AIRFOILS

Primary Symbols

a	velocity of sound
A, B, C, and D	Busemann coefficients
c	chord of airfoil section
c_d	section drag coefficient (Drag force/qc)
c_f	section skin friction drag coefficient
c_ℓ	section lift coefficient (Lift force/qc)
c_m	section moment coefficient
c.p.	center of pressure, distance from leading edge in fraction of chord length
c_p	pressure coefficient $((p-p_\infty)/q_\infty)$
M	Mach number (V/a)
p	static pressure
q	dynamic pressure $(1/2\ \rho\ V^2)$
t	thickness of airfoil section
V	velocity of airfoil
x	distance along chord from leading edge
y	distance measured normal to chord
α	angle of attack of airfoil
δ	half-wedge angle of airfoil at leading edge
δ_x	local angle of airfoil profile measured with respect to the chord positive in a counter-clockwise direction
η	angle shock wave makes with undisturbed flow direction
γ	ratio of specific heat at constant pressure to specific heat at constant volume of ambient fluid
ω	flow deflection angle relative to free-stream direction

ρ	density of ambient fluid
θ	local change in flow deflection angle

Auxiliary Symbols

Subscripts

a	axial component
d	drag
ℓ	lift
n	normal component
t	tangential component or stagnation condition
1, 2, 3, 4	four surfaces of a double wedge airfoil (cf., figure on 601.21 page 1)
∞	undisturbed free stream
ℓ	lower surface
u	upper surface

SECTION 6 - TWO-DIMENSIONAL AIRFOILS

This section of the Handbook of Supersonic Aerodynamics was prepared at the Applied Physics Laboratory of The Johns Hopkins University. Many of the formulae and charts of two-dimensional airfoil characteristics were especially prepared for this section by the Defense Research Laboratory of The University of Texas.

600 Introduction

This section of the Handbook serves as an introduction to the more practical design considerations which will be treated in Section 7, "Three-Dimensional Airfoils". No missile wing can be completely analyzed from two-dimensional data, but certain significant trends may be determined from these data. Two-dimensional data may be used for guidance in estimating the effect of changing Mach number, angle of attack, thickness ratio, camber, position of maximum thickness, and viscosity effects. In addition, a comparison of higher order theories and the linearized theory can be made.

600.1 General Scope of Contents

This section of the Handbook provides the designer with data pertaining to two-dimensional airfoils. The theoretical airfoil characteristics computed by the shock expansion method for section lift coefficient (c_ℓ), drag coefficient (c_d), and center of pressure (c.p.) are presented in graphical form for double-symmetrical sharp-edge airfoil sections of the double wedge, flattened double wedge, and biconvex types. Supplementary data are provided for modifications of the double-symmetrical airfoil sections, including the effects of camber and position of maximum thickness. Data for estimating the effect of viscosity upon drag coefficients are also presented.

A short résumé of the theories applicable to these airfoils is presented; several charts are included to compare the results of the cited theories.

Available experimental data are presented for comparison with the results predicted by the various theories.

601 Methods for Determining Pressure Coefficients

The theoretical characteristics of two-dimensional airfoils may be determined once the theoretical pressure distribution is known. This distribution is usually specified in terms of local pressure coefficients (c_p) defined by

$$c_p = \frac{\Delta p}{q_\infty} = \frac{p - p_\infty}{\frac{\rho_\infty V_\infty^2}{2}} = \frac{p - p_\infty}{\frac{\gamma}{2} p_\infty M_\infty^2} = \frac{\frac{p}{p_\infty} - 1}{\frac{\gamma}{2} M_\infty^2} \qquad (601\text{-}1)$$

(All symbols are defined at the beginning of this section.) Methods for the computations of c_p will form the principal part of this subsection of the Handbook.

601.1 Basic Assumptions for all Theoretical Treatments

In all the theoretical treatments described in Subsection 601 the following assumptions are made:

(a) The shock wave at the leading edge is attached. This limits the treatments to sharp-nosed airfoils, and to Mach numbers greater than the critical value which is a function of the leading-edge wedge angle and the angle of attack.

(b) The fluid is inviscid. This eliminates all effects due to viscosity, such as boundary layer, flow separation, and interactions between shock wave and boundary layer.

(c) There is no heat transfer. This restriction applies to transfer between streamlines, between boundary layers and the wall surface, and through shock waves.

(d) The gas obeys the perfect gas law with constant specific heats. Thus, no dissociation occurs and the ratio of the specific heats (γ) is constant.

(e) The motion of the fluid is confined to two dimensions.

(f) The flow is irrotational. This condition limits the treatment to plane shock waves or infinitely weak shock waves, where there is no vorticity. (An exception to this restriction is made in applying the "Method of Characteristics", which is mentioned briefly in Subsection 601.4.)

447269 O - 58 - 2

601.2 Power Series Method

By using a power series expansion (Ref. 1, Article 16.9)* one obtains from Eq. 2.76 of Volume I of this Handbook, (Ref. 2) a third-degree equation for the pressure coefficient.

$$c_p = A\omega + B\omega^2 + (C - D)\omega^3, \qquad (601.2\text{-}1)$$

where:

for expansion flows, ω is negative;

for compression flows, ω is positive;

for expansion flows and isentropic compressions, $D = 0$; and

for single oblique shock compressions, D is not equal to zero.

The coefficients are functions of the free-stream Mach number, as follows:

$$A = \frac{2}{\sqrt{M_\infty^2 - 1}},$$

$$B = \frac{\frac{\gamma + 1}{2} M_\infty^4 - 2(M_\infty^2 - 1)}{(M_\infty^2 - 1)^2},$$

$$C = \frac{1}{(M_\infty^2 - 1)^{7/2}} \left[\frac{\gamma + 1}{6} M_\infty^8 - \left(\frac{5 + 7\gamma - 2\gamma^2}{6} \right) M_\infty^6 + \frac{5(\gamma + 1)}{3} M_\infty^4 - 2M_\infty^2 + \frac{4}{3} \right],$$

$$D = \frac{(\gamma + 1) M_\infty^4}{12 (M_\infty^2 - 1)^{7/2}} \left[\frac{5 - 3\gamma}{4} M_\infty^4 - (3 - \gamma) M_\infty^2 + 2 \right].$$

The numerical values of the coefficients A, B, C, and D (for use when ω is in radians) are tabulated in Table 505.111, Section 5, Volume 2 of this Handbook (Ref. 2). Values are given only for $\gamma = 1.4$.

Equation 601.2-1 is known as the Busemann Higher-Order Equation for Pressure Coefficients; in linearized form it becomes

$$c_p = A\omega = \frac{2\omega}{\sqrt{M_\infty^2 - 1}}. \qquad (601.2\text{-}2)$$

Ackeret (Ref. 3), by an independent solution, was the first to obtain Eq. 601.2-2.

* References are listed on reference page following Subsection 606.2.

601.21 Numerical Example with Symmetric Double Wedge Airfoil

It is recognized that theoretically the power series method is strictly applicable only to wedge-type flow--that is, flow which experiences only one finite change in direction from that of the free stream. However, it is found that pressure distributions over most of the conventional supersonic wing sections computed by means of the power series method conform reasonably well with the values computed by the shock expansion method outlined in Subsection 601.3. To illustrate the power series method, a typical numerical example is given. Consider the double-symmetrical double wedge airfoil section shown in the following figure.

Let $M_\infty = 3$,
$\alpha = 8$ degrees,
$(t/c)_{max} = 0.06$,
δ = arc tan 0.06 = 3.434 degrees.

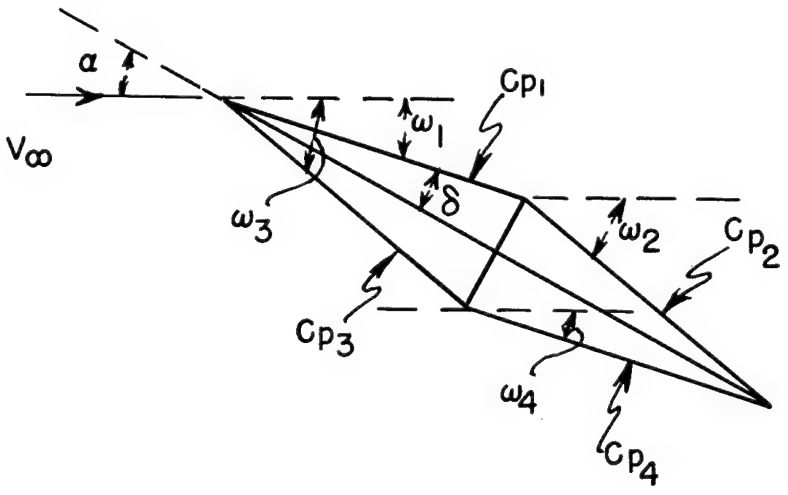

By properly combining the angle of attack (α) and the wedge half angle (δ), the flow deflections (ω) relative to the free-stream over each of the four surfaces are as follows:

Deflection Angle	ω_1	ω_2	ω_3	ω_4
Degrees	-4.566	-11.434	+11.434	+4.566
Radians	-0.0797	- 0.1996	+ 0.1996	+0.0797

Taking for the M_1 of Table 505.111 the value $M_\infty = 3$, the coefficients in Eq. 601.2-1 are:

$A = 0.7071 \text{ radian}^{-1}$, $B = 1.2688 \text{ radians}^{-2}$,

$C = 1.112 \text{ radians}^{-3}$, $D = 0.043 \text{ radian}^{-3}$.

Therefore the pressure coefficients over each of the four surfaces of this airfoil, when computed by Eq. 601.2-1 to various orders, are given in the following table. Also listed for comparison are the shock expansion values computed in Subsection 601.32.

Pressure Coefficient	c_{p_1}	c_{p_2}	c_{p_3}	c_{p_4}
1st Order	-0.0564	-0.1411	+0.1411	+0.0564
2nd Order	-0.0483	-0.0906	+0.1916	+0.0645
3rd Order, without D	-0.0489	-0.0994	+0.2005	+0.0650
3rd Order, with D	-0.0489	-0.0994	+0.2001	+0.0650
Shock Expansion	-0.0488	-0.0988	+0.1995	+0.0650

601.3 Shock Expansion Method

The shock expansion method utilizes the exact expressions for flow through a plane oblique-compression shock wave and for an expansion flow. It will give exact results for those configurations which do not produce a curved shock wave.

In treating configurations as the double wedge of the preceding subsection, the results will be exact as long as the reflected waves produced by the interaction of the Mach waves originating at the shoulder of the profile and the leading-edge shock wave do not strike the after part of the profile. The results are exact for the double wedge, at all Mach numbers and angles of attack shown in the figures. However, at higher angles of attack than shown, the reflected Mach waves will strike the after portion of the double wedge thereby modifying the pressure distribution there. The flattened double wedge will experience this difficulty at the higher Mach numbers at high angles of attack given in Fig. 603.2-1(b). Although sometimes applied to the biconvex airfoil, the shock expansion method will not give exact results under any condition (Ref. 1, page 568). The intersection of the Mach waves with the leading edge shock produce a curved shock wave and vorticity (cf. Subsection 601.1). Nevertheless, the shock expansion method gives results sufficiently accurate for most engineering applications. The use of the method of characteristics, which will give exact results in these last cases (discussed briefly in Subsection 601.4 to follow) is rarely justified in practice.

601.31 Attached Shock Waves

The fluid flow across the upper and lower airfoil surfaces at the leading edge are independent of each other as long as the shock waves are attached to the leading edge. The shock waves will be attached as long as the greater of the two angles of flow deflection at the leading edge, for a given Mach number, is equal to or less than a certain critical value for that Mach number. Values for this maximum flow deflection angle (ω_{max}) are tabulated as a function of Mach number in Table 503.211, Volume 2 of the Handbook (Ref. 2), and are also shown in Fig. 601.31-1 of this volume.

601.311 Pressure Coefficient Behind Shock Wave at Leading Edge

The flow through a plane compression shock wave at the leading edge of an airfoil (Ref. 4, Page 72) for an upstream Mach number of M_∞ and a flow deflection angle of ω is shown in the following figure.

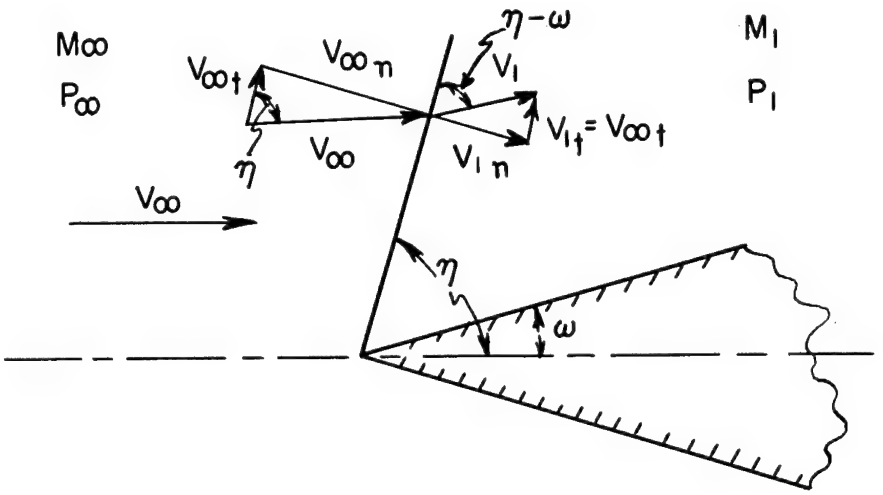

To calculate the pressure coefficient (c_p) behind the leading edge on the surface producing a compressive shock, the following procedure is suggested:

(a) For the known values of M_∞ and ω, read the shock angle (η) from Table 503.111, Section 5, Volume 2. (It should be noted that in Table 503.111 the shock angle is designated by α instead of η and Mach number ahead of the shock as M_1 instead of M_∞.)

(b) Compute the component of the Mach number normal to the shock front (M_{∞_n}) by means of the equation,

$$M_{\infty_n} = M_\infty \sin \eta .$$

(c) Using M_{∞_n} as the independent variable, determine the ratio of static pressure on the downstream side to that on the upstream side of the shock wave (p_1/p_∞) from Table 502.111, Section 5, Volume 2.

(d) Compute the pressure coefficient (c_p) by means of Eq. 601-1,

$$c_p = \frac{\frac{p_1}{p_\infty} - 1}{\frac{\gamma}{2} M_\infty^2} .$$

601.312 Pressure Coefficient Behind Expansion Fan at Leading Edge

The following figure depicts the flow for an expansion fan at the leading edge, when the upstream Mach number is M_∞ and the flow deflection angle is ω.

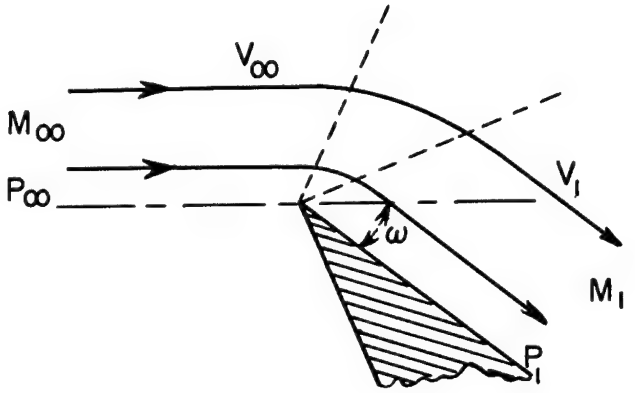

To calculate the pressure coefficient (c_p) behind the leading edge on the surface, the following procedure is suggested:

(a) Find the Prandtl-Meyer angle (ω_∞), corresponding to the upstream Mach number (M_∞) from Table 504.111, Section 5, Volume 2 of the Handbook (Ref. 2).

(b) Then the Prandtl-Meyer angle (ω_1), for an expansion flow from sonic velocity when the flow deflection angle is ω, is obtained from the relation $\omega_1 = \omega_\infty + \omega$.

(c) Find the downstream Mach number M_1 corresponding to ω_1 from Table 504.211.

(d) From Table 501.111, find the ratios of static to stagnation pressures, $\frac{p_\infty}{p_t}$ and $\frac{p_1}{p_t}$ for M_∞ and M_1 respectively.

(e) Then $\frac{p_1}{p_\infty} = \frac{p_1}{p_t} \Big/ \frac{p_\infty}{p_t}$.

(f) Compute the pressure coefficient (c_p) by means of

$$c_p = \frac{\frac{p_1}{p_\infty} - 1}{\frac{\gamma}{2} M_\infty^2} .$$

601.313 Pressure Coefficient for Points Other Than Leading Edge

In all usual cases, in which the airfoil surface is convex, c_p at any point may be calculated by the use of expansion-fan techniques. For a biconvex airfoil section, for example, divide the surface into a number of elements, considering the surface within each element to be a straight line. Relate local pressure (p_n) to that ahead of the leading edge (p_∞) by

$$\frac{p_n}{p_\infty} = \left(\frac{p_n}{p_{n-1}}\right) \cdots \left(\frac{p_2}{p_1}\right)\left(\frac{p_1}{p_\infty}\right),$$

where ratios p_1/p_∞, p_2/p_1, etc. are calculated as above. Then the pressure coefficient at this point is

$$c_{p_n} = \frac{\frac{p_n}{p_\infty} - 1}{\frac{\gamma}{2} M_\infty^2}.$$

When the shock expansion method is used to compute pressures over a biconvex airfoil, or certain other cases, the results are not exact (cf. Subsection 601.3).

601.32 Numerical Example for Symmetrical Double Wedge Airfoil

The following figure shows the flow field about the airfoil:

Let $M_\infty = 3$,

$\alpha = 8$ degrees,

$(t/c)_{max} = 0.06$,

$\delta = 3.434$ degrees.

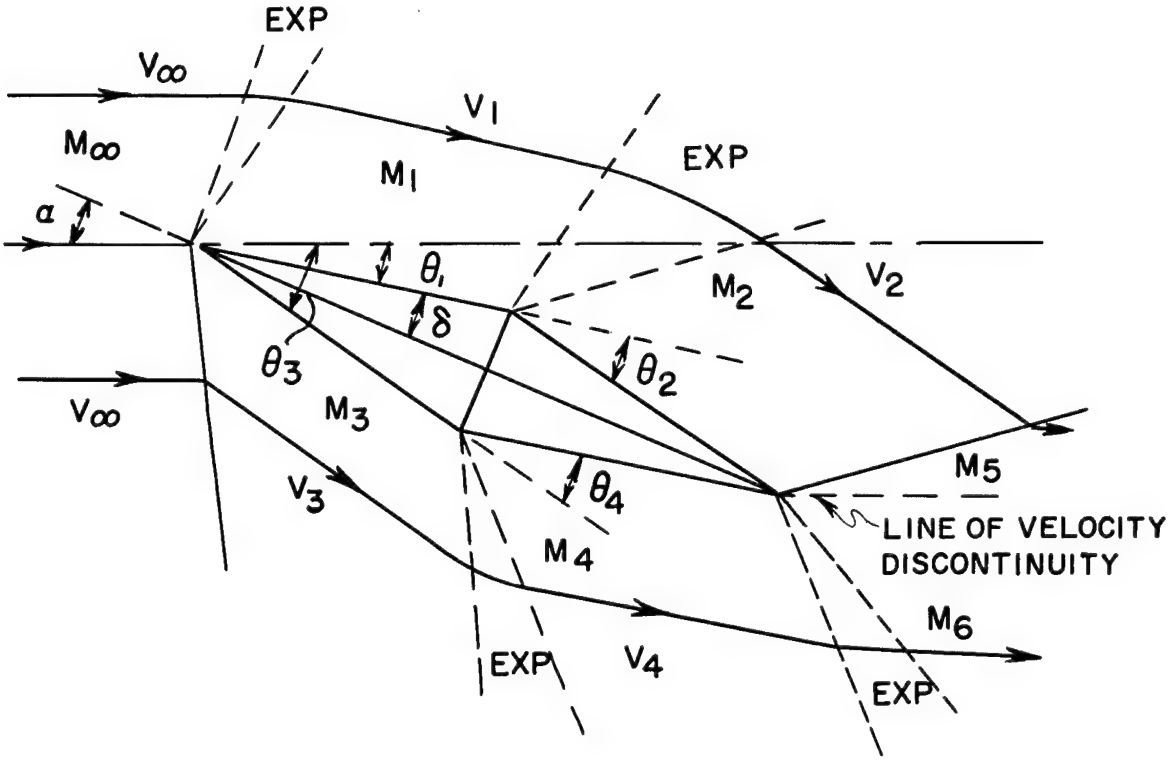

If the angle of attack (α) and the wedge half angle (δ) are properly combined the local changes in flow deflection angle (θ) for each of the four surfaces are as follows:

Angle	θ_1	θ_2	θ_3	θ_4
Degrees	-4.566	-6.868	+11.434	-6.868

For surface No. 1, at angle $\theta_1 = -4.566$ degrees (expansion) with original flow direction:

(a) By Table 504.111, $\omega_\infty = 49.757$ degrees,

(b) $\omega_1 = 49.757 + 4.566 = 54.323$ degrees,

(c) By Table 504.211, $M_1 = 3.248$,

(d) By Table 501.111, $p_\infty/p_t = 0.02722$,

$p_1/p_t = 0.01886$,

(e) $\frac{p_1}{p_\infty} = \frac{0.01886}{0.02722} = 0.6929$,

(f) $c_{p_1} = \frac{0.6929 - 1}{0.7 \times 9} = -0.0487$.

For surface No. 2, at angle $\theta_2 = -6.868$ degrees (expansion) with surface No. 1:

(a) $\omega_1 = 54.323$ degrees,

(b) $\omega_2 = 54.323 + 6.868 = 61.191$ degrees,

(c) $M_2 = 3.673$,

(d) $\frac{p_1}{p_t} = 0.01886$,

$\frac{p_2}{p_t} = 0.01028$,

(e) $\frac{p_2}{p_1} = \frac{0.01028}{0.01886} = 0.5451,$

(f) $\frac{p_2}{p_\infty} = \left(\frac{p_2}{p_1}\right)\left(\frac{p_1}{p_\infty}\right) = 0.5451 \times 0.6929 = 0.3777,$

(g) $c_{p_2} = \frac{0.3777 - 1}{0.7 \times 9} = -0.0988.$

For surface No. 3, at angle $\theta_3 = 11.433$ degrees (compression) with original flow direction:

(a) By Table 503.111, $\eta_3 = 28.71$ degrees, (designated as α in Table 503.111)

$\sin \eta_3 = 0.4804,$

(b) $M_{\infty_n} = M_\infty \sin \eta_3 = 3.0 \times 0.4804 = 1.441,$

(c) By Table 502.111, $M_{3_n} = 0.7231,$

$\frac{p_3}{p_\infty} = 2.256,$

(d) $M_3 = \frac{M_{3_n}}{\sin (\eta_3 - \theta_3)} = \frac{0.7230}{\sin 17.28} = \frac{0.7230}{0.2970} = 2.435,$

(e) $c_{p_3} = \frac{2.257 - 1}{0.7 \times 9} = 0.1994.$

For surface No. 4, at angle $\theta_4 = -6.868$ degrees (expansion) with surface No. 3:

(a) By Table 504.111, $\omega_3 = 37.589$ degrees,

(b) $\omega_4 = 37.565 + 6.868 = 44.457$ degrees,

(c) By Table 504.211, $M_4 = 2.739$,

(d) By Table 501.111, $p_3/p_t = 0.06477$,

$$p_4/p_t = 0.04045,$$

(e) $$\frac{p_4}{p_3} = \frac{0.04052}{0.06487} = 0.6245,$$

(f) $$\frac{p_4}{p_\infty} = 0.6246 \times 2.257 = 1.4089,$$

(g) $$c_{p_4} = \frac{1.4097 - 1}{0.7 \times 9} = 0.0649.$$

601.4 Characteristics Method

As was pointed out in Subsection 601.3, the shock expansion method is not exact for those profiles that produce expansion wavelets intersecting the leading-edge shock wave at such points that the reflected waves from these intersections reach the profile and thereby modify the pressure distribution over the rearward portion of the profile. The biconvex airfoil, or any continuous curved profile, falls in this class.

Normally, for the biconvex profiles, the curvature of the profile is sufficiently small that the effects of the reflected wavelets may be neglected. In this case, if sufficiently small intervals are selected along the profile, the shock expansion method will give satisfactory results.

Where a more accurate pressure distribution for a continuous curved profile is required, the method of characteristics may be employed. Details of the method of characteristics may be found in numerous volumes (e.g., Ref. 5, page 591 ff).

601.5 Comparison of Various Methods

Following the method of Ref. 6, page 239, there is presented in Fig. 601.5-1, a graph that shows, for Mach numbers from 1.0 to 5.0, the range of flow deflection angles (ω) for which the pressure calculated by use of the third-order equation differs from the value obtained by the second-order equation by not more than one per cent of the latter value. The equations used in computing this set of curves are:

$$\frac{2}{\gamma M^2} = - A\omega - B\omega^2 + 100(C - D)\omega^3, \qquad (601.5\text{-}1)$$

for flow deflections involving compressions (ω positive), and

$$\frac{2}{\gamma M^2} = - A\omega - B\omega^2 - 100C\omega^3, \qquad (601.5\text{-}2)$$

for isentropic expansions (ω negative).

Figure 601.5-1 also shows the maximum expansion angle which, if exceeded, according to the second-order theory, will result in an increase in pressure with an increase in flow expansion angle, and thus will falsely indicate a compression (Ref. 6, page 238). The equation used for this practical limit on the use of the second-order theory for expansion flows is

$$\omega = - \frac{A}{2B} . \qquad (601.5\text{-}3)$$

Also shown on Fig. 601.5-1 is the upper limit of shock-compression flow deflection angle beyond which shock detachment will occur (see Subsection 601.31). None of the aforementioned theories are applicable for those large deflection angles that result in shock detachment.

As an aid in determining limiting conditions, graphs of half-wedge angle (δ) versus thickness ratio, (t/c), for double-symmetric airfoils of double wedge, flattened double wedge, and circular arc sections are given in Fig. 601.5-2. The flattened double wedge here considered is defined in Subsection 603.

For the symmetrical circular arc profile there is also plotted in Fig. 601.5-2 the chord-to-radius ratio against thickness ratio.

In order to compare the results of the computations based on each of the various methods (excluding the characteristics method which is rarely ever justified for airfoil computations), a number of graphs are presented in the following subsection for both double-symmetrical double wedge and circular arc airfoils.

601.51 Pressure Distributions

For the double-symmetrical double wedge airfoil a comparison of the pressure coefficients (c_p) obtained by the power-series method and the shock expansion method is made in the table in Subsection 601.21 and Fig. 601.51-1. The airfoil used in this comparison has a maximum thickness ratio of 0.06 for which the half wedge angle is 3.434 degrees. The mid-chord line of the airfoil is at an angle of attack of 8 degrees with the direction of the undisturbed flow. For these conditions the critical Mach number at which the shock wave begins to detach is 1.474. This comparison covers a Mach number range from shock detachment to 5.

In all instances the second-order theory gives pressure coefficients that approximate more closely the exact shock expansion values than do the first order results. Furthermore, the third-order values of pressure coefficients are almost indistinguishable from the shock expansion values, except as shock detachment is approached.

In the table in Subsection 601.21 of pressure coefficients, it is apparent that, at $M_\infty = 3$, the effect of the D-coefficient in the third-order term is negligible. Over the Mach number range from shock detachment to 5, the largest difference due to the D-coefficient is only 0.6 per cent of the c_p. Consequently, in Fig. 601.51-1 (and in all subsequent figures), there is shown for the third order, only one curve which represents both sets of values--with and without the coefficient "D".

Pressure coefficients for this same double wedge airfoil section, at zero angle of attack, are shown in Fig. 601.51-2.

The chordwise variation of pressure coefficient over a double circular arc airfoil with a thickness ratio of 0.06 at $M_\infty = 2$ is shown in Fig. 601.51-3. The pressure coefficients over both the lower and upper surfaces when the airfoil is at an angle of attack of 12 degrees, as well as at zero angle of attack, are shown. The results of using the first-, second-, and third-order and shock-expansion methods of computation are presented. Since all biconvex airfoils produce rotational flow for which the shock expansion method is not precisely valid, none of the curves for this class of airfoil gives exact values (see Subsection 601.3). However, the errors resulting from use of the shock expansion method are smaller than for any of the power-series methods. For exact values the method of characteristics must be used, but generally it is not considered necessary to resort to this more laborious method in the determination of airfoil characteristics.

That the pressure coefficients obtained from the higher-order power series conform more closely to the shock expansion results than do the lower-order series is demonstrated in the foregoing paragraph.

447269 O - 58 - 3

602 Lift, Drag and Center of Pressure

The primary aerodynamic characteristics of the two-dimensional airfoil are readily determined from the pressure distribution. In this section, lift and drag coefficients, per unit section, c_ℓ and c_d, and the center of pressure, c.p., are determined for double wedge and circular arc airfoils. The various methods of determining pressures given in Subsection 601 are used so that the results of higher-order theories may be compared.

The standard force coefficients, c_ℓ and c_d, refer to air forces normal and tangential to free stream direction. As here computed, only the pressure, or "wave" drag is accounted for in c_d. The total drag may be estimated by adding the skin friction drag (Subsection 605.1) to this pressure drag.

In terms of forces normal to and parallel to the chord (or axis) of the airfoil, we may write c_ℓ and c_d as follows:

$$c_\ell = c_n \cos \alpha - c_a \sin \alpha, \qquad (602\text{-}1)$$

$$c_d = c_n \sin \alpha + c_a \cos \alpha,$$

where the coefficients c_n and c_a can be shown to be, (see for example, Ref. 6):

$$c_n = \frac{1}{c} \int_0^c (c_{p_\ell} - c_{p_u})\, dx,$$

$$c_a = \frac{1}{c} \int_0^c \left[(c_{p_u} - c_{p_\ell}) \tan \delta_x \right] dx. \qquad (602\text{-}2)$$

The element of length dx is measured along the chord from leading edge; tan δ_x is the slope of the wing surface with respect to the chord, and the subscripts ℓ and u refer to the lower and upper surfaces of the airfoil.

The center of pressure is defined as the point of intersection of the line of action of the resultant air force with the chord of the airfoil. The distance from leading edge to center of pressure, c.p., is then

$$\text{c.p.} = -c_m/c_n, \tag{602-3}$$

where c_m is the moment coefficient about the leading edge. The negative sign arises as c_m conventionally is taken positive when the trailing edge is forced down.

$$c_m = \frac{1}{c^2}\int_0^c (c_{p_u} - c_{p_\ell})\, x\,dx + \frac{1}{c^2}\int_{y_\ell}^{y_u} (c_{p_u} - c_{p_\ell})\, y\,dy,$$

where the distance y is measured from the chord in the direction normal to the chord, positive in the direction of the upper surface.

602.1 Continuation of the Numerical Example for Symmetrical Double Wedge Airfoil

The double wedge symmetrical wing section has been taken as the configuration for which pressure coefficients were calculated to illustrate the power series method (Subsection 601.21) and the shock expansion method (Subsection 601.32). The pressure coefficients are constants over the four surfaces and c_n, c_a, and c_m become simply:

$$c_n = \frac{1}{2}\left(-c_{p_1} - c_{p_2} + c_{p_3} + c_{p_4}\right),$$

$$c_a = \frac{t}{2c}\left(+c_{p_1} - c_{p_2} + c_{p_3} - c_{p_4}\right),$$

$$c_m = \frac{1}{8}\left[\left(c_{p_1} - c_{p_3}\right) + 3\left(c_{p_2} - c_{p_4}\right) + \left(\frac{t}{c}\right)^2 \left(c_{p_1} - c_{p_2} - c_{p_3} + c_{p_4}\right)\right].$$

Taking values of c_p from the table, Subsection 601.21, the coefficients c_ℓ and c_d and the c.p. may be computed from the defining Eqs. 602-1 and 602-3 and the above. These computed values are given in the table below and in Fig. 602.1-1. The values of c.p. are given in decimal fractions of the chord from the leading edge.

Aerodynamic Coefficients	c_ℓ	c_d	c.p.
1st order	0.1948	0.0325	0.5000
2nd order	0.1948	0.0325	0.4465
3rd order without D	0.2041	0.0343	0.4488
3rd order with D	0.2039	0.0343	0.4490
Shock expansion	0.2032	0.0342	0.4489

Since the pressure coefficients for the diagonally opposite surfaces of this airfoil as computed by the second-order theory differ from those obtained by the first-order theory by the same amount ($B\omega^2$) and since these second-order terms cancel each other in all computations of aerodynamic forces, it follows that the second-order values of any of these forces are identical with the first-order values. The moments produced by these forces over the four surfaces of the airfoil, however, do not cancel, and consequently the computed values of moment coefficient (and of center of pressure) by second-order computations are different from the first-order results. For the third-order theory, however, the third-order terms in the expression for pressure coefficient do not cancel when they are used in the computation of the aerodynamic forces. In addition, even though the third-order values for the pressure coefficients differ only slightly from the shock-expansion values, it is conceivable that the difference may be much larger in the case of the computed values for the center of pressure.

Since the second-order theory gives values of force coefficients that are no better than the first-order values, and also since it is desirous to give the designer a feeling for the difference in results obtained by the various orders of power series, all three orders are included in the figures.

For the double-symmetric double wedge airfoil whose pressure coefficients at an angle of attack of 8 degrees are presented in Table 601.51-1 and Fig. 601.51-1, there are shown the section lift and drag coefficients and center of pressure in Fig. 602.1-1. The Mach number range is from 1.474 (shock detachment) to 5. The centers of pressure are in decimal fractions of the chord from the leading edge.

602.2 Comparison of Results Given by Various Methods

The results of computations, by the various theories, of c_ℓ, c_d and c.p. on double wedge and circular arc airfoils at angles of attack up to 20 degrees, for t/c = 0.06, are shown in Fig. 602.2-1 plotted against Mach number.

The aerodynamic coefficients for double wedge airfoils are computed from Eqs. 602-4 and 602-5.

For the circular arc profiles, the computations were made by determining the pressure coefficients at five points equally spaced along the chord (so as to divide it into four equal segments) and five other points similarly dispersed along the half maximum-thickness line. Simpson's "one-third rule" was then used in integrating these pressures so as to obtain lift and drag coefficients, and centers of pressure. As a result of the comparison with results obtained when twice as many points are used, it is concluded that this procedure, using four segments only, leads to negligible errors in computed values of c_ℓ, c_d, and c.p.

For constant Mach numbers, $M_\infty = 2$ and $M_\infty = 3$, another similar group of curves is presented in Figs. 602.2-2 and 602.2-3, plotted against thickness ratio.

The variation of center of pressure with angle of attack at $M_\infty = 2$ for double wedge airfoils of 6 and 12 per cent thickness is shown in Fig. 602.2-4.

603. Double-Symmetric Airfoil Sections with Sharp Edges

Two-dimensional airfoil characteristics (c_ℓ, c_d, and c.p.) calculated by the Defense Research Laboratory of The University of Texas (Ref. 7), using the shock-expansion method outlined in Subsections 601.3 - 601.32 and the tables of the Handbook, Section 5 (Ref. 2), are presented in this subsection for double-symmetric sharp-edged sections. More specifically, the characteristics are for the double wedge, the "flattened double wedge" and the biconvex circular arc airfoil sections. The "flattened double wedge" here reported on is defined as shown in the middle sketch below.

(a) Double wedge

(b) Flattened double wedge

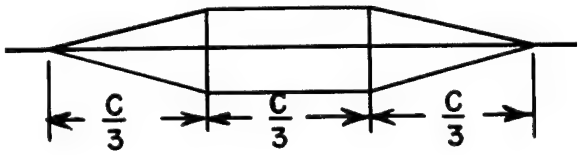

(c) Circular arc

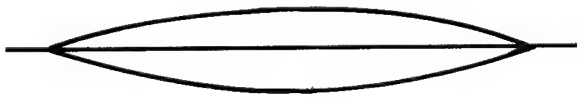

Double symmetric airfoil sections here considered.

Three independent variables have been chosen; Mach number, angle of attack, and thickness ratio. The three principal characteristics--lift coefficient, drag coefficient, and center of pressure--for certain groupings of these variables are presented in graphical form in the following subsections.

603.1 Airfoil Characteristics - Variable Thickness Ratio

Figure 603.1-1 shows the airfoil characteristics c_ℓ, c_d and c.p. for symmetric double wedge, flattened double wedge and circular arc airfoil sections for Mach number of two ($M_\infty = 2$). Figure 603.1-2 presents corresponding data for $M_\infty = 3$. These data cover the range of thickness ratios from zero to 0.12. The arbitrary parameter used is the angle of attack (α = 0, 4, 8, 12, 16 and 20 degrees).

603.2 Airfoil Characteristics - Variable Mach Number

Figure 603.2-1 shows the variation with Mach number of the airfoil characteristics c_ℓ, c_d and c.p. for double symmetric double wedge, flattened double wedge, and circular arc airfoil sections, with a constant thickness ratio of 0.06. These data cover a range up to $M_\infty = 5$, from minimum values of Mach number that depend upon shock detachment at the leading edge. The arbitrary parameter used is the angle of attack (α = 0, 4, 8, 12, 16 and 20 degrees).

604 Unsymmetrical Two-Dimensional Airfoil Sections

This subsection is concerned with the effects on the airfoil characteristics in supersonic flow of certain modifications of the foregoing double-symmetrical airfoil sections. These modifications result in airfoils that no longer have double symmetry.

604.1 Effect of Changing Position of Maximum Thickness

Changing the position of maximum thickness eliminates symmetry about an axis perpendicular to the chord, but retains symmetry about the chord. Figure 604.1-1 shows the change in pressure drag coefficient for double wedge airfoils (of 0.06 thickness ratio) at zero angle of attack (zero lift), for M_∞ = 2, 3, 4, 5, 6, and 8, plotted against the position of maximum thickness. The shock-expansion method was used for this computation.

It is seen that at low Mach numbers there is a well defined minimum value of drag coefficient when the maximum thickness is at about 0.55 of the chord back from the leading edge. At higher Mach numbers the chordwise position for minimum pressure drag shifts aft (Ref. 8), and at M_∞ = 8 is approximately 65 per cent of the chord from the leading edge.

604.2 Effect of Changing Camber of Airfoil

Starting with a double-symmetric double wedge airfoil (zero camber) of thickness ratio 0.06, both positive and negative cambers* have been introduced by converting the airfoil to triangular sections, and maintaining the thickness ratio at 0.06. In particular, the cases of a triangular section with 3 per cent positive camber (base down), and another with 3 per cent negative camber (base up) are considered. Values of c_ℓ and c_d have been computed by the shock-expansion method for several angles of attack at M_∞ = 2, and the results are shown in the diagram of Fig. 604.2-1.

It is seen that when only the wave drag component is considered, the uncambered airfoil has the best lift-to-drag ratio. A positive camber is next best, according to these calculations.

*Camber. Ratio of departure of median airfoil line from the straight line joining its extremities, to the length of this line. The sign is positive when the departure is upward.

The effect, at a free-stream Mach number of 4, of a 1.25 per cent positive camber on the section lift, drag coefficient and the lift-to-drag ratio for a double-symmetric double wedge airfoil with a maximum thickness ratio of 0.05, according to Ref. 8, is shown in Fig. 604.2-2.

Positive camber results in a positive angle of attack for zero lift in the case of the three cambered Guidonia airfoils (G.U. 3, G.U. 4, and G.U. 5) for which there are adequate experimental data. Theoretical values for the angle of zero lift based on the shock-expansion method (Ref. 8) and experimental values as reported in Ref. 9 are given in the following figure together with the configurations of these three airfoils.

Guidonia Airfoils

Angle of Attack for Zero Lift (degrees)

Airfoil	G.U. 3	G.U. 4	G.U. 5
Theoretical (Ref. 8)	1.68	0.44	0.28
Experiemntal (Ref. 9)	1.89	0.45	0.26

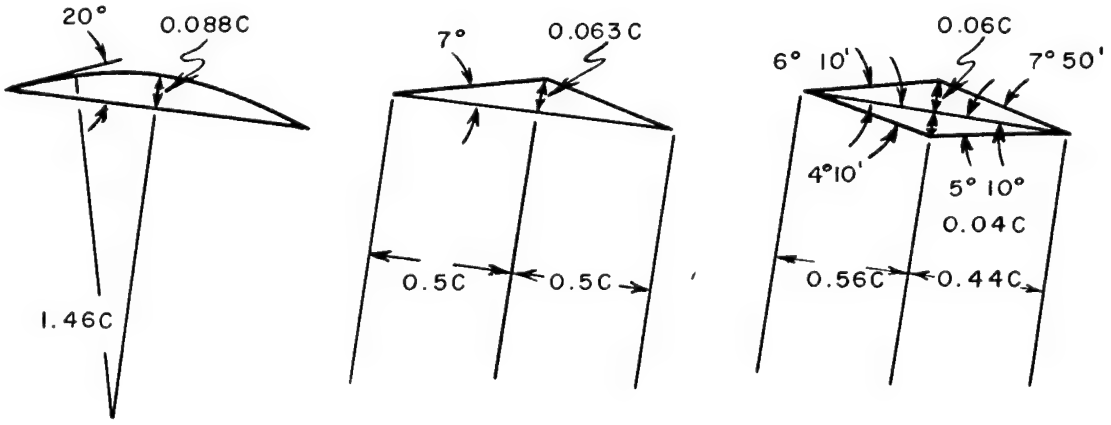

G.U. 3 G.U. 4 G.U. 5

605 Viscosity Effects

The effects of viscosity and heat transfer are restricted to a thin layer close to the surface of the solid body, the boundary layer. These effects are treated in some detail in Sections 13 and 14 of the Handbook. This subsection therefore includes only a brief resumé of these effects as they pertain to two-dimensional airfoils.

605.1 Skin Friction Drag

As a result of both theory and experiment it has been established that there are two general types of boundary layer flow over a surface. These depend in part upon the nature of the surface--the Mach number and the Reynolds number of the flow. The flow may be either laminar or turbulent, or a combination of both. In order to set forth some indications as to trends, Figs. 605.1-1 and 605.1-2 have been included to illustrate the mean skin friction drag coefficients for completely laminar and turbulent flows, respectively, over one side only of an insulated flat plate. Figure 605.1-1 is based on an equation by A. D. Young in Ref. 10; Fig. 605.1-2 is based on an equation by E. R. Van Driest in Ref. 11. It is apparent that the laminar flow drag coefficients are appreciably less than those for turbulent flow. An estimate of the total drag can be obtained by adding these skin friction drag coefficients to the pressure drag coefficients.

605.2 Flow Separation

The viscous flow in a boundary layer will, under certain conditions of adverse pressure gradients, cause a separation of the boundary layer. This results in an alteration of the flow, to the extent that loss of lift and large increases in drag and moment may result. Separation effects are more serious at low Reynolds numbers, and increase rapidly with increasing angle of attack. The separation may be temporary, permanent, or oscillatory, depending on the shape of the airfoil as well as the nature of the boundary layer, and whether transition precedes separation or follows it. No general quantitative data are available showing the effects of separation on lift, drag and moment. One experimental study (Ref. 13) of flow separation on a double wedge and a biconvex airfoil with $t/c = 0.10$ at $M_\infty = 1.86$ and $M_\infty = 2.48$, and a Reynold's number of about 5×10^5 is described in Subsections 606.1 and 606.2 below. Although some separation was present at all angles of attack greater than zero in these studies, the effect on lift and drag was small; the effect on center of pressure quite large. It should be noted that the theoretical values of c.p. are brought into fair agreement with the experiment here if separation is taken into account. The most reliable method of ascertaining separation effects in relation to particular airfoil sections is by experiment.

605.3 Heat Transfer

The phenomenon of heat transfer underlies all boundary layer effects and cannot be separated completely from them. It has been shown that cooling the body surface stabilizes a laminar boundary layer and thereby increases the Reynolds number at which transition from laminar to turbulent flow occurs. Heating the body surface destabilizes a laminar boundary layer. Cooling usually decreases the skin friction whether the boundary layer is fully laminar or turbulent, whereas heating usually increases the skin friction.

606 Experimental Data

The first experimental supersonic data on two-dimensional airfoil characteristics are believed to be that of T. E. Stanton, published in 1928. These data were on a cambered biconvex airfoil of 10 per cent thickness ratio. There are no available results of comprehensive experimental studies of two-dimensional airfoils at supersonic speeds. A limited body of data is available, however, for uncambered biconvex and double wedge airfoils. Selected portions of these data are presented here along with pertinent theoretical results.

606.1 Double-Symmetric Double Wedge Airfoils

The results of tests made at the United Aircraft Corporation's supersonic wind tunnel on a series of 6-inch chord double wedge airfoils without camber have been reported (Ref. 12). Tests were made at Mach numbers of 1.38, 1.48, and 1.58. The thickness ratios of the airfoils tested were 0.035, 0.070, and 0.105. More recent tests carried out in Great Britain (Ref. 13) are for a double wedge with $t/c = 0.10$ and $M_\infty = 1.86$ and $M_\infty = 2.48$. Pressure measurements were made at a number of points on the surfaces of the airfoils. These pressures were used exclusively in both studies in reporting the various force and moment coefficients, and center of pressure, recorded therein.

The experimental results were compared with theoretical values that were computed by the shock-expansion method. No allowance was made for the effect of skin friction upon the reported quantities. In general, satisfactory agreement between theory and experiment was demonstrated.

Some data for the airfoils are reproduced here. The pressure distribution over the upper surface of one airfoil is compared with the prediction from shock expansion theory in Fig. 606.1-1(a). It can be seen that the predicted abrupt pressure change at maximum thickness is smoothed by the presence of a boundary layer and that boundary layer separation occurs at all positive angles of attack.

The values of lift and drag computed from the pressure distribution (Figs. 606.1-1(b) and 606.1-1(c)) show good agreement with the theory. The c.p. computations are less satisfactory (Fig. 606.1-1(d)). The effect of separation on c.p. was computed for an 8° angle of attack in Ref. 13 and is shown in the figure, indicating that separation accounts for about one half the difference between the shock expansion theory and experiment.

606.2 Double-Symmetric Biconvex Airfoils

The tests on a biconvex airfoil reported in Ref. 13 give results similar to the above on a double wedge. Separation occurred at all positive angles of attack (Fig. 606.2-1) and is reported to account for nearly all the difference between the theoretical c.p. and the center of pressure computed from the experimental pressure distribution. Experimental data on lift and drag from the Guidonia tunnel (Ref. 9) were obtained as force measurements from a wind tunnel equipped with a balance system. Thus, the c_d obtained included friction drag. In addition to the theoretical curves shown in Ref. 9, there is also presented in Fig. 606.2-2(a) a modified curve that includes the skin friction drag effect determined from Fig. 605.1-2. It should be noted that the viscous effects are for a completely turbulent boundary layer with zero heat transfer. The experimental and theoretical results for c_d are in good agreement. The curves presented are for a 10 per cent thick biconvex airfoil at $M_\infty = 2.13$. Pressure measurements made in the same tests are compared with the predicted values (based on shock-expansion theory) in Fig. 606.2-2(b).

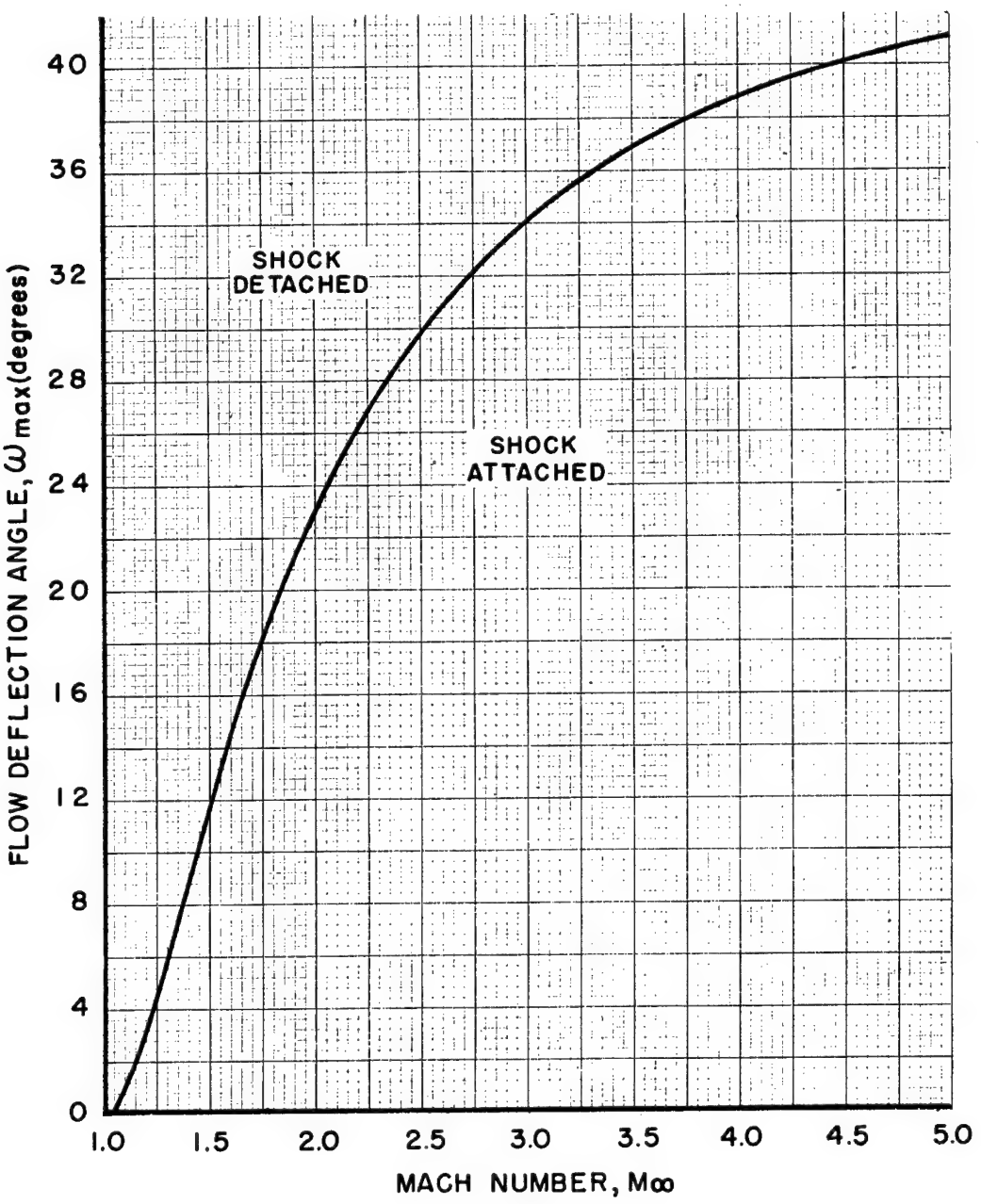

Figure 601.31-1 MAXIMUM FLOW DEFLECTION ANGLE FOR SHOCK ATTACHMENT AS A FUNCTION OF MACH NUMBER; REF. 2, TABLE 503.211, VOLUME 2

447269 O - 58 - 4

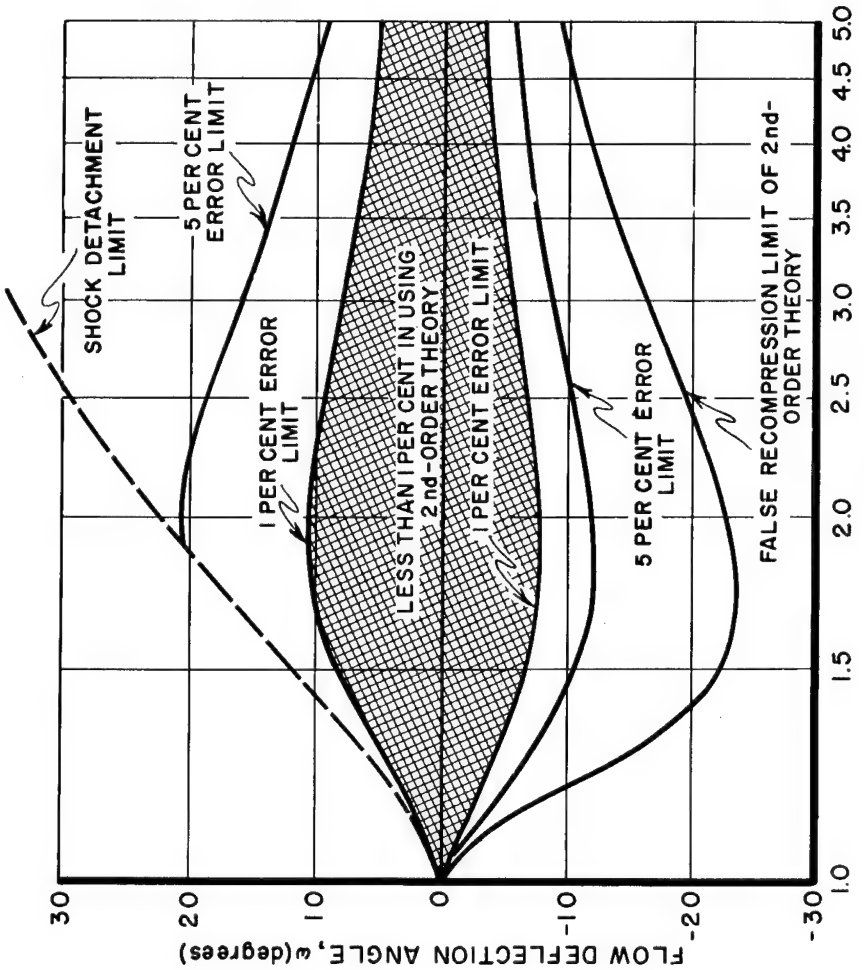

Figure 601.5-1 LIMITS OF ACCURACY FOR SECOND-ORDER THEORY IN TWO-DIMENSIONAL FLOW

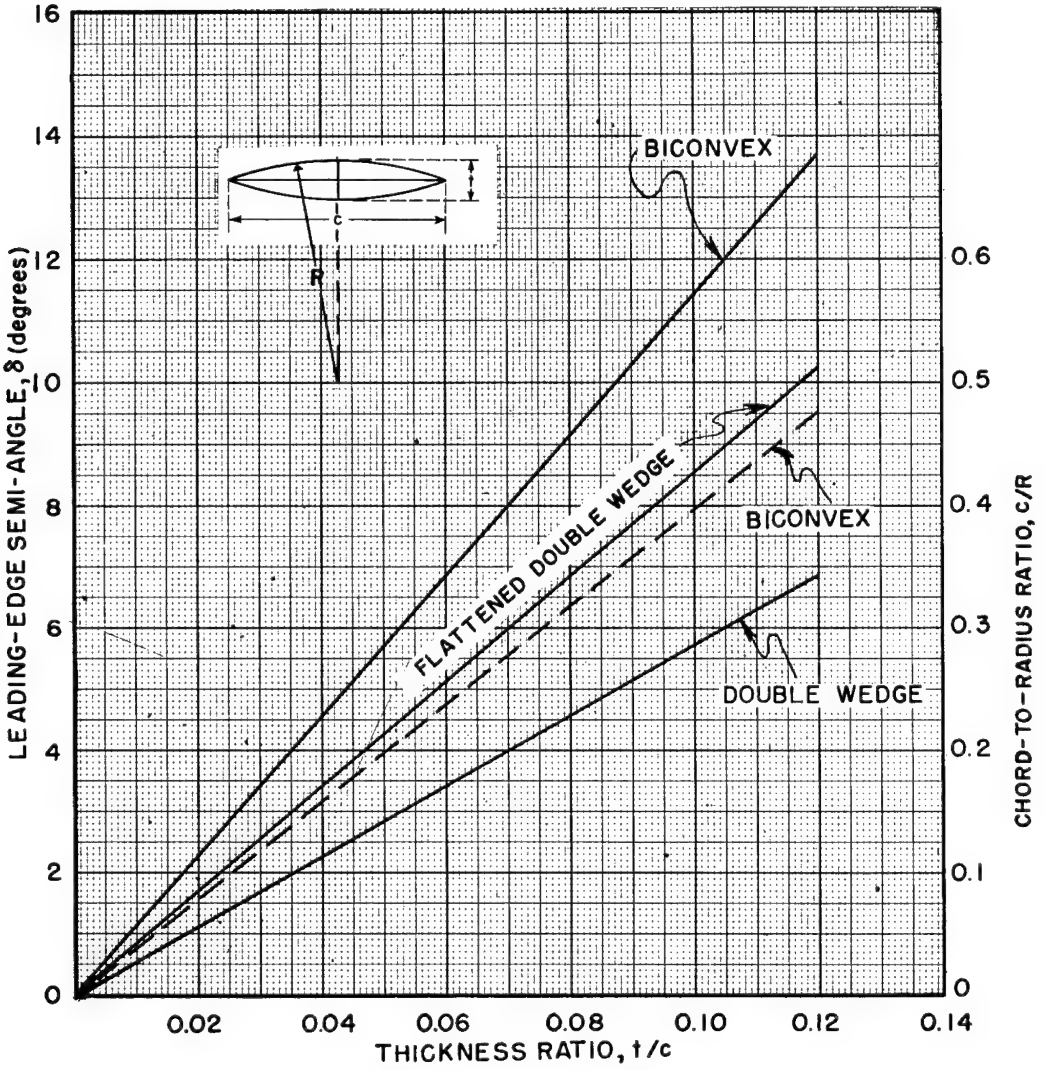

Figure 601.5-2 LEADING-EDGE SEMI-ANGLES AND CHORD-TO-RADIUS RATIO AS FUNCTIONS OF THICKNESS RATIO; BICONVEX, DOUBLE WEDGE, AND FLATTENED DOUBLE WEDGE PROFILES

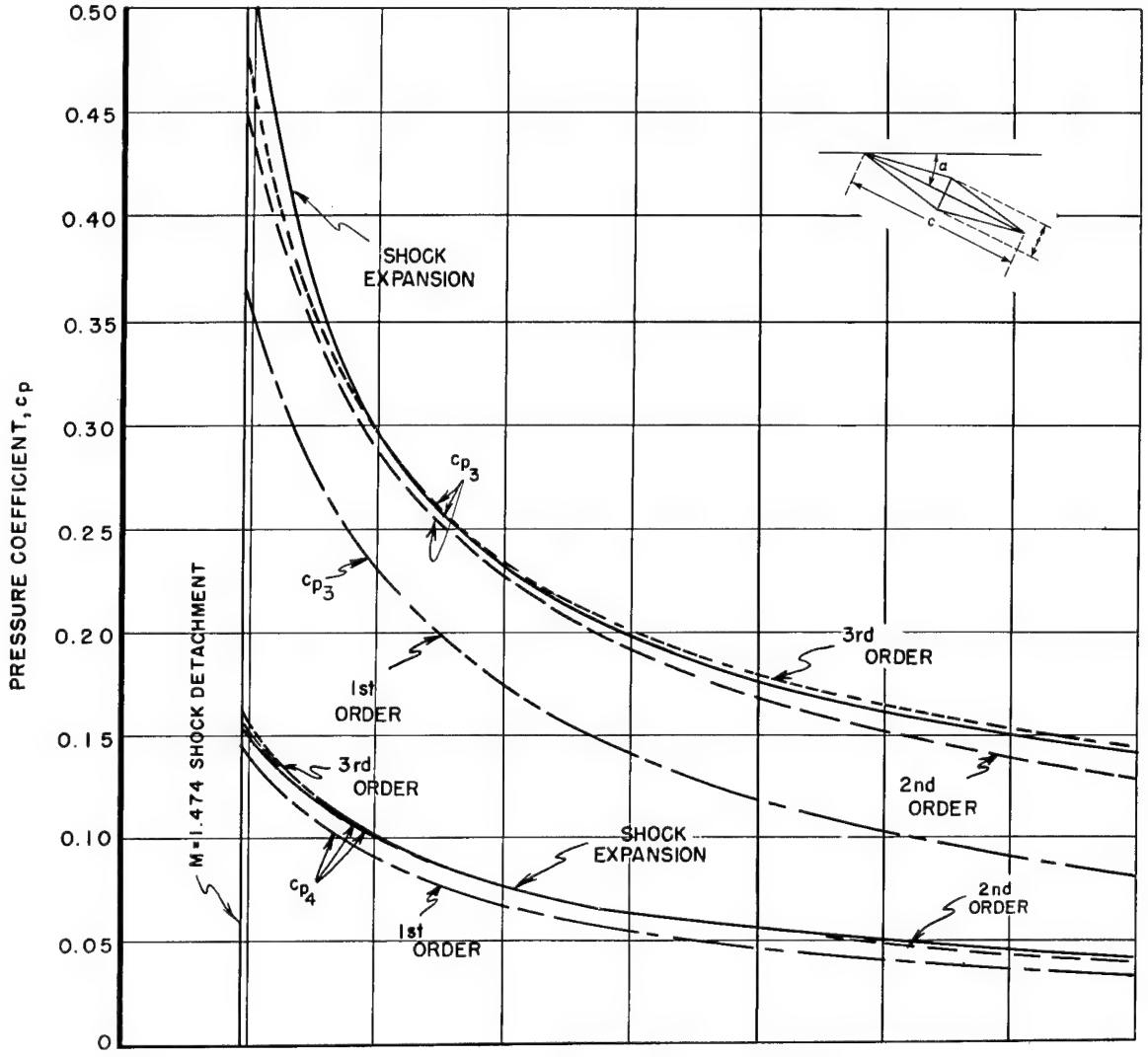
PRESSURE COEFFICIENT, c_p
0.50
0.45
0.40
0.35
0.30
0.25
0.20
0.15
0.10
0.05
0
M=1.474 SHOCK DETACHMENT
SHOCK EXPANSION
c_{p_3}
c_{p_3}
1st ORDER
3rd ORDER
2nd ORDER
3rd ORDER
SHOCK EXPANSION
c_{p_4}
1st ORDER
2nd ORDER
a
c

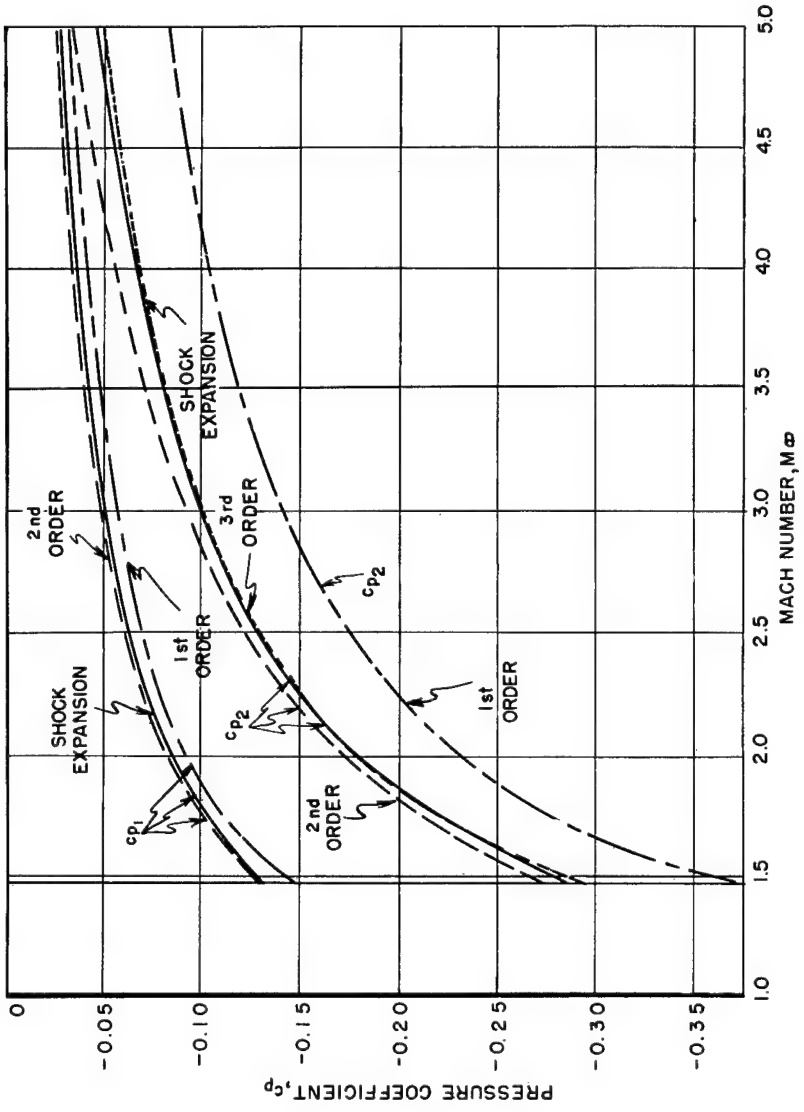

Figure 601.51-1 COMPARISON OF THEORETICAL APPROXIMATIONS; VARIATION OF PRESSURE COEFFICIENT WITH MACH NUMBER; DOUBLE WEDGE AIRFOIL; $t/c = 0.06$; $\alpha = 8°$

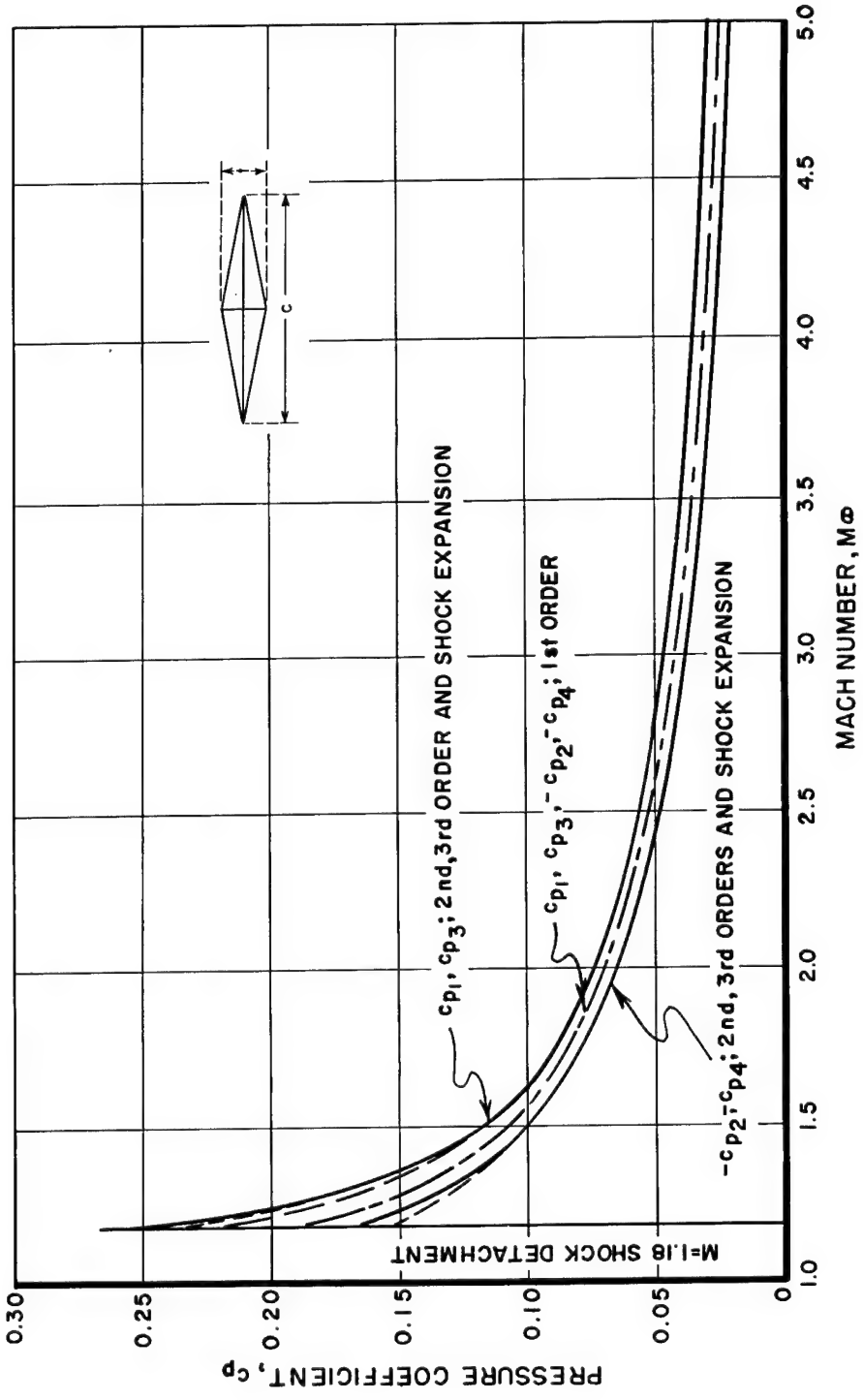

Figure 601.51-2 COMPARISON OF THEORETICAL APPROXIMATIONS; VARIATION OF PRESSURE COEFFICIENT WITH MACH NUMBER; DOUBLE WEDGE AIRFOIL; $t/c = 0.06$; $\alpha = 0°$

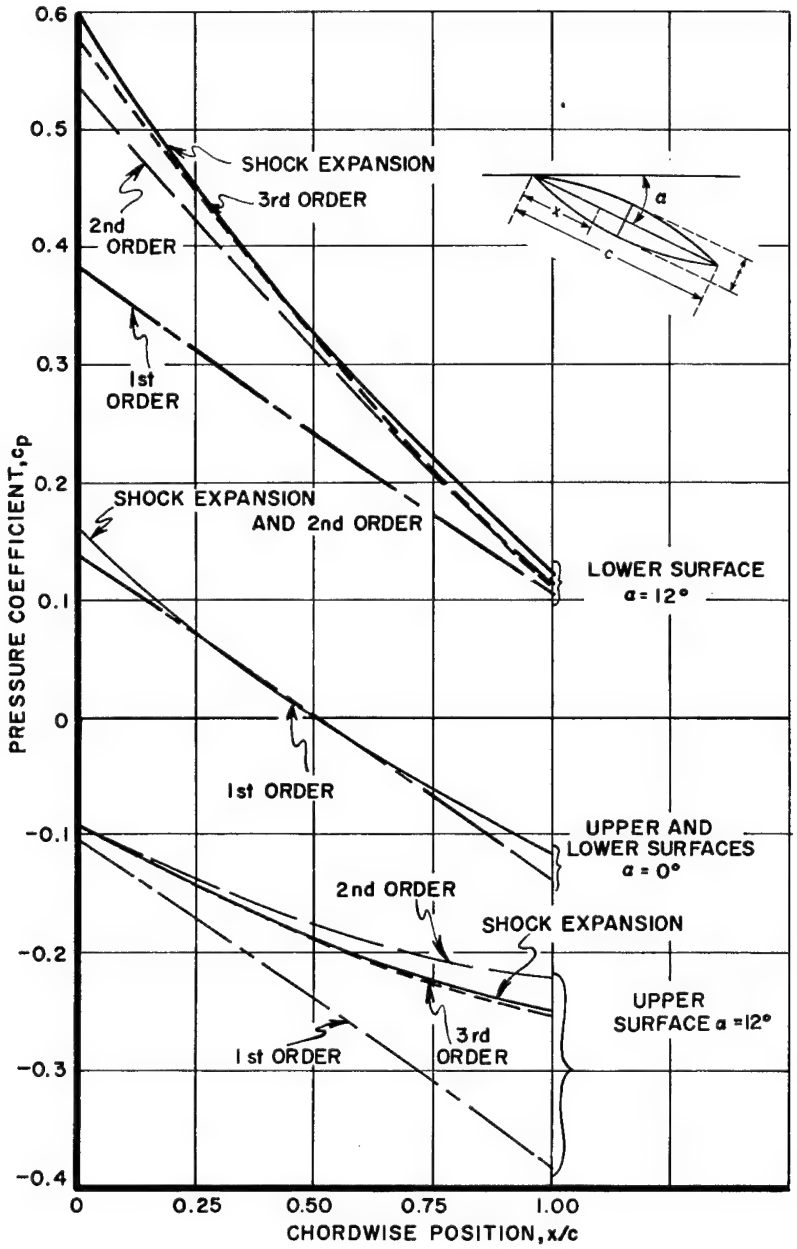

Figure 601.51-3 COMPARISON OF THEORETICAL APPROXIMATIONS; CHORDWISE PRESSURE DISTRIBUTION FOR A BICONVEX AIRFOIL; $M_\infty = 2$; $t/c = 0.06$; $\alpha = 0°, 12°$

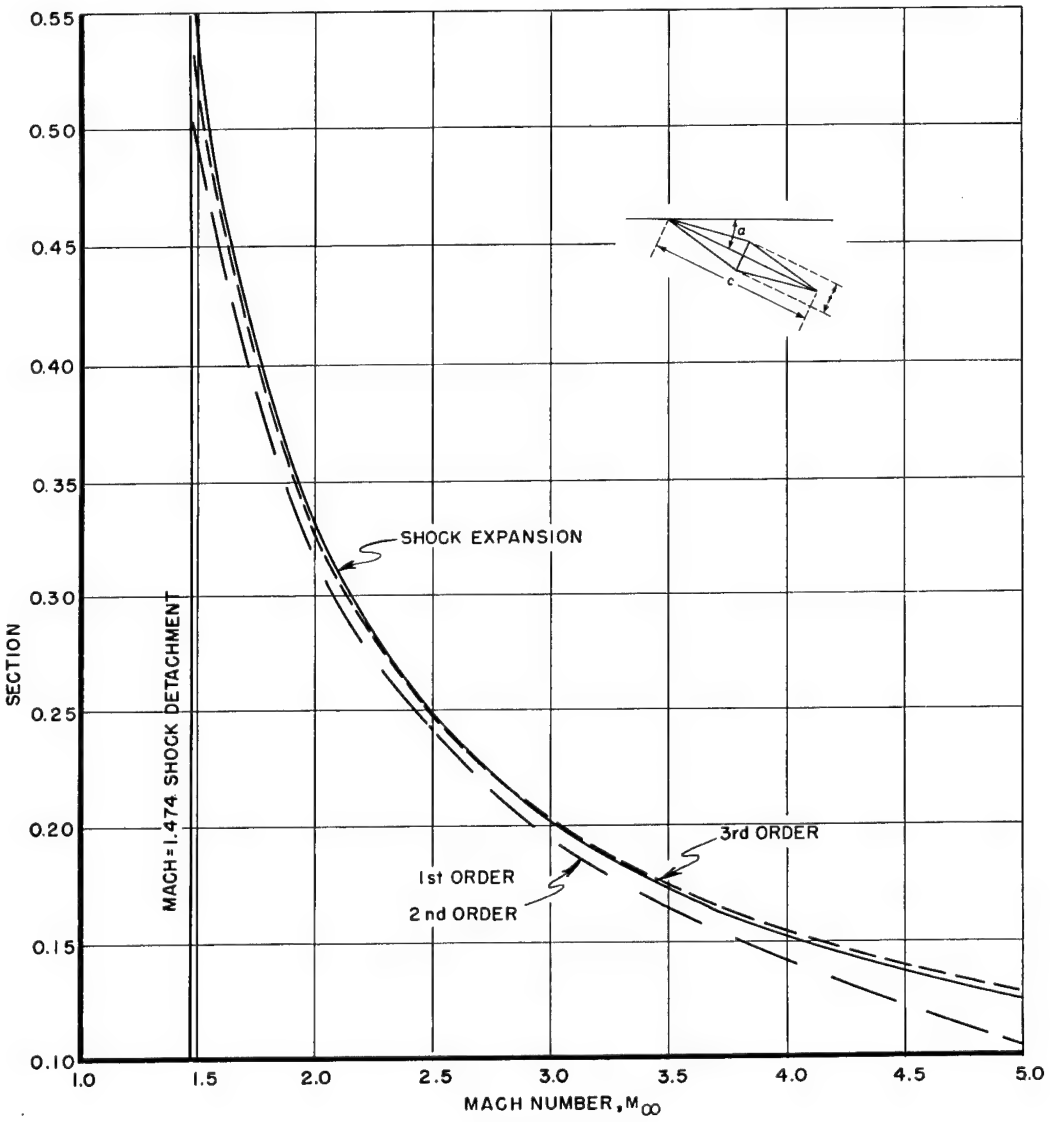

Figure 602.1-1(a) COMPARISON OF THEORETICAL APPROXIMATIONS; VARIATION OF SECTION LIFT COEFFICIENT WITH MACH NUMBER; DOUBLE WEDGE AIRFOIL; $t/c = 0.06$; $\alpha = 8°$

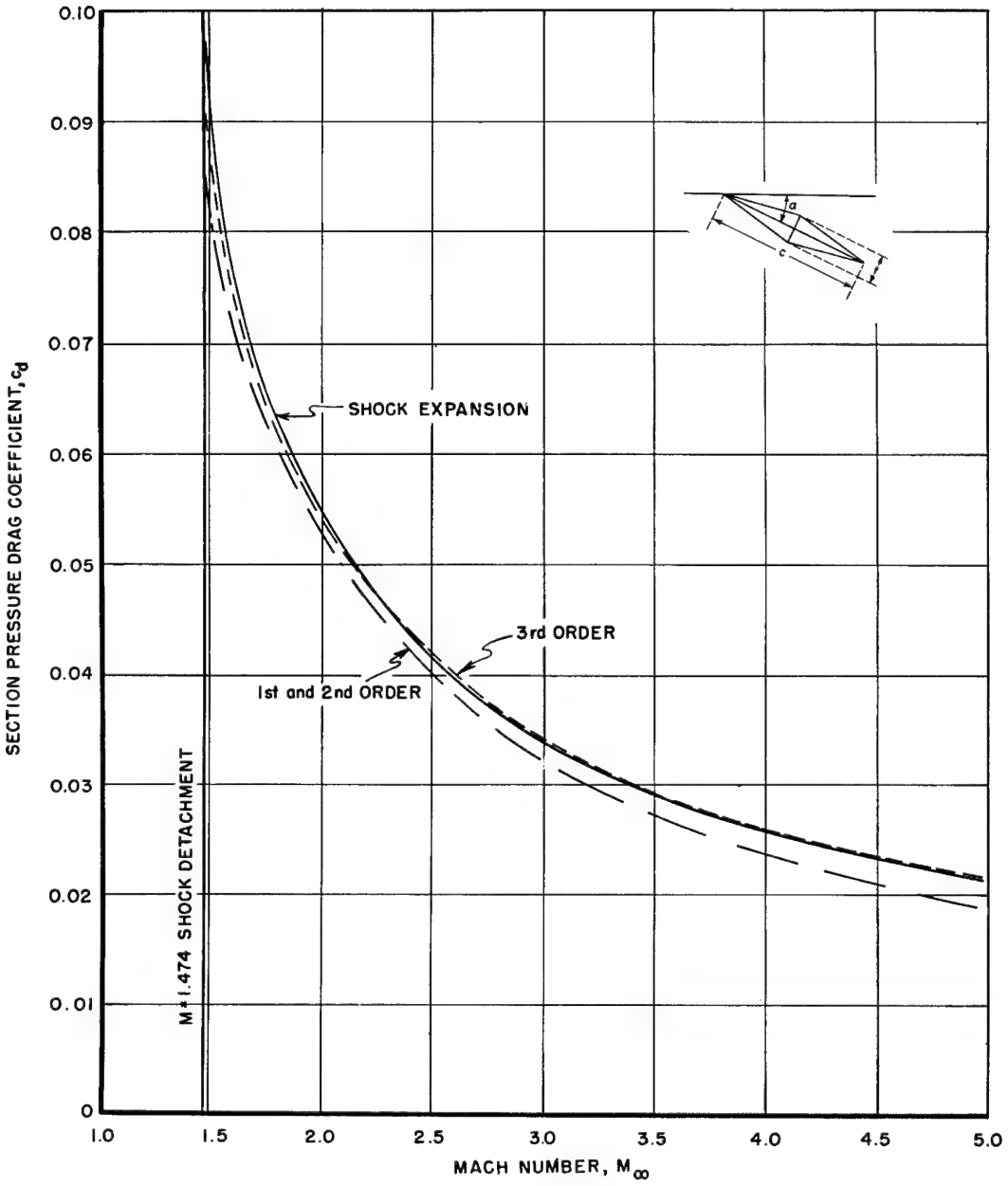

Figure 602.1-1(b) COMPARISON OF THEORETICAL APPROXIMATIONS; VARIATION OF SECTION PRESSURE DRAG COEFFICIENT WITH MACH NUMBER; DOUBLE WEDGE AIRFOIL; $t/c = 0.06$; $\alpha = 8°$

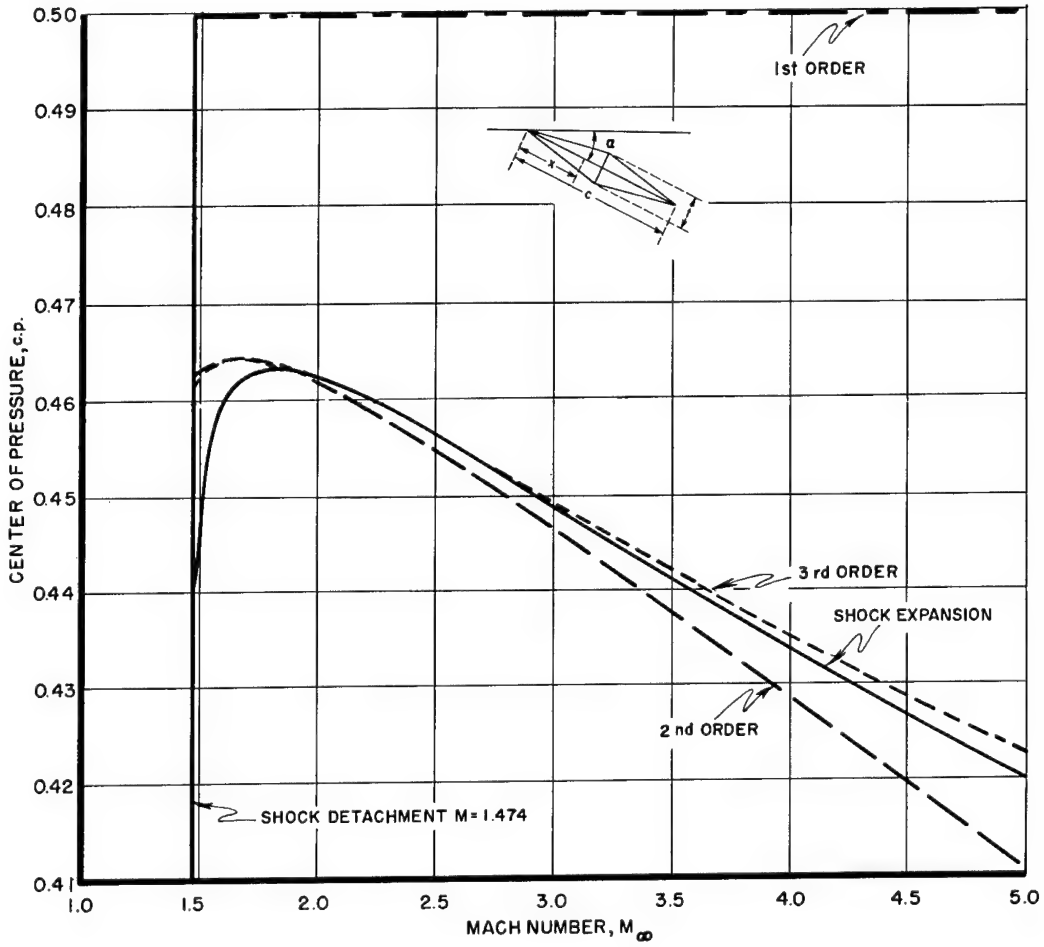

Figure 602.1-1(c) COMPARISON OF THEORETICAL APPROXIMATIONS; VARIATION OF CENTER OF PRESSURE WITH MACH NUMBER; DOUBLE WEDGE AIRFOIL; $t/c = 0.06$; $\alpha = 8°$

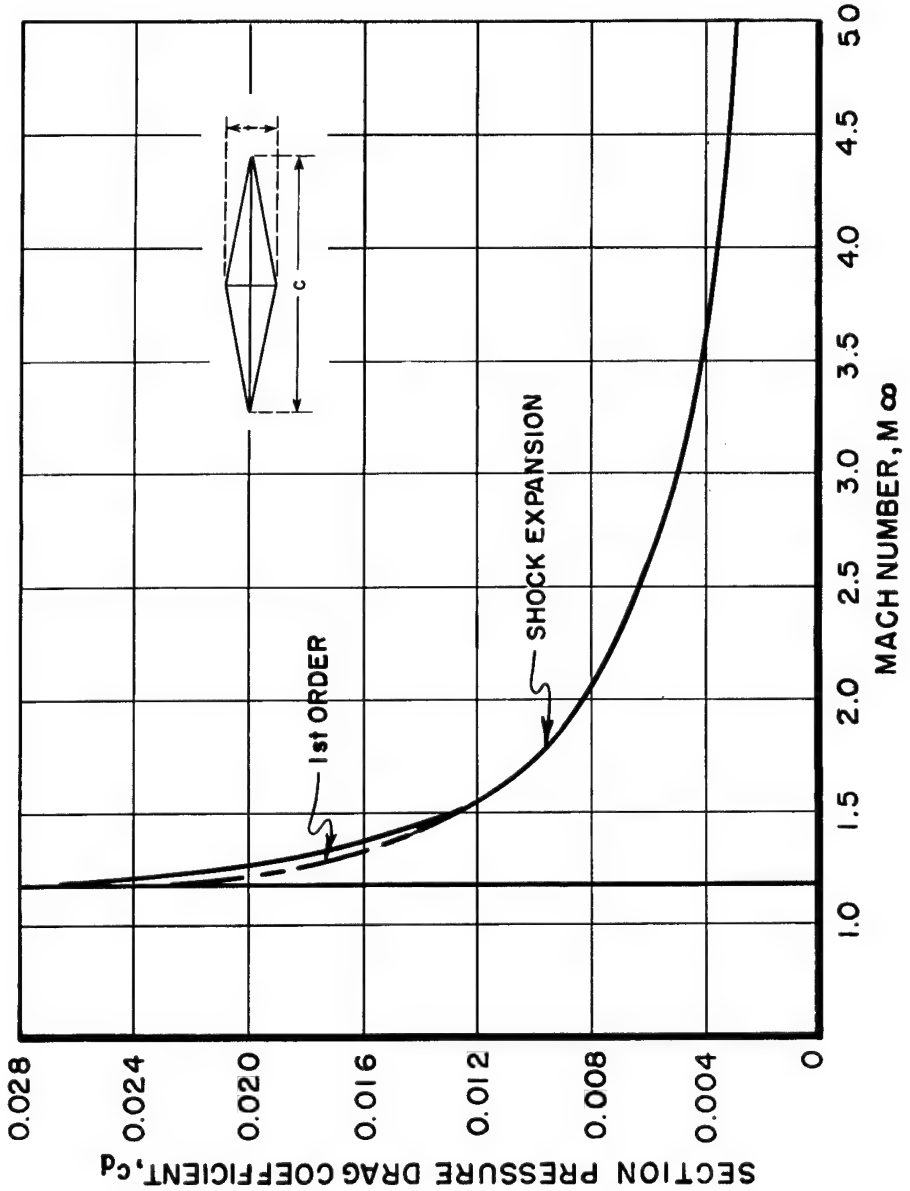

Figure 602.1-2 COMPARISON OF THEORETICAL APPROXIMATIONS; VARIATION OF SECTION PRESSURE DRAG COEFFICIENT WITH MACH NUMBER; DOUBLE WEDGE AIRFOIL; $t/c = 0.06$; $\alpha = 0°$

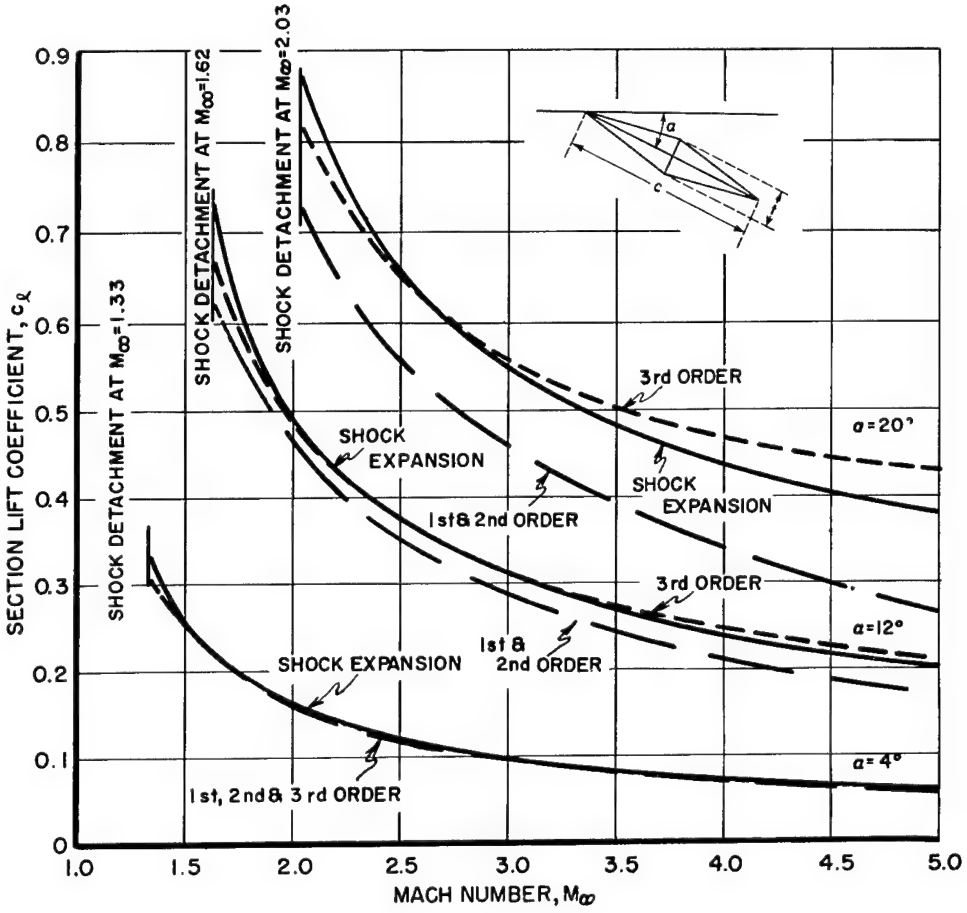

Figure 602.2-1(a) COMPARISON OF THEORETICAL APPROXIMATIONS; VARIATION OF SECTION LIFT COEFFICIENT WITH MACH NUMBER; DOUBLE WEDGE AIRFOIL; $t/c = 0.06$; $\alpha = 4°, 12°, 20°$

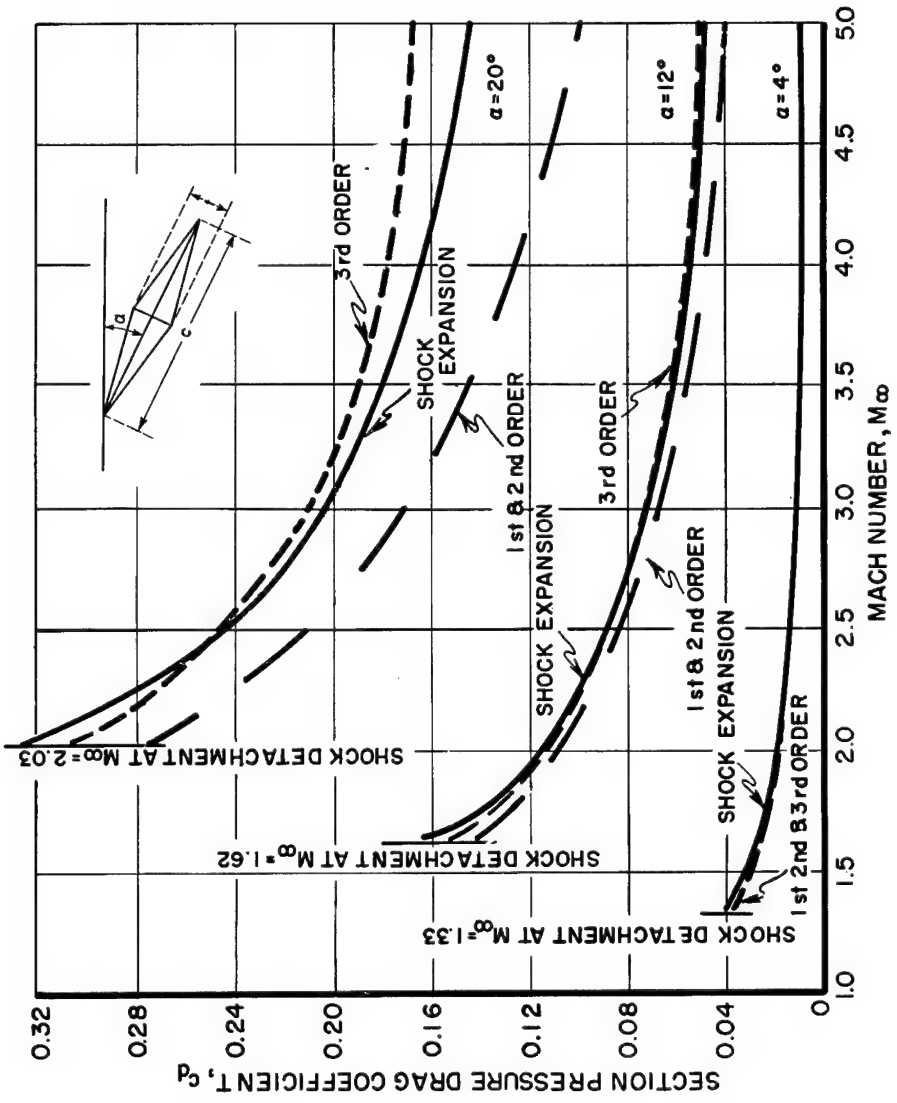

Figure 602.2-1(b) COMPARISON OF THEORETICAL APPROXIMATIONS; VARIATION OF SECTION PRESSURE DRAG COEFFICIENT WITH MACH NUMBER; DOUBLE WEDGE AIRFOIL; $t/c = 0.06$; $\alpha = 4°, 12°, 20°$

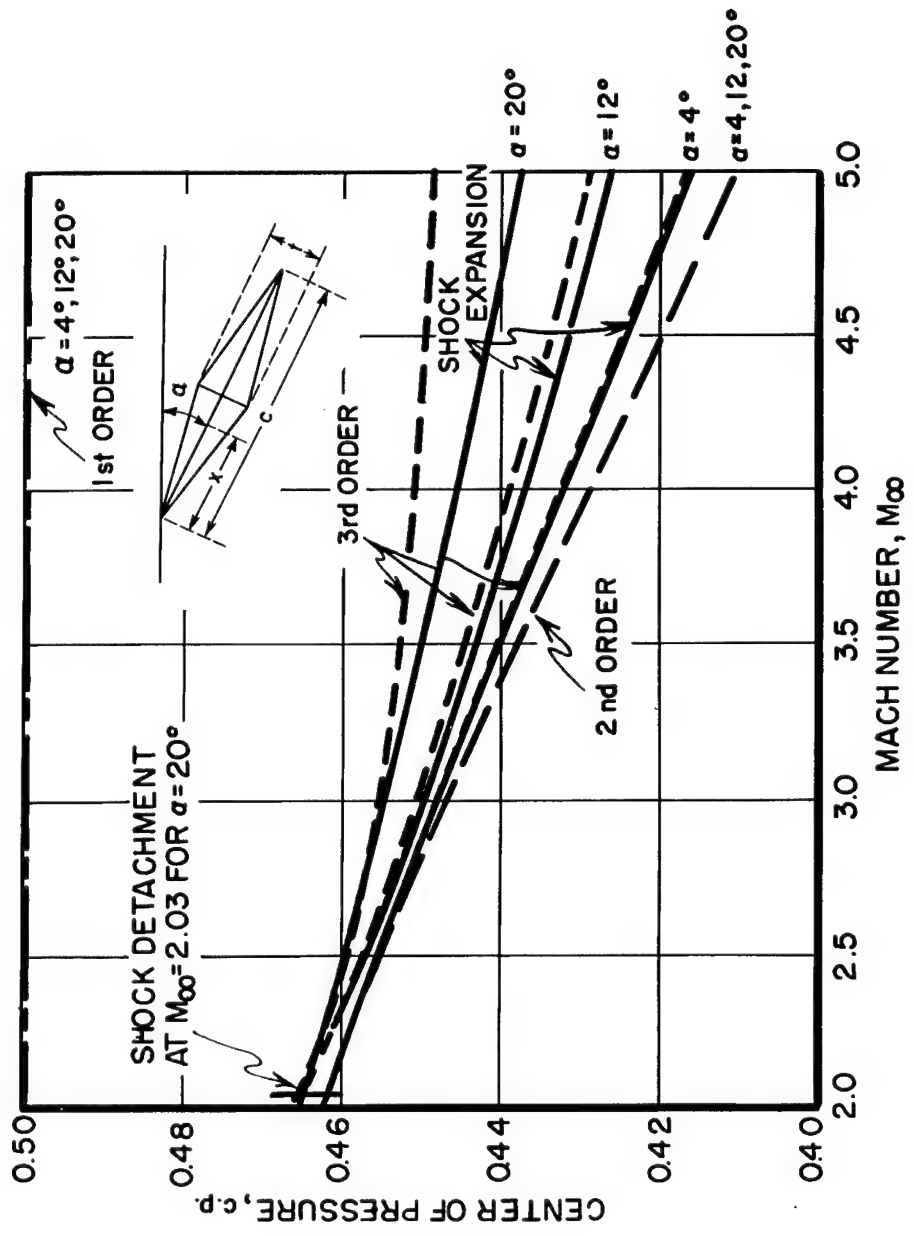

Figure 602.2-1(c) COMPARISON OF THEORETICAL APPROXIMATIONS; VARIATION OF CENTER OF PRESSURE WITH MACH NUMBER; DOUBLE WEDGE AIRFOIL; $t/c = 0.06$; $\alpha = 4°$, $12°$, $20°$

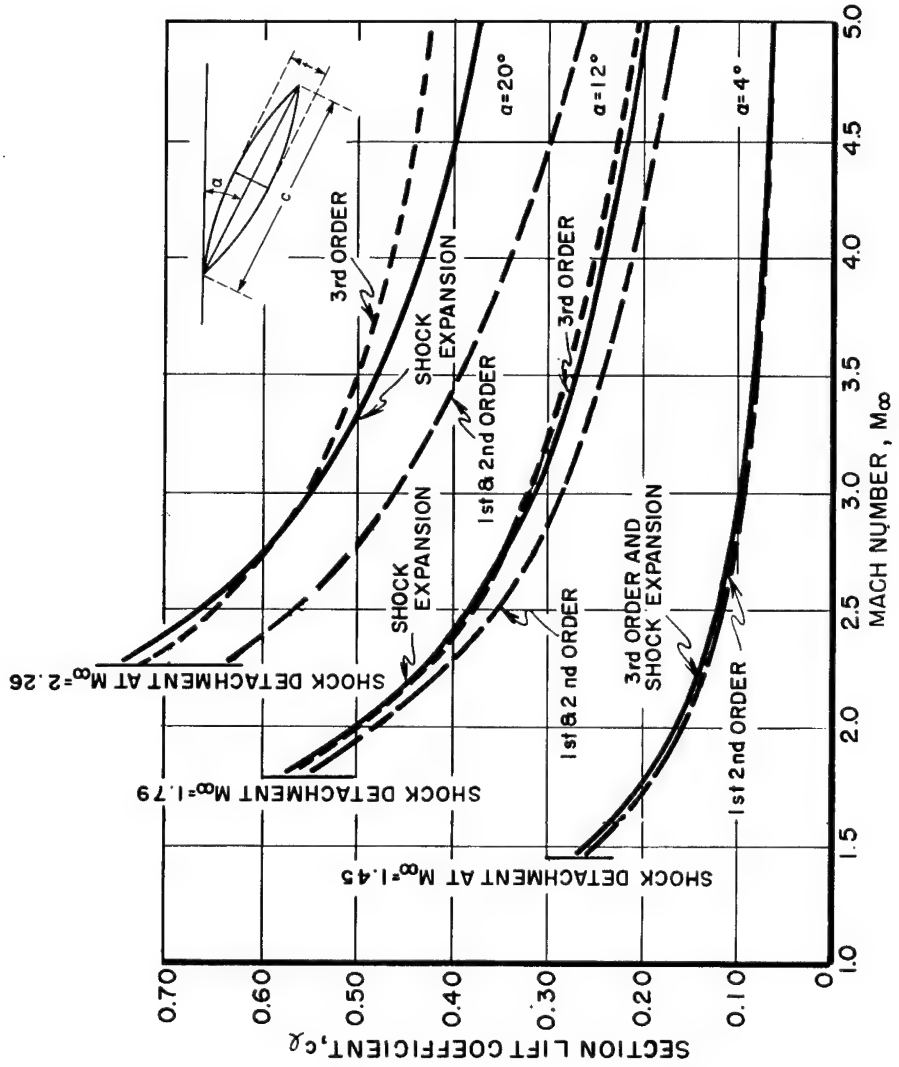

Figure 602.2-1(d) COMPARISON OF THEORETICAL APPROXIMATIONS; VARIATION OF SECTION LIFT COEFFICIENT WITH MACH NUMBER; BICONVEX AIRFOIL; $t/c = 0.06$; $\alpha = 4°, 12°, 20°$

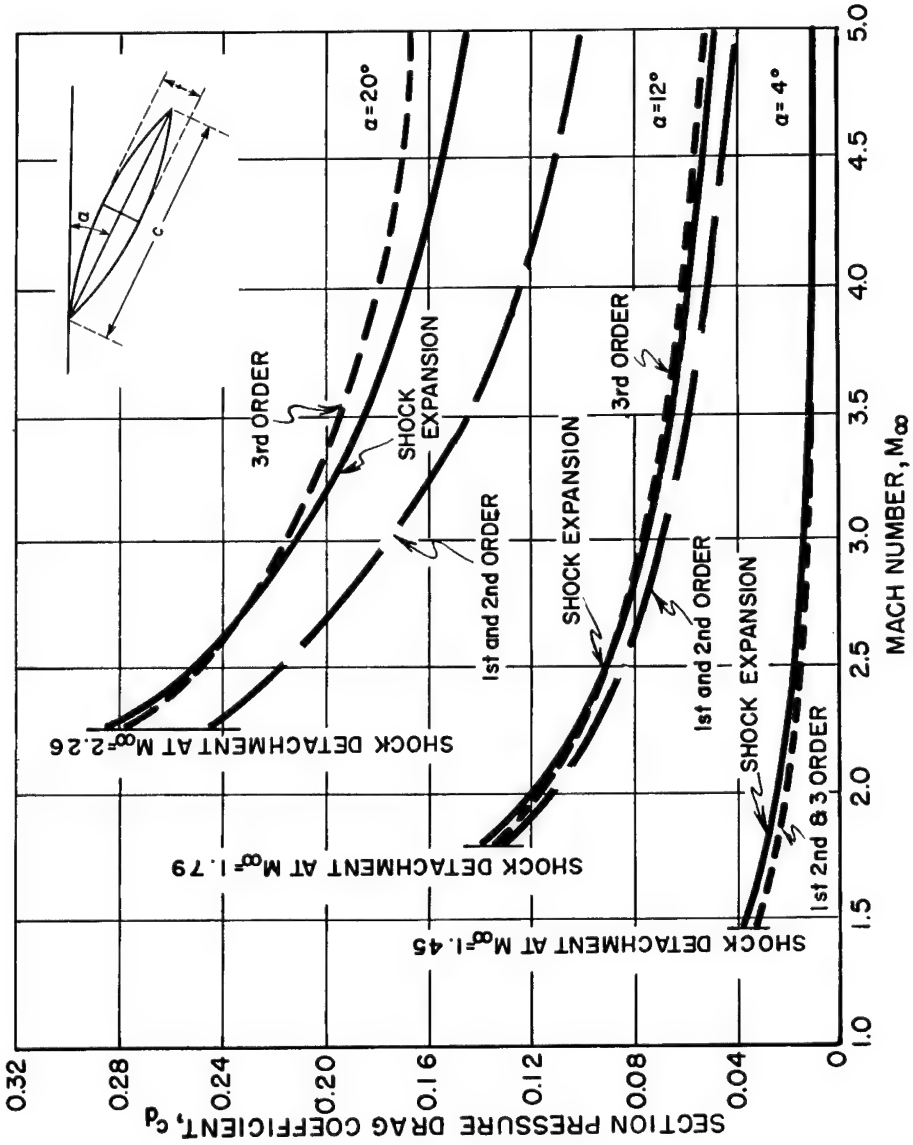

Figure 602.2-1(e) COMPARISON OF THEORETICAL APPROXIMATIONS; VARIATION OF SECTION PRESSURE DRAG COEFFICIENT WITH MACH NUMBER; BICONVEX AIRFOIL; $t/c = 0.06$; $\alpha = 4°, 12°, 20°$

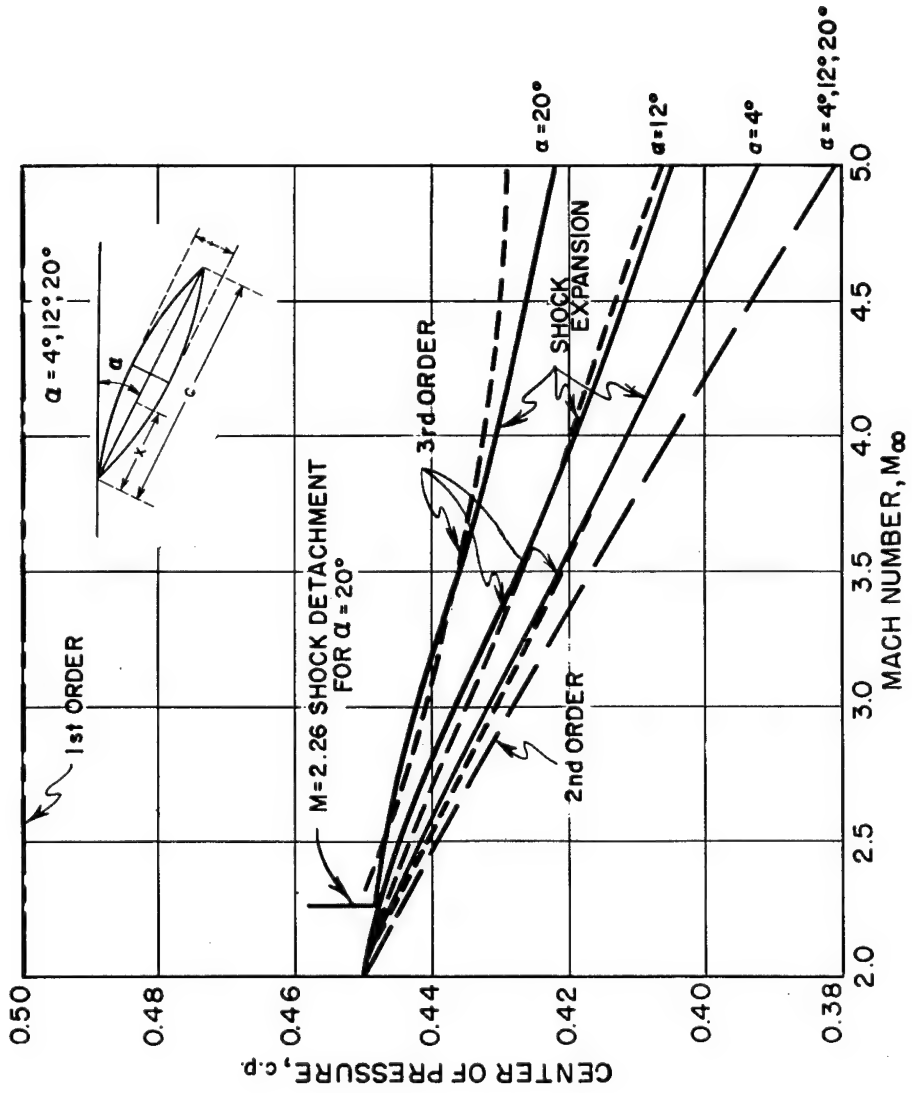

Figure 602.2-1(f) COMPARISON OF THEORETICAL APPROXIMATIONS; VARIATION OF CENTER OF PRESSURE WITH MACH NUMBER; BICONVEX AIRFOIL; t/c = 0.06; α = 4°, 12°, 20°

447269 O - 58 - 5

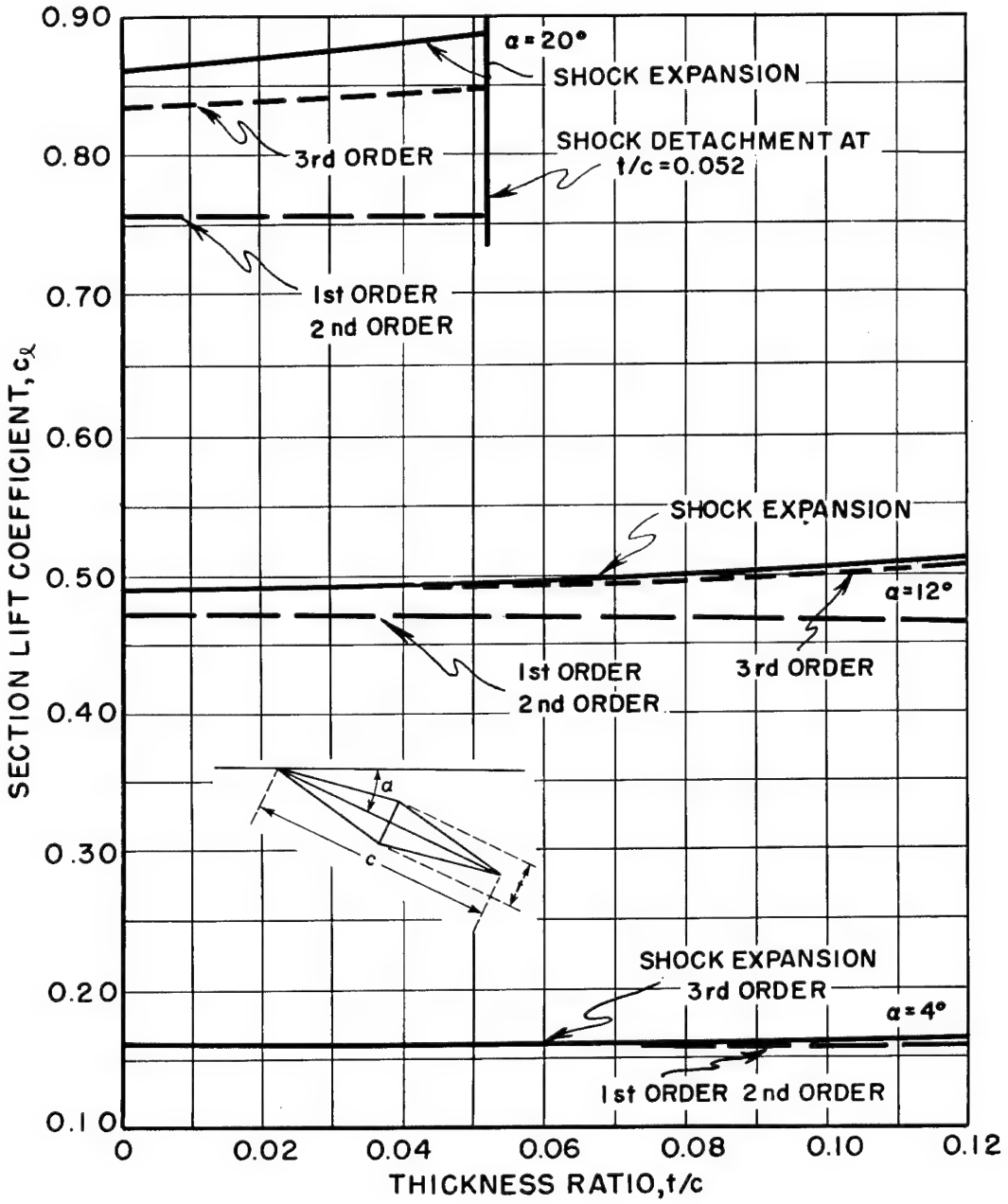

Figure 602.2-2(a) COMPARISON OF THEORETICAL APPROXIMATIONS; VARIATION OF SECTION LIFT COEFFICIENT WITH THICKNESS RATIO; DOUBLE WEDGE AIRFOIL; $M_\infty = 2$; $\alpha = 4°, 12°, 20°$

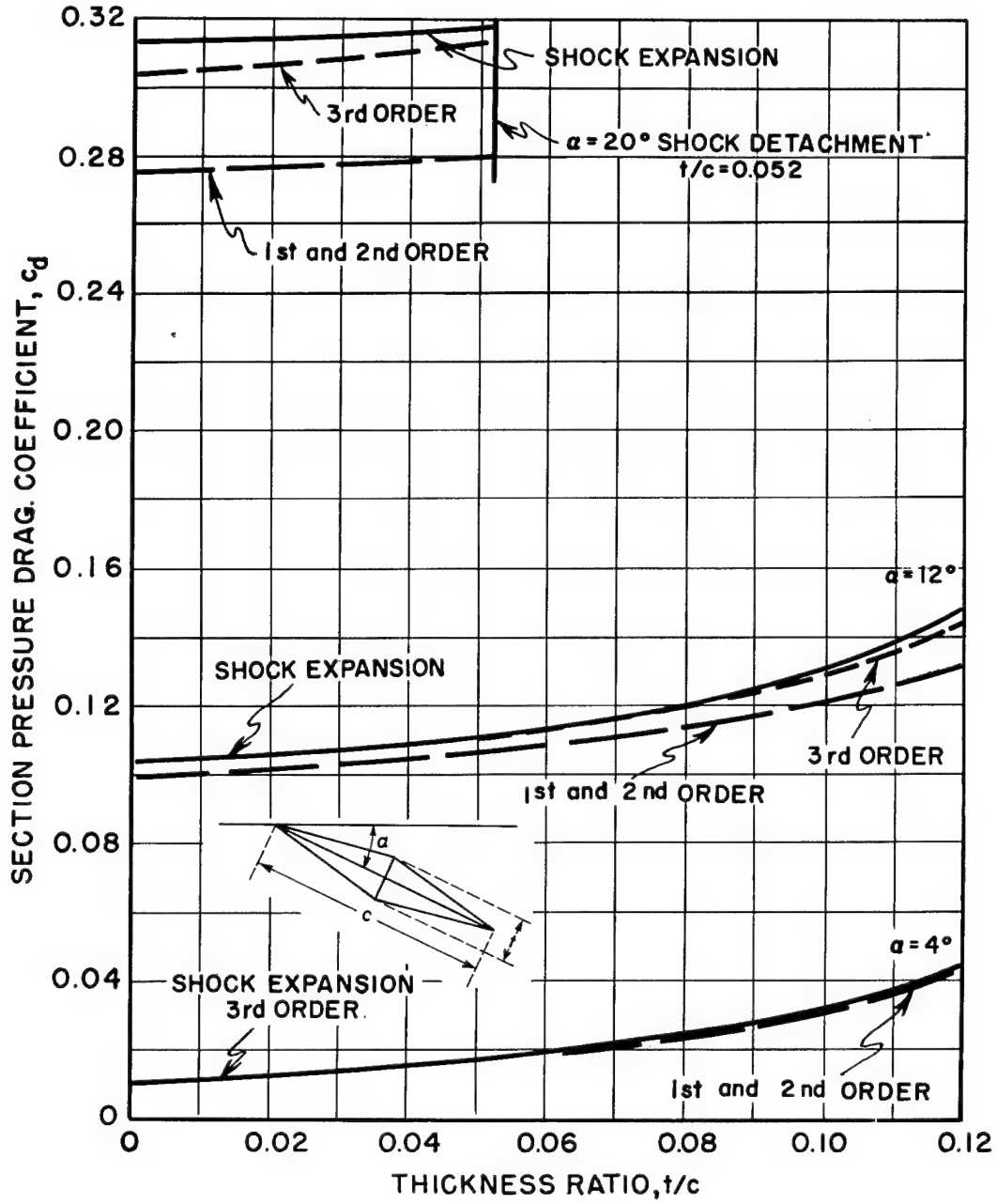

Figure 602.2-2(b) COMPARISON OF THEORETICAL APPROXIMATIONS; VARIATION OF SECTION PRESSURE DRAG COEFFICIENT WITH THICKNESS RATIO; DOUBLE WEDGE AIRFOIL; $M_\infty = 2$; $\alpha = 4°, 12°, 20°$

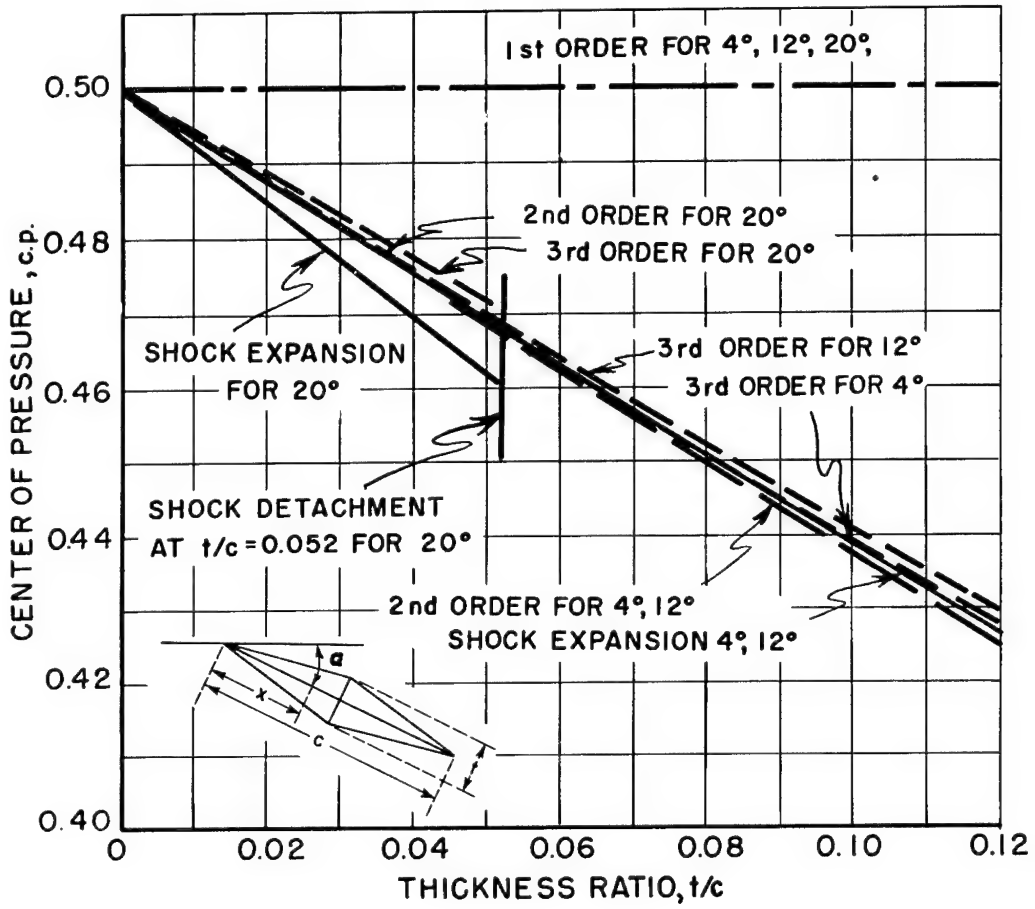

Figure 602.2-2(c) COMPARISON OF THEORETICAL APPROXIMATIONS; VARIATION OF CENTER OF PRESSURE WITH THICKNESS RATIO; DOUBLE WEDGE AIRFOIL; $M_\infty = 2$; $\alpha = 4°, 12°, 20°$

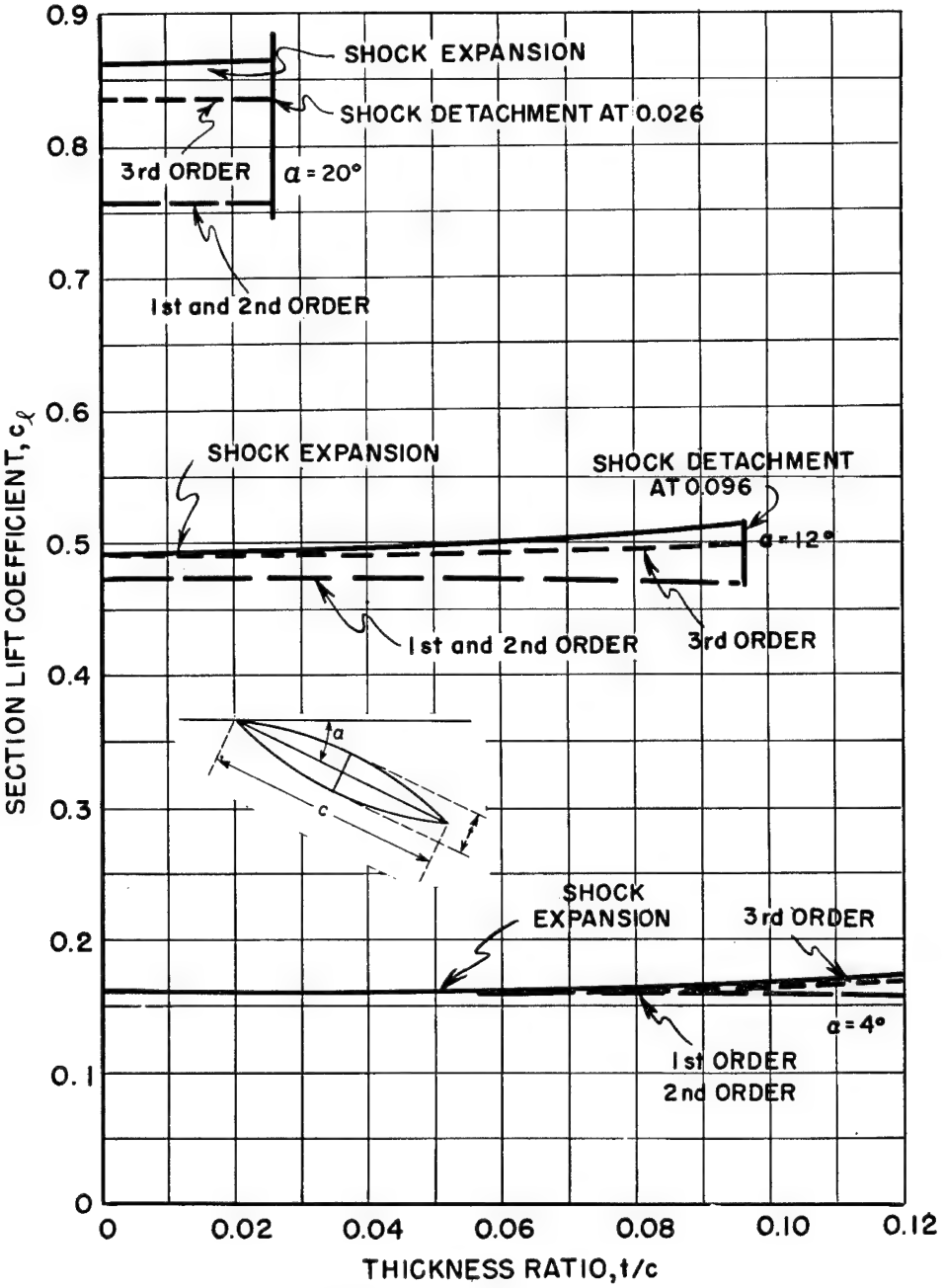

Figure 602.2-2(d) COMPARISON OF THEORETICAL APPROXIMATIONS; VARIATION OF SECTION LIFT COEFFICIENT WITH THICKNESS RATIO; BICONVEX AIRFOIL; $M_\infty = 2$; $\alpha = 4°, 12°, 20°$

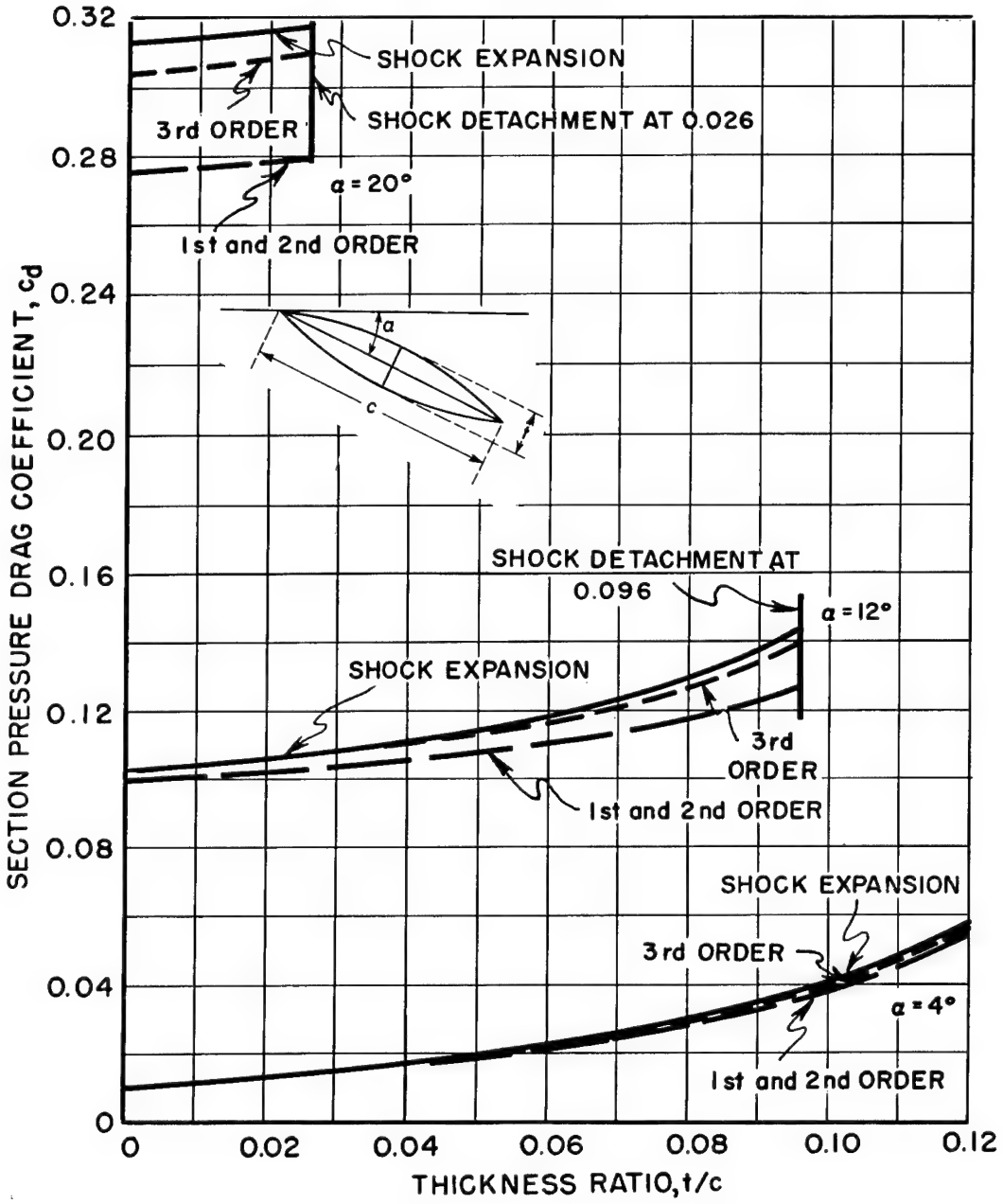

Figure 602.2-2(e) COMPARISON OF THEORETICAL APPROXIMATIONS; VARIATION OF SECTION PRESSURE DRAG COEFFICIENT WITH THICKNESS RATIO; BICONVEX AIRFOIL; $M_\infty = 2$; $\alpha = 4°, 12°, 20°$

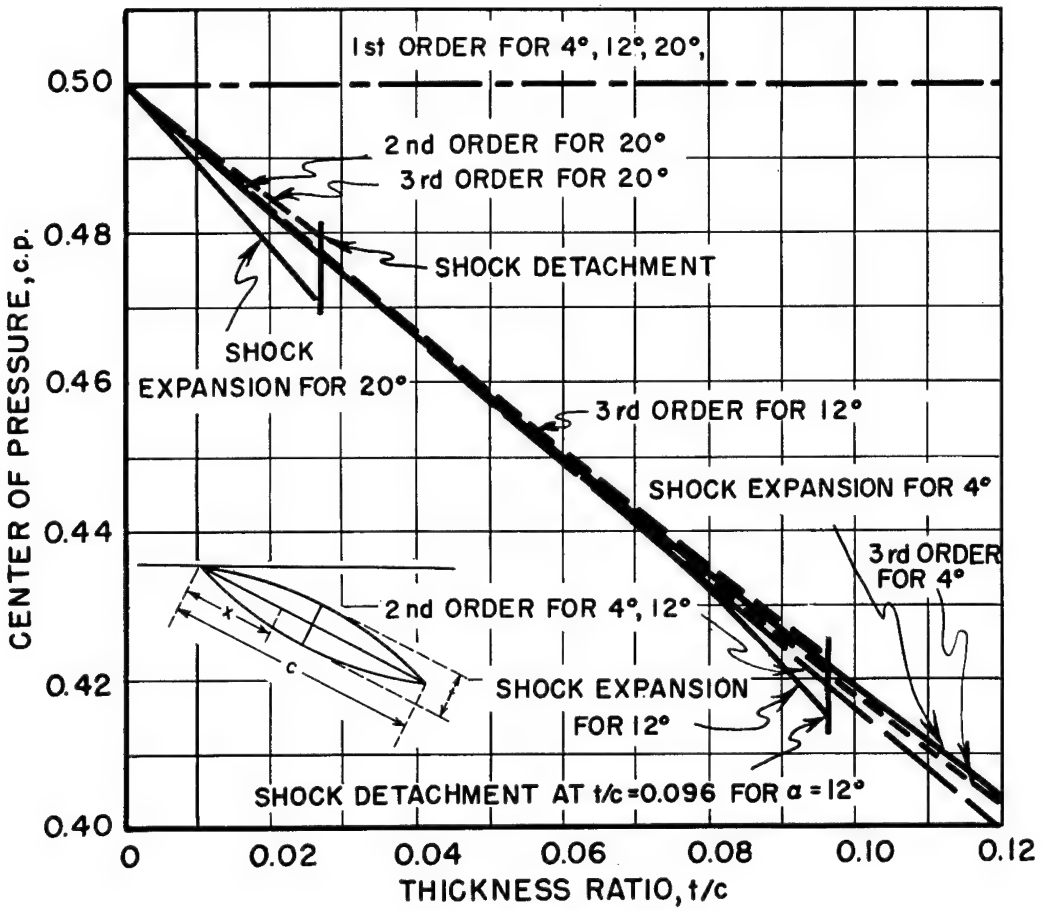

Figure 602.2-2(f) COMPARISON OF THEORETICAL APPROXIMATIONS; VARIATION OF CENTER OF PRESSURE WITH THICKNESS RATIO; BICONVEX AIRFOIL; $M_\infty = 2$; $\alpha = 4°, 12°, 20°$

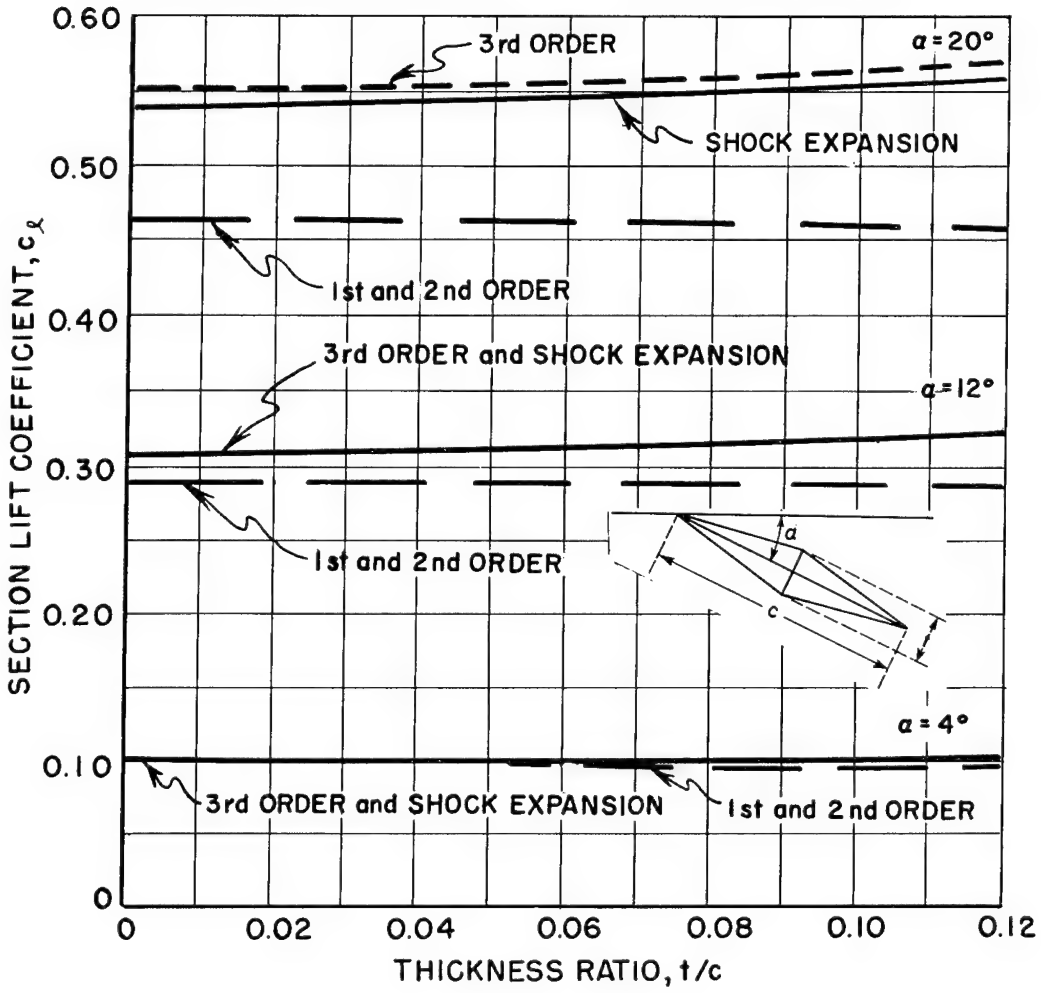

Figure 602.2-3(a) COMPARISON OF THEORETICAL APPROXIMATIONS; VARIATION OF SECTION LIFT COEFFICIENT WITH THICKNESS RATIO; DOUBLE WEDGE AIRFOIL; $M_\infty = 3$; $\alpha = 4°, 12°, 20°$

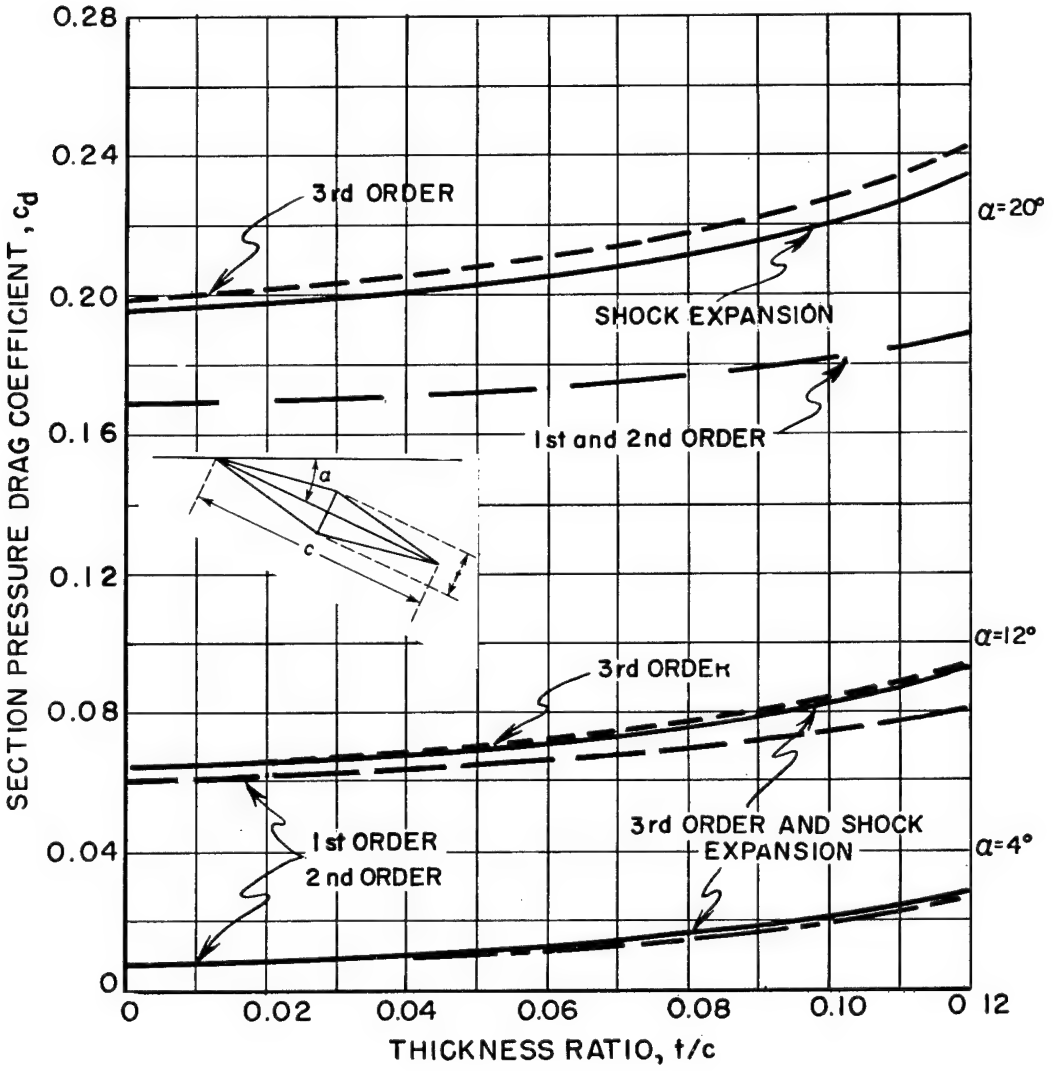

Figure 602.2-3(b) COMPARISON OF THEORETICAL APPROXIMATIONS; VARIATION OF SECTION PRESSURE DRAG COEFFICIENT WITH THICKNESS RATIO; DOUBLE WEDGE AIRFOIL; $M_\infty = 3$; $\alpha = 4°, 12°, 20°$

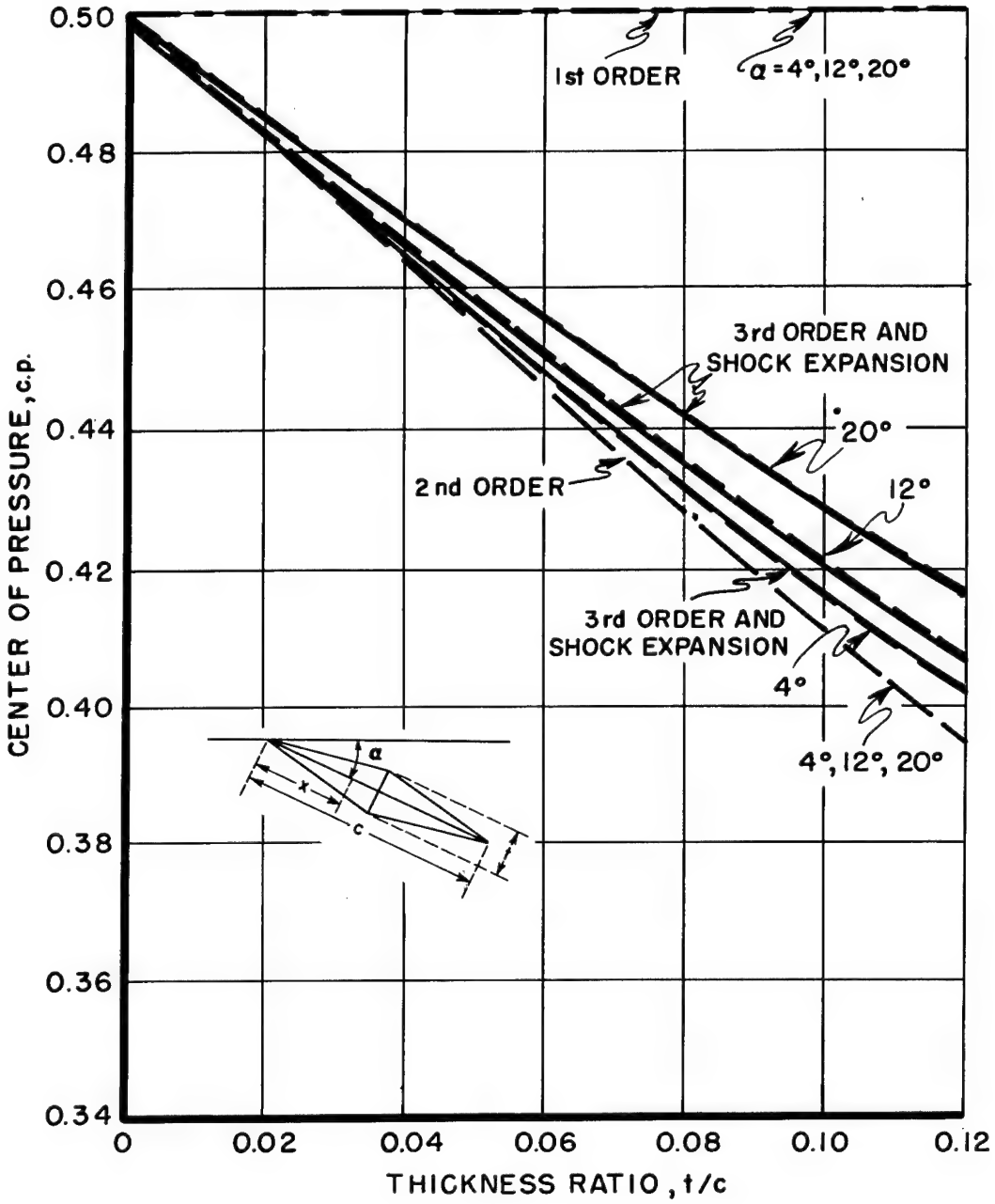

Figure 602.2-3(c) COMPARISON OF THEORETICAL APPROXIMATIONS; VARIATION OF CENTER OF PRESSURE WITH THICKNESS RATIO; DOUBLE WEDGE AIRFOIL; $M_\infty = 3$; $\alpha = 4°, 12°, 20°$

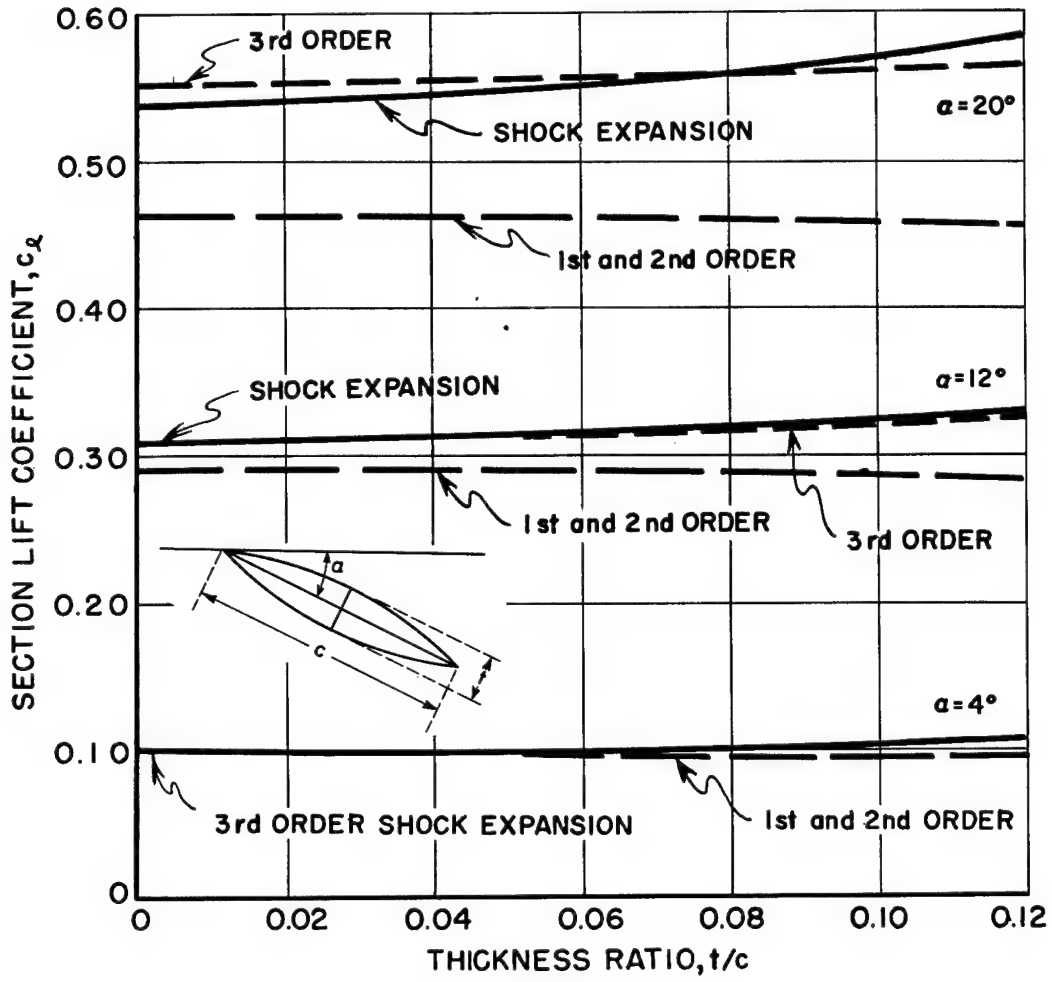

Figure 602.2-3(d) COMPARISON OF THEORETICAL APPROXIMATIONS; VARIATION OF SECTION LIFT COEFFICIENT WITH THICKNESS RATIO; BICONVEX AIRFOIL; $M_\infty = 3$; $\alpha = 4°, 12°, 20°$

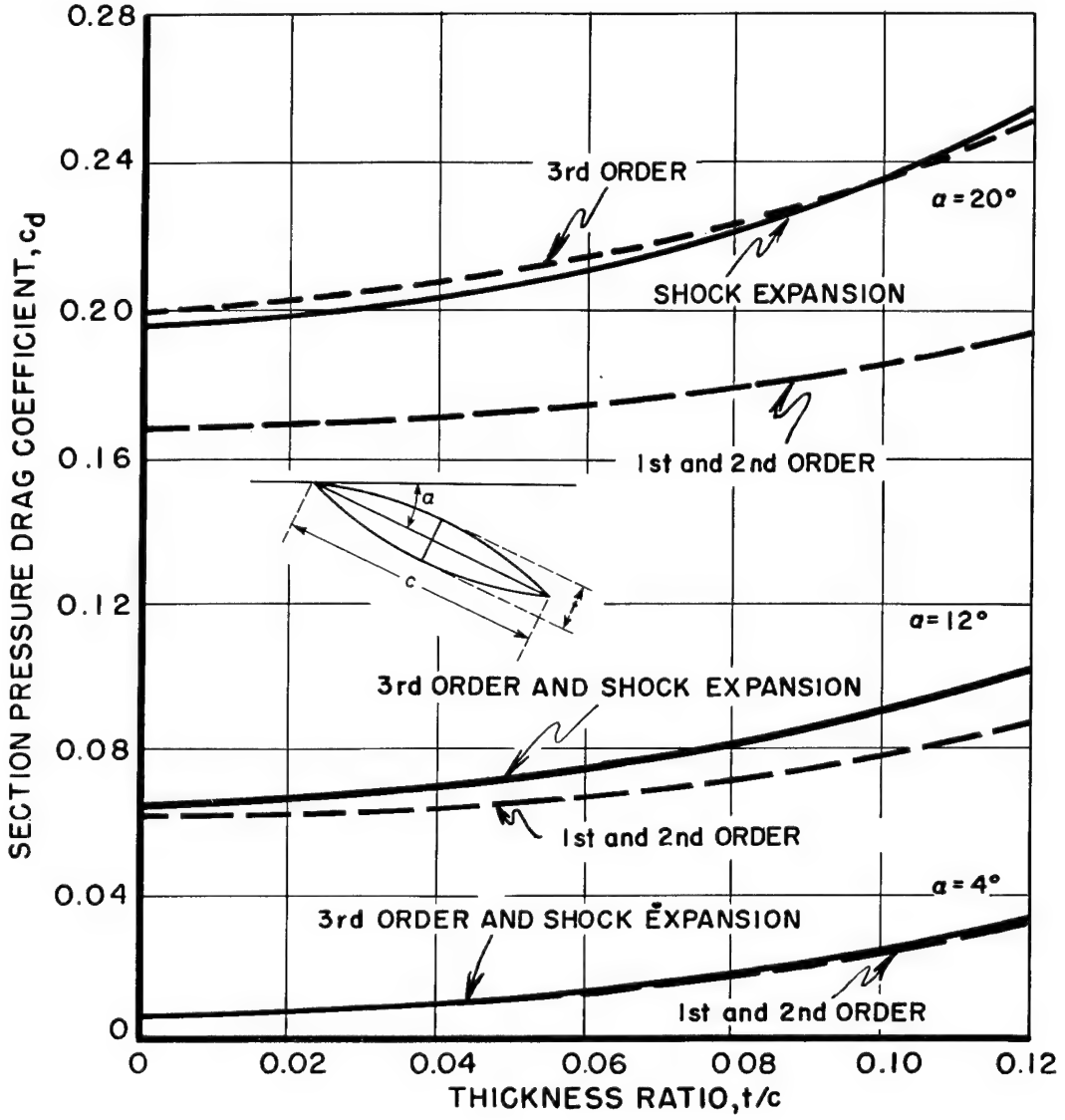

Figure 602.2-3(e) COMPARISON OF THEORETICAL APPROXIMATIONS; VARIATION OF SECTION PRESSURE DRAG COEFFICIENT WITH THICKNESS RATIO; BICONVEX AIRFOIL; $M_\infty = 3$; $\alpha = 4°, 12°, 20°$

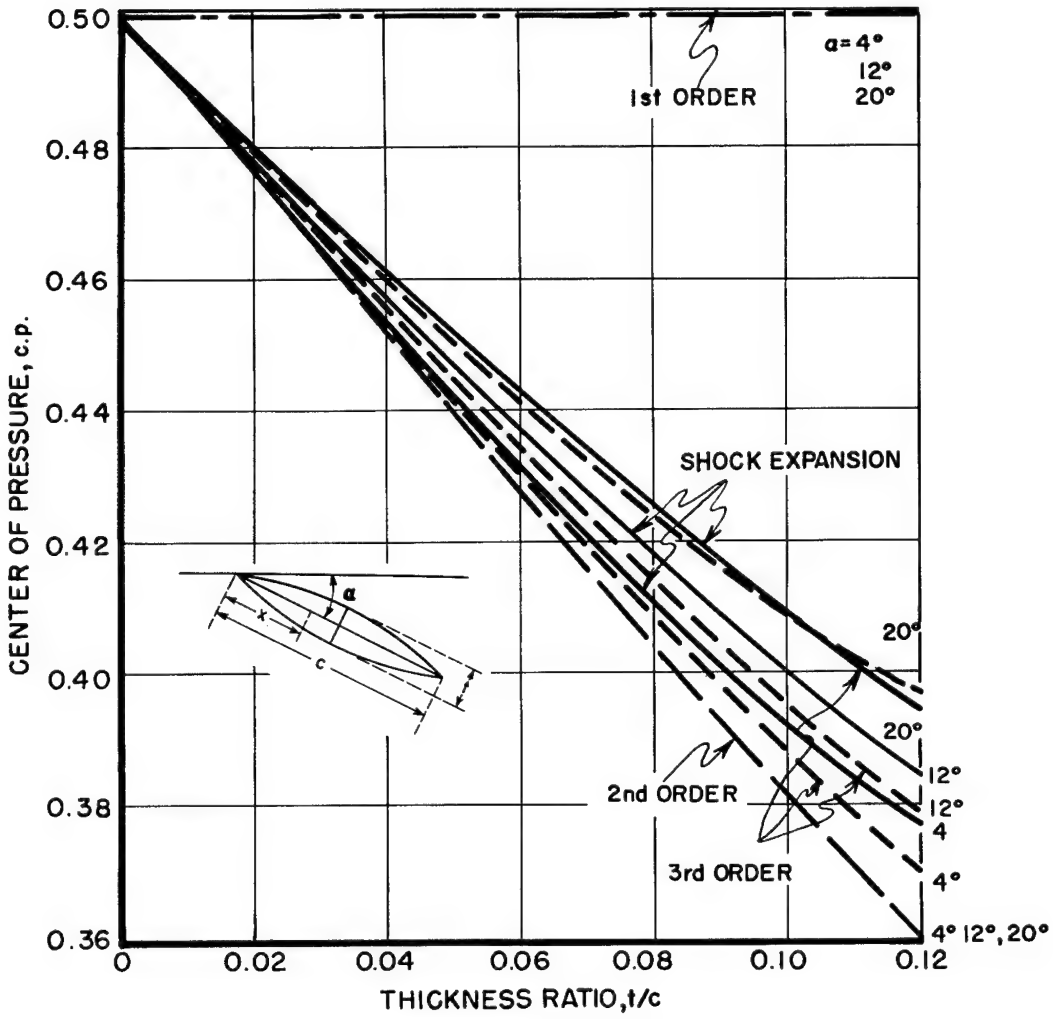

Figure 602.2-3(f) COMPARISON OF THEORETICAL APPROXIMATIONS; VARIATION OF CENTER OF PRESSURE WITH THICKNESS RATIO; BICONVEX AIRFOIL; $M_\infty = 3$; $\alpha = 4°, 12°, 20°$

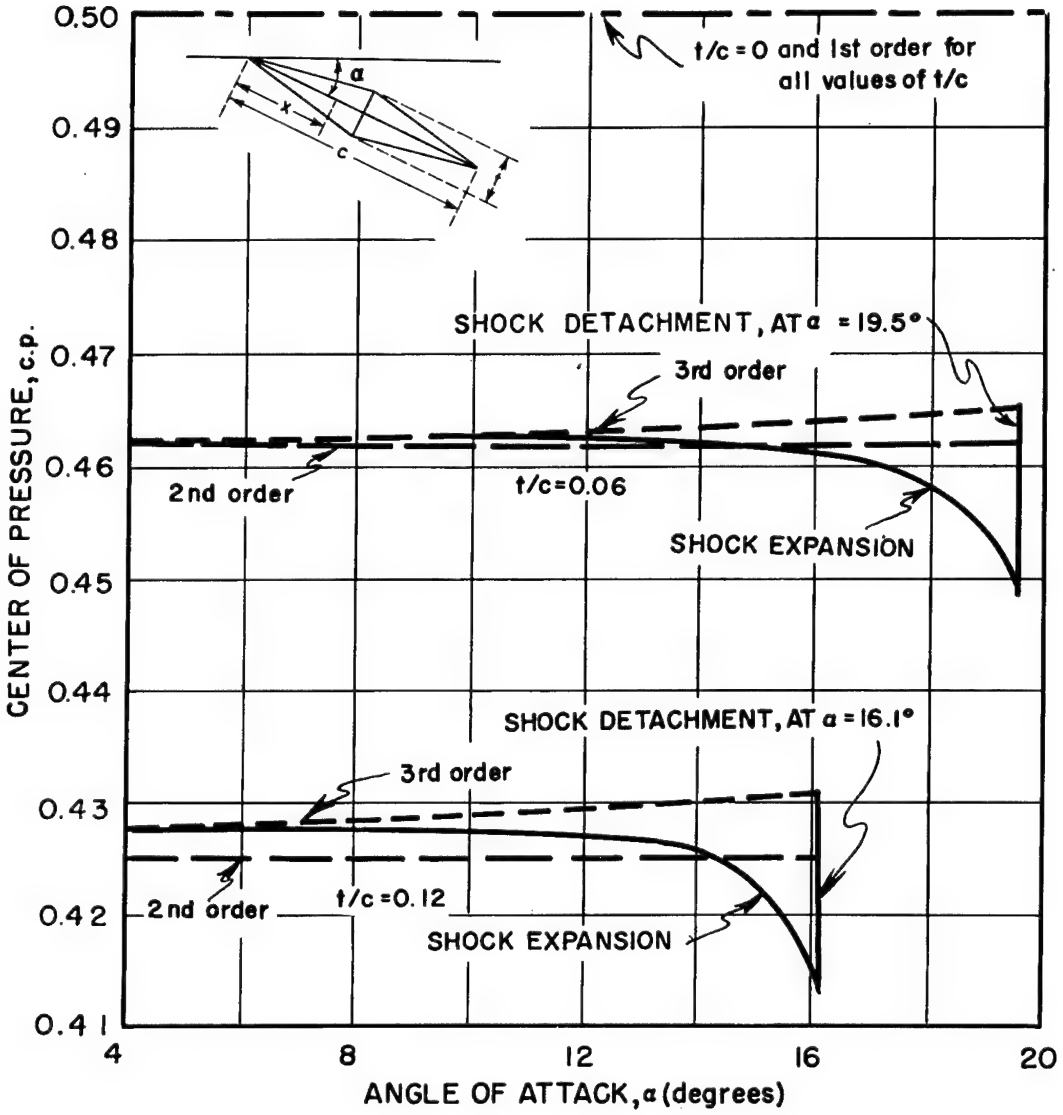

Figure 602.2-4 COMPARISON OF THEORETICAL APPROXIMATIONS; VARIATION OF CENTER OF PRESSURE WITH ANGLE OF ATTACK; DOUBLE WEDGE AIRFOIL; $M_\infty = 2$; $t/c = 0, 0.06, 0.12$

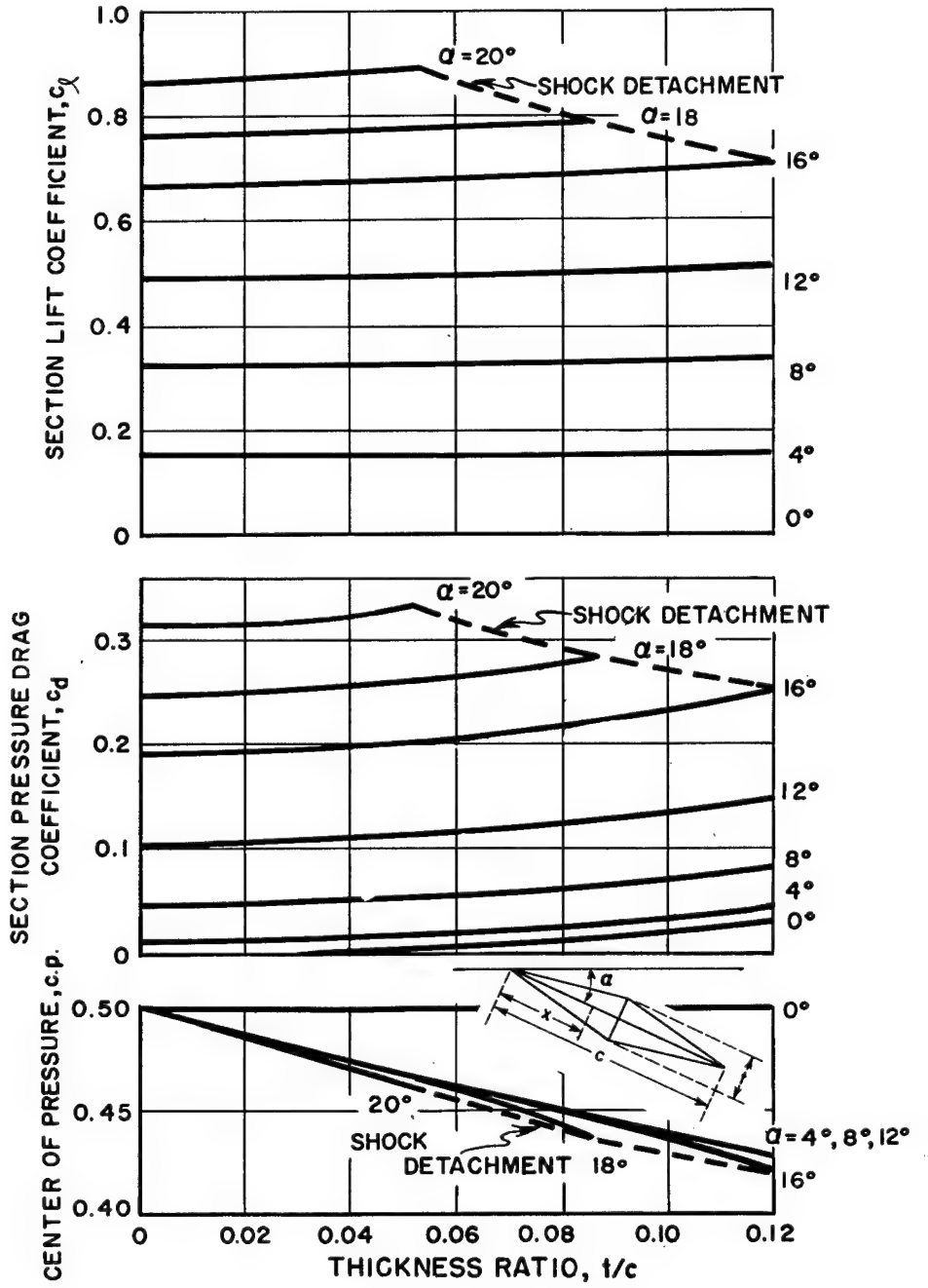

Figure 603.1-1(a) VARIATION OF DOUBLE WEDGE AIRFOIL CHARACTERISTICS WITH THICKNESS RATIO USING SHOCK EXPANSION METHOD; $M_\infty = 2$; $\alpha = 0°, 4°, 8°, 12°, 16°, 18°, 20°$

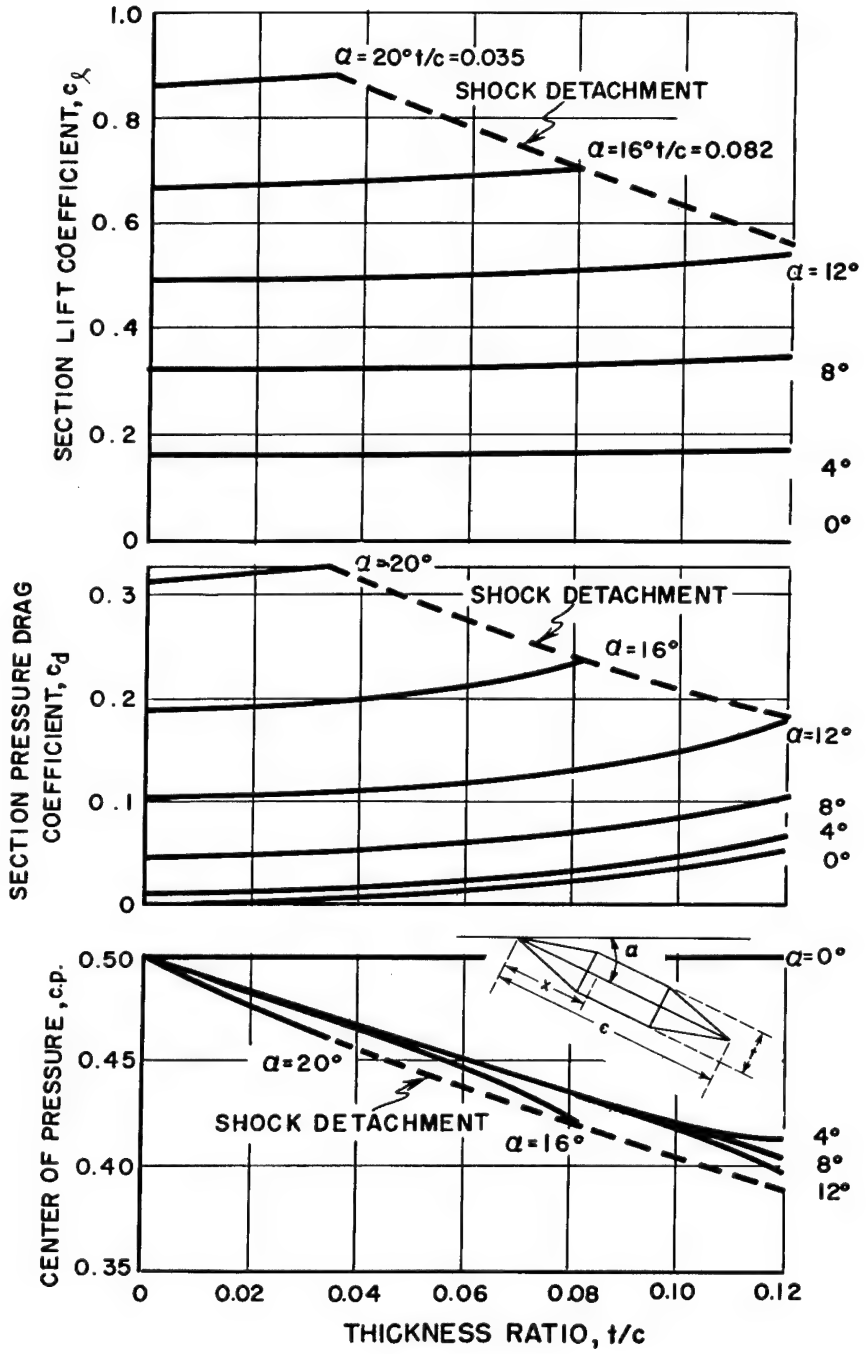

Figure 603.1-1(b) VARIATION OF FLATTENED DOUBLE WEDGE AIRFOIL CHARACTERISTICS WITH THICKNESS RATIO USING SHOCK EXPANSION METHOD; $M_\infty = 2$; $\alpha = 0°, 4°, 8°, 12°, 16°, 20°$

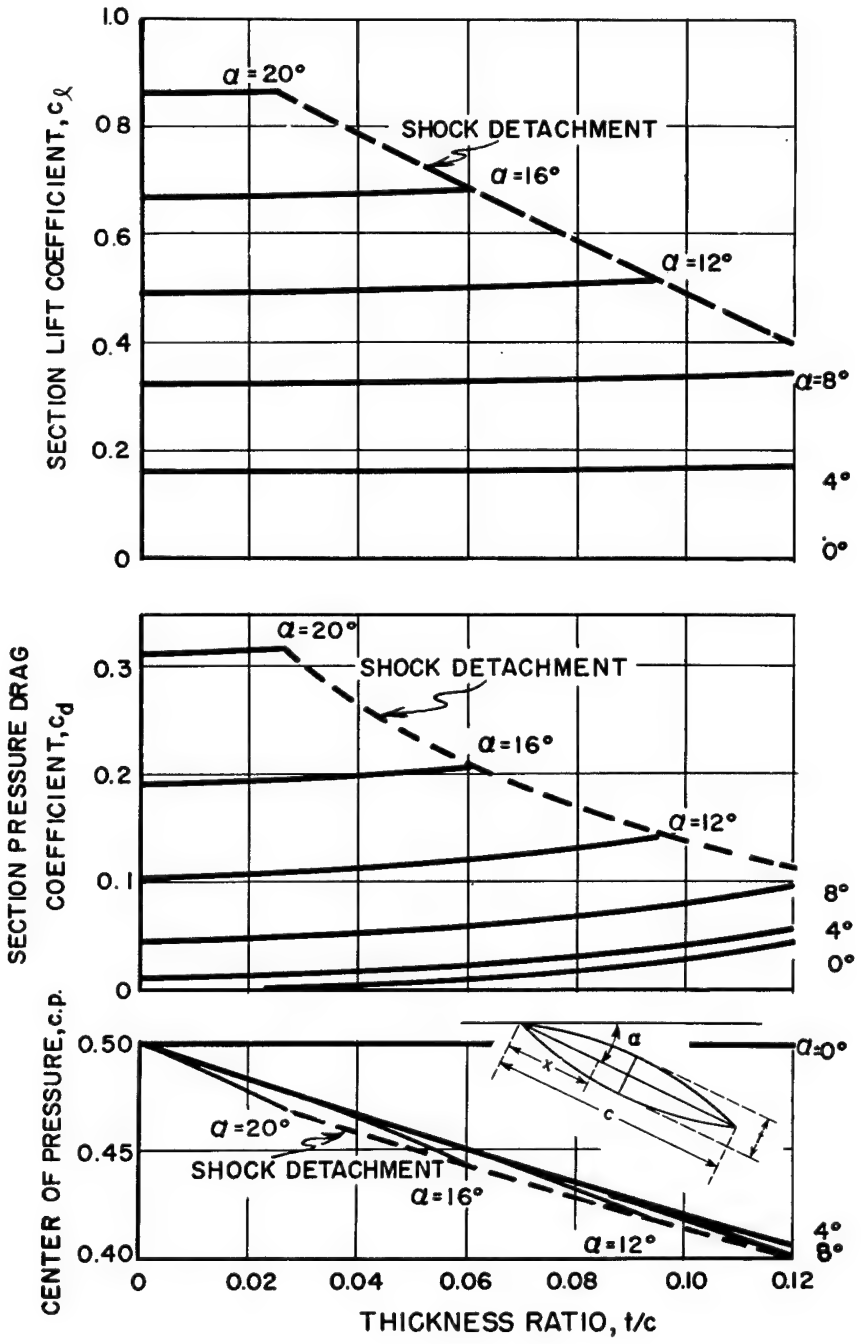

Figure 603.1-1(c) VARIATION OF BICONVEX AIRFOIL CHARACTERISTICS WITH THICKNESS RATIO USING SHOCK EXPANSION METHOD; $M_\infty = 2$; $\alpha = 0°, 4°, 8°, 12°, 16°, 20°$

447269 O - 58 - 6

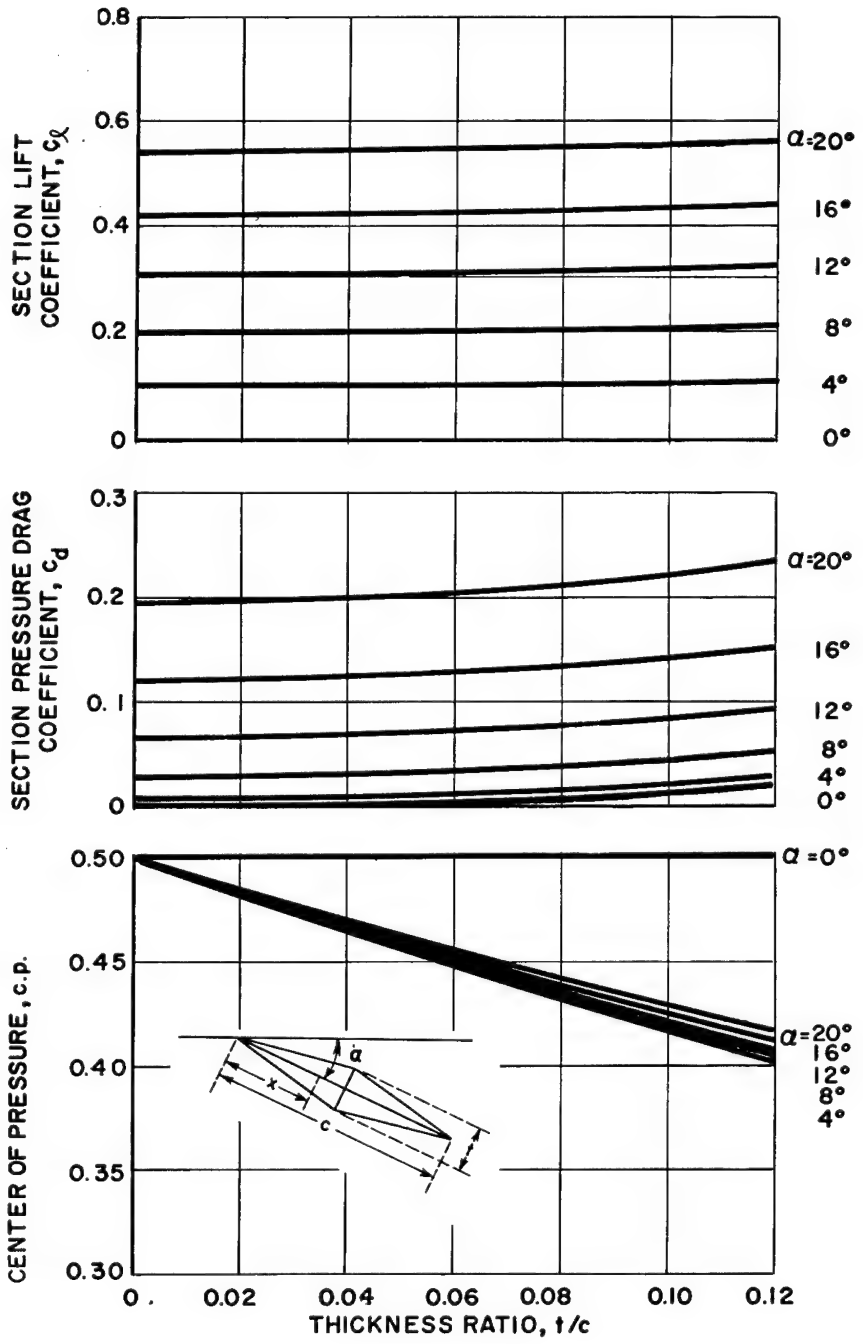

Figure 603.1-2(a) VARIATION OF DOUBLE WEDGE AIRFOIL CHARACTERISTICS WITH THICKNESS RATIO USING SHOCK EXPANSION METHOD; $M_\infty = 3$; $\alpha = 0°, 4°, 8°, 12°, 16°, 20°$

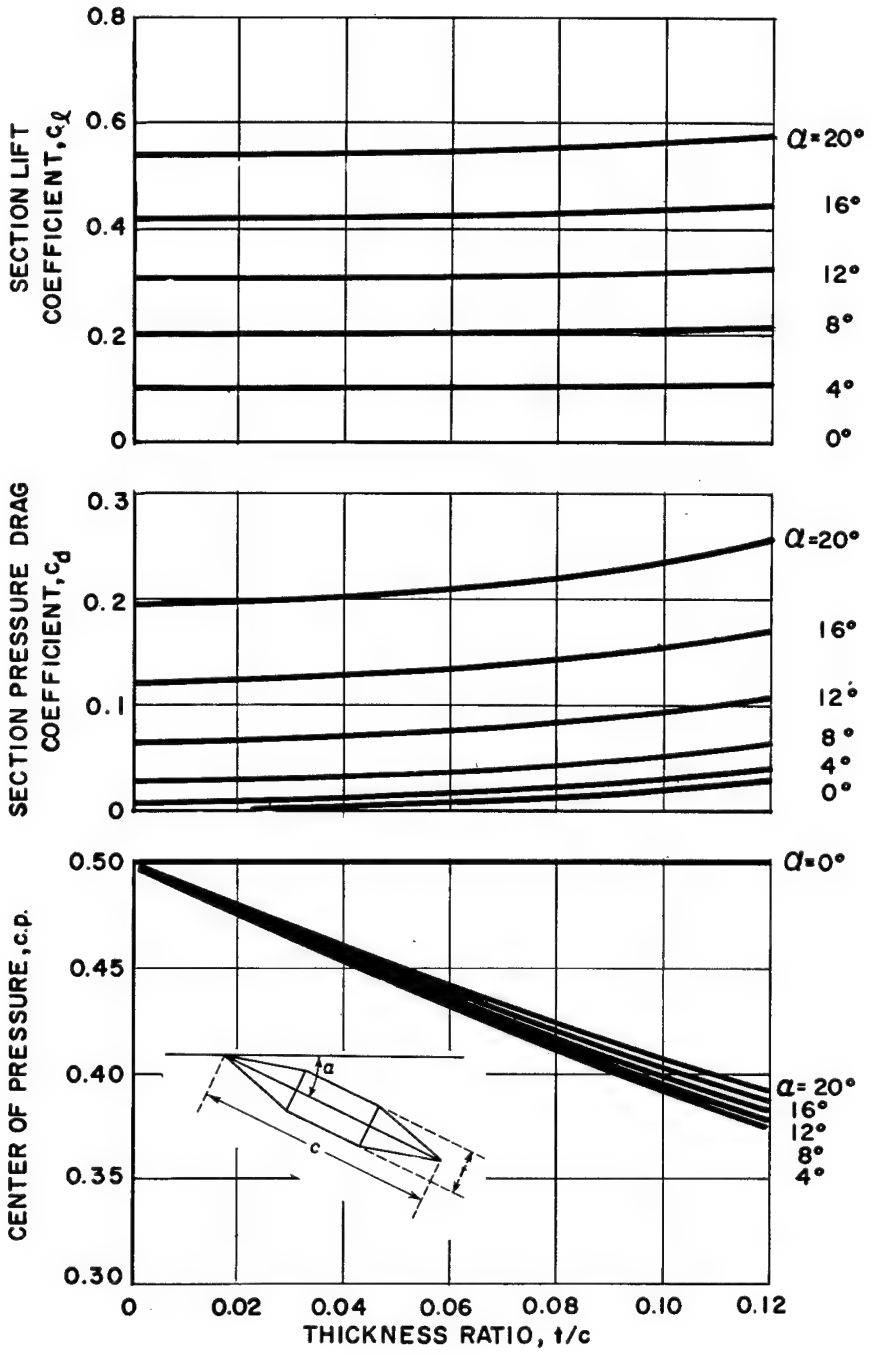

Figure 603.1-2(b) VARIATION OF FLATTENED DOUBLE WEDGE AIRFOIL CHARACTERISTICS WITH THICKNESS RATIO USING SHOCK EXPANSION METHOD; $M_\infty = 3$; $\alpha = 0°, 4°, 8°, 12°, 16°, 20°$

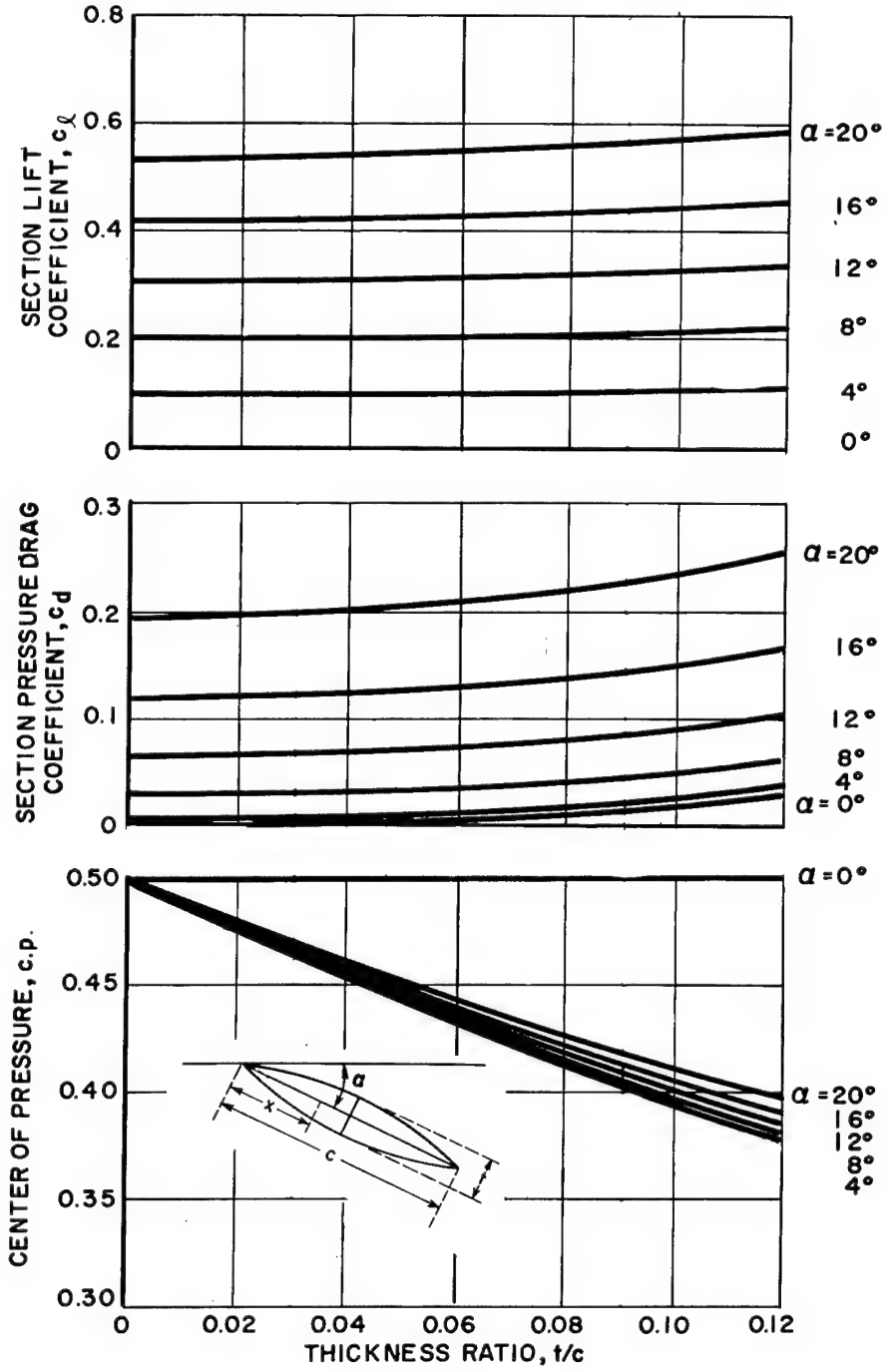

Figure 603.1-2(c) VARIATION OF BICONVEX AIRFOIL CHARACTERISTICS WITH THICKNESS RATIO USING SHOCK EXPANSION METHOD; $M_\infty = 3$; $\alpha = 0°, 4°, 8°, 12°, 16°, 20°$

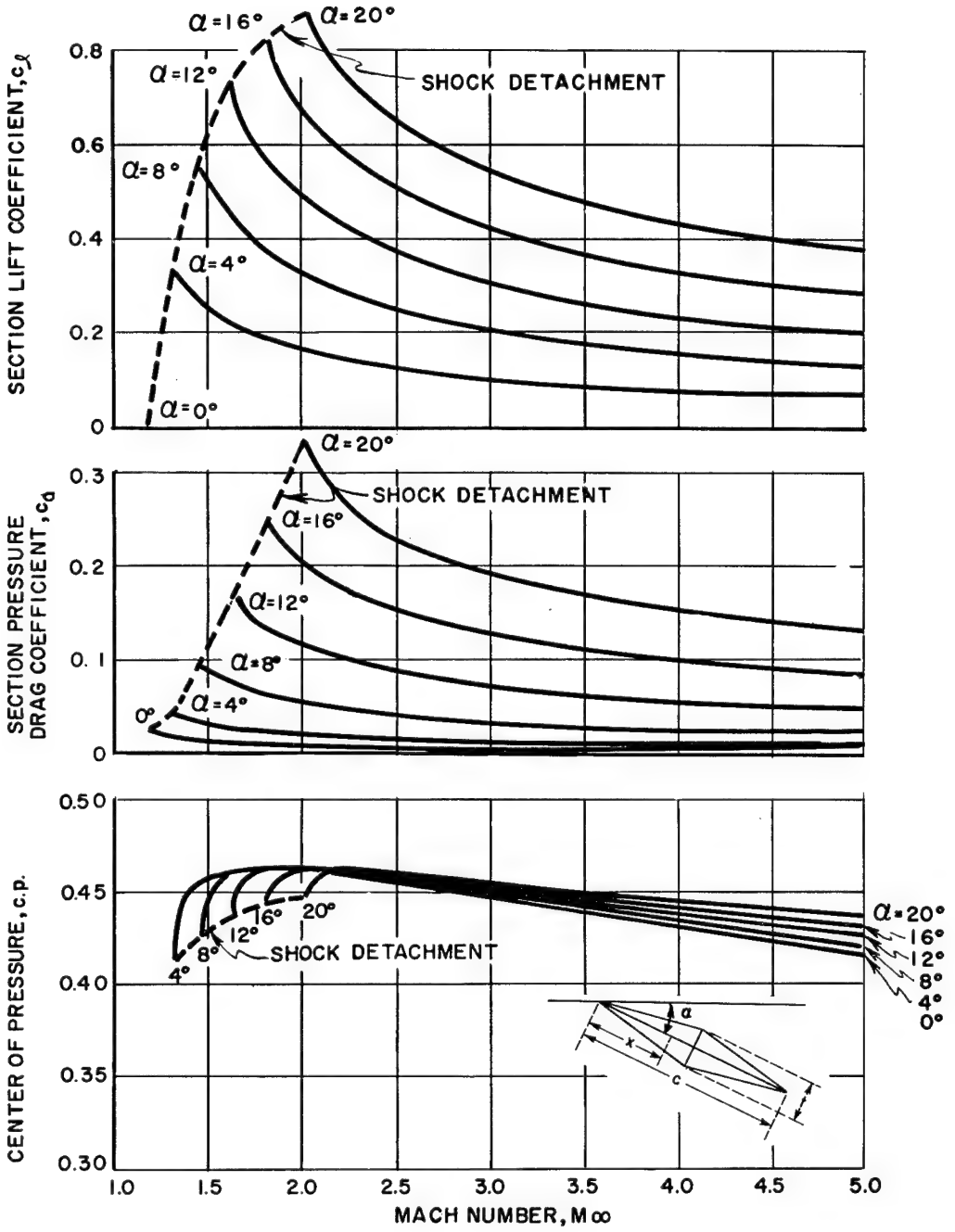

Figure 603.2-1(a) VARIATION OF DOUBLE WEDGE AIRFOIL CHARACTERISTICS WITH MACH NUMBER USING SHOCK EXPANSION METHOD; t/c = 0.06; α = 0°, 4°, 8°, 12°, 16°, 20°

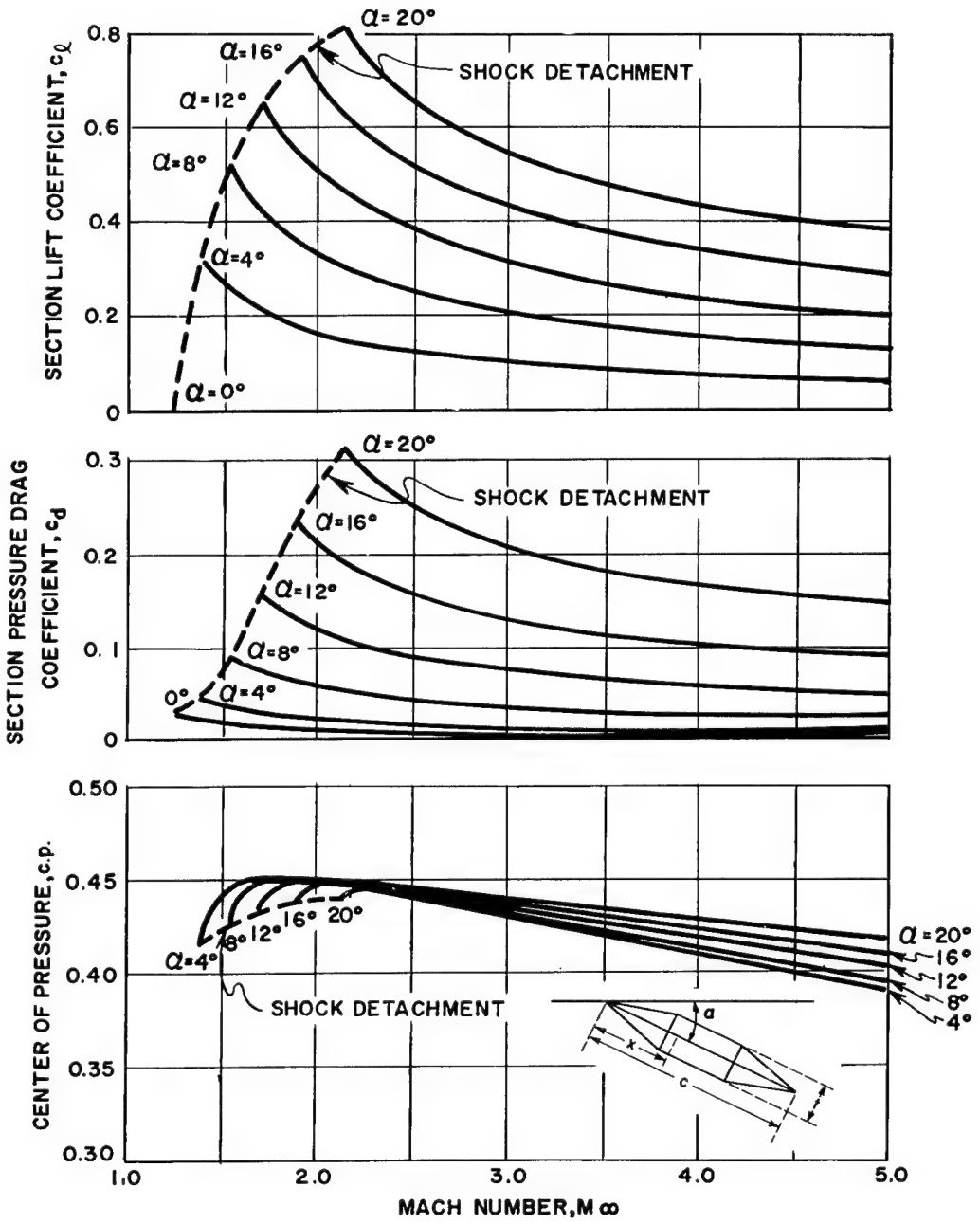

Figure 603.2-1(b) VARIATION OF FLATTENED DOUBLE WEDGE AIRFOIL CHARACTERISTICS WITH MACH NUMBER USING SHOCK EXPANSION METHOD; t/c = 0.06; α = 0°, 4°, 8°, 12°, 16°, 20°

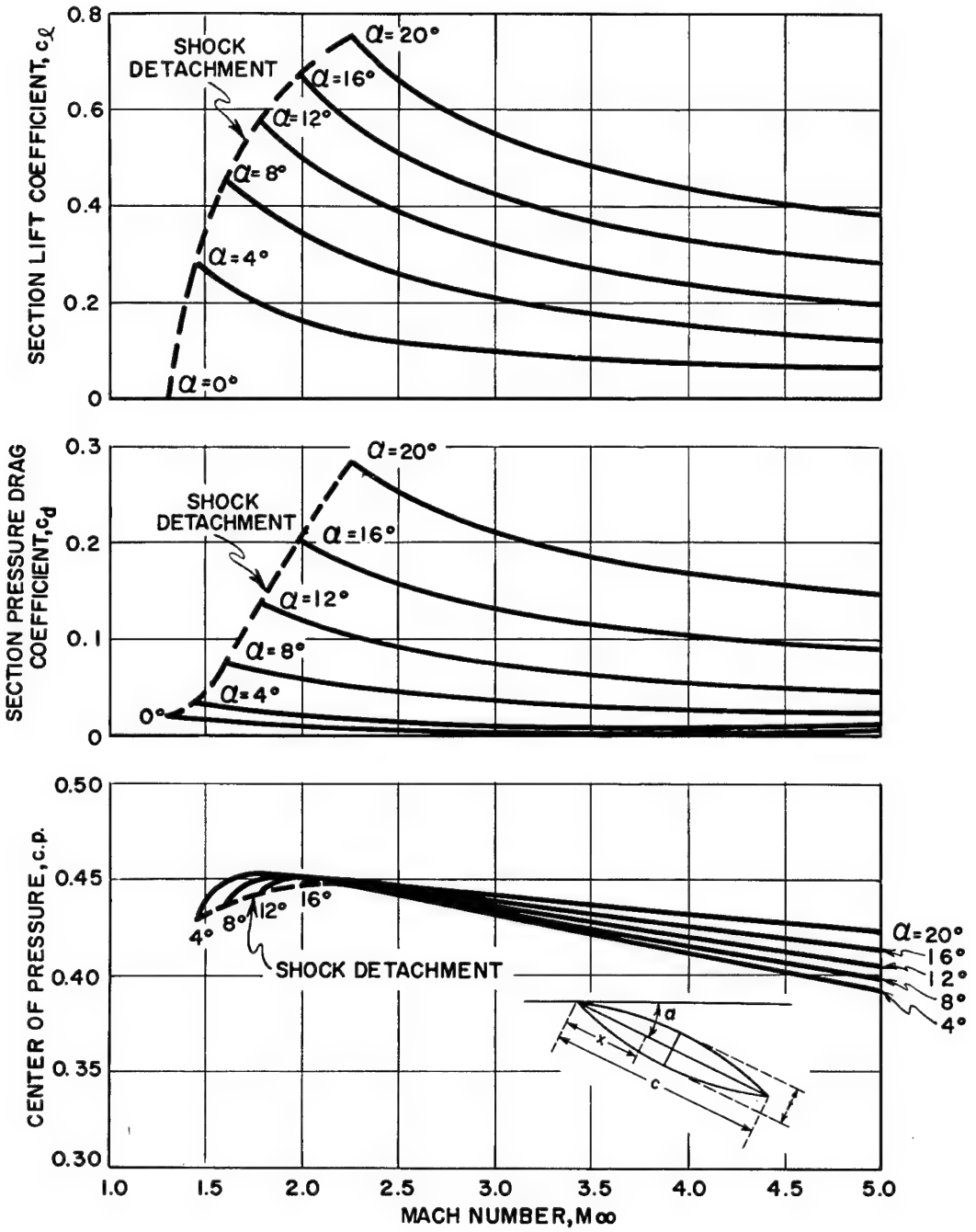

Figure 603.2-1(c) VARIATION OF BICONVEX AIRFOIL CHARACTERISTICS WITH MACH NUMBER USING SHOCK EXPANSION METHOD; t/c = 0.06; α = 0°, 4°, 8°, 12°, 16°, 20°

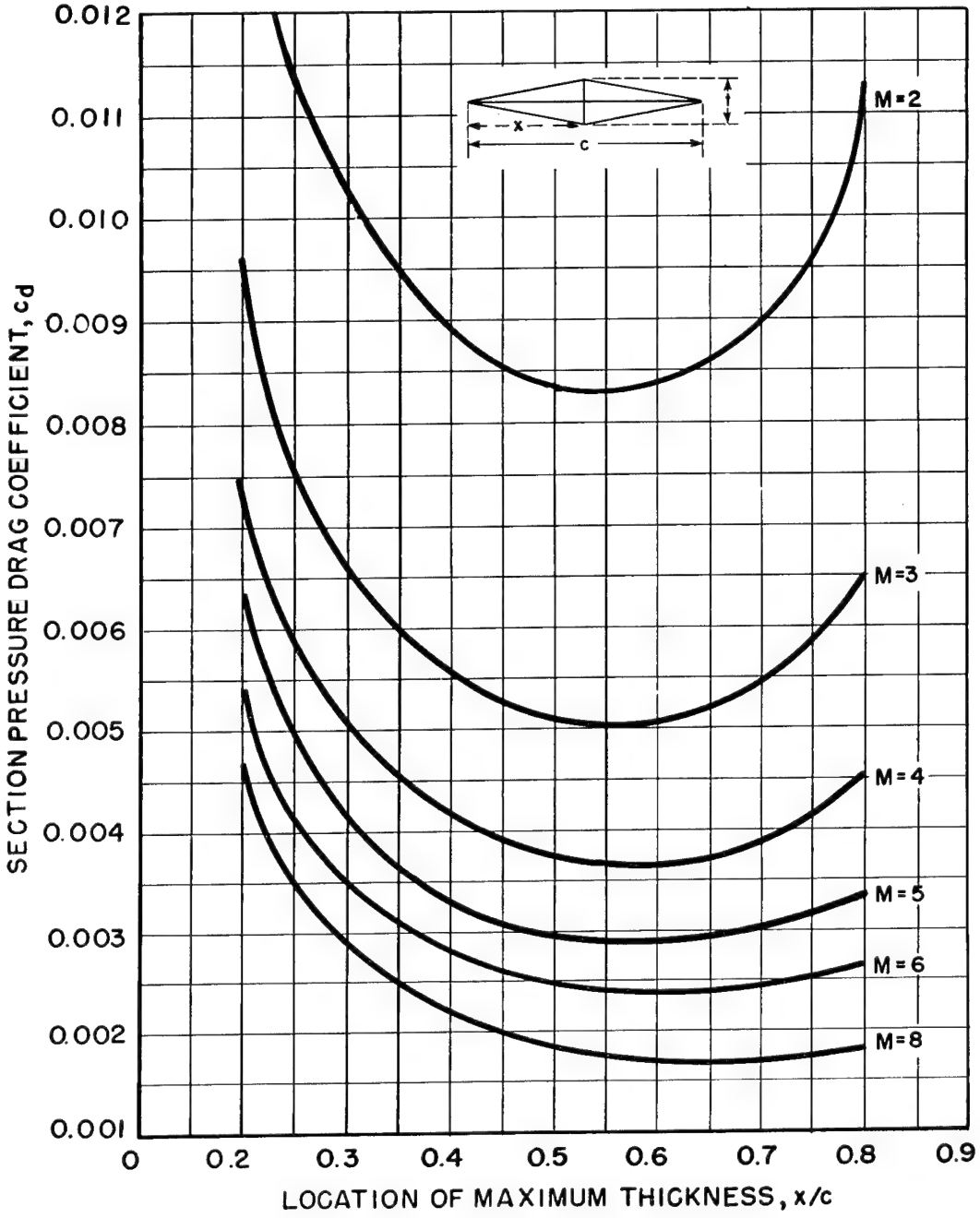

Figure 604.1-1 VARIATION OF SECTION PRESSURE DRAG COEFFICIENT WITH POSITION OF MAXIMUM THICKNESS; DOUBLE WEDGE AIRFOIL; SHOCK EXPANSION METHOD; M_∞ = 2, 3, 4, 5, 6, 8; t/c = 0.06; α = 0°

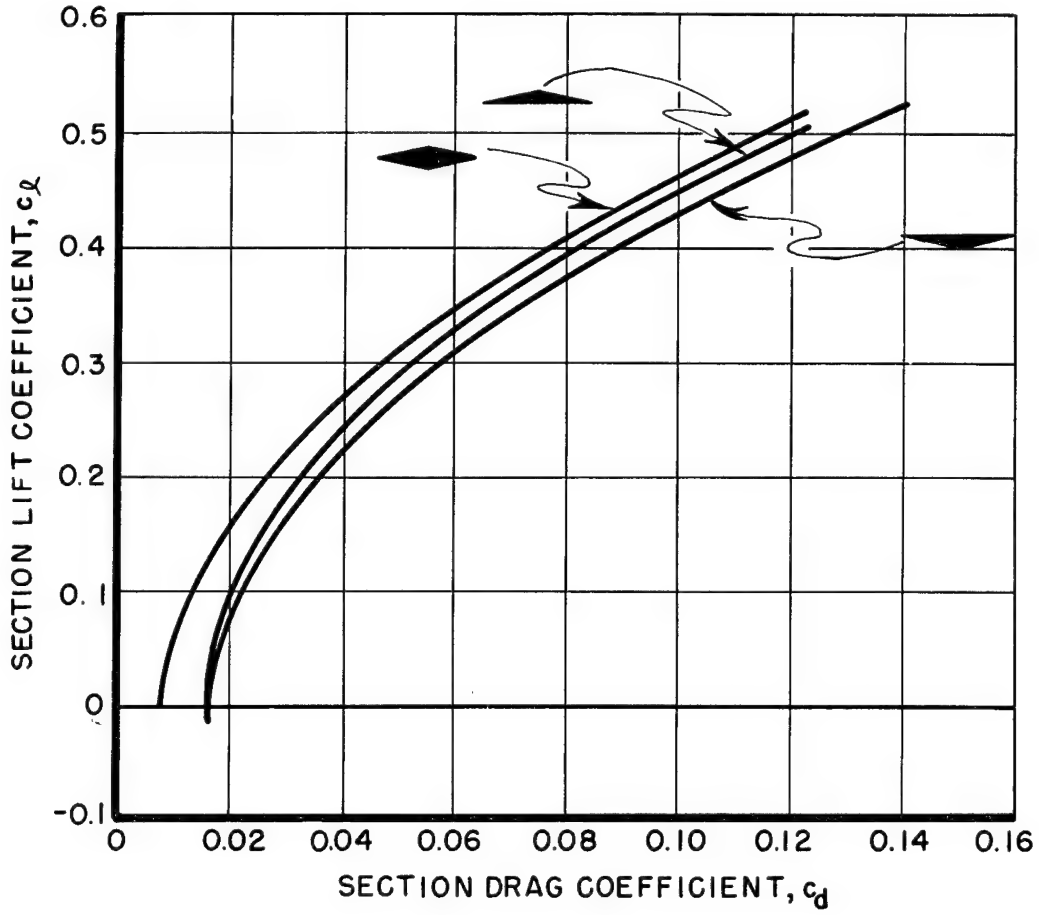

Figure 604.2-1 EFFECT OF CAMBER ON CHARACTERISTICS OF WEDGE AIRFOILS; DRAG POLAR DIAGRAM; SHOCK EXPANSION METHOD; $M_\infty = 2$; $(t/c)_{max} = 0.06$

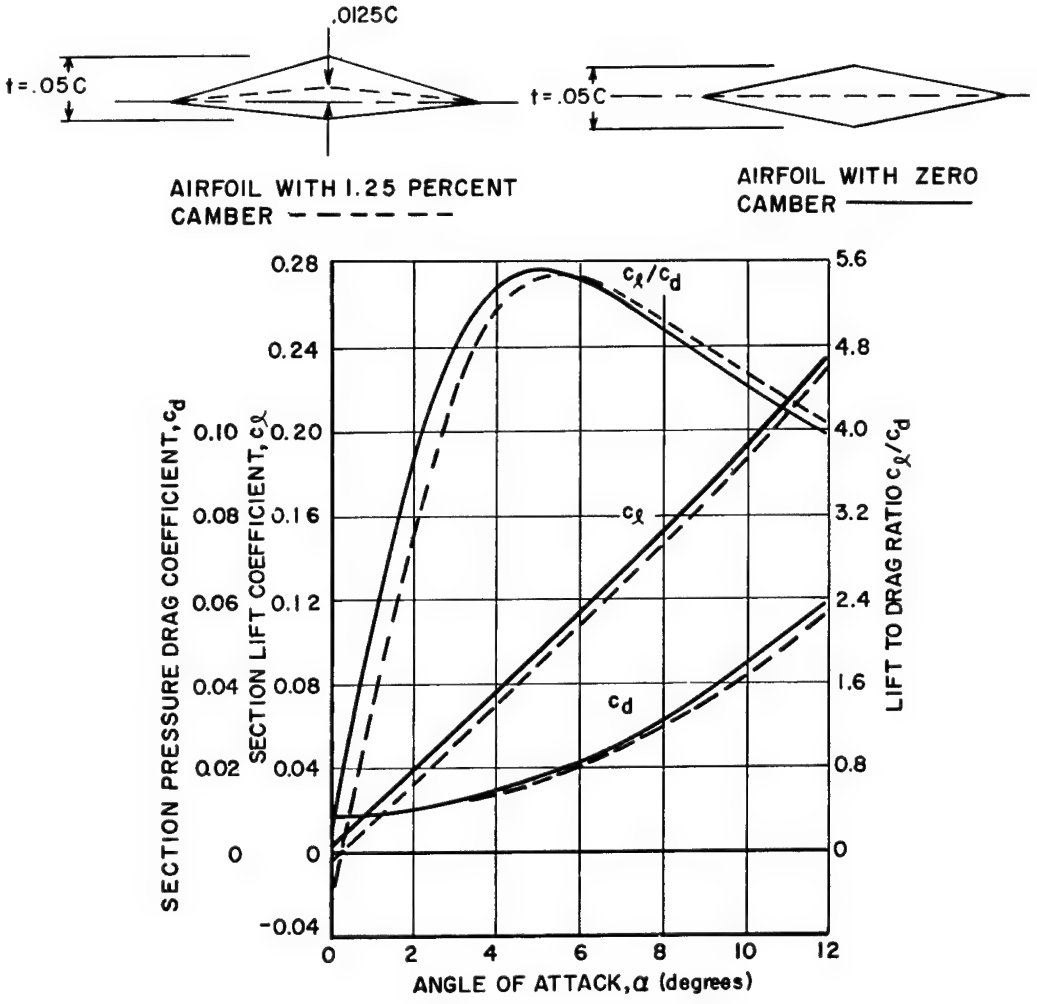

Figure 604.2-2 EFFECT OF CAMBER ON CHARACTERISTICS OF AIRFOIL; $M_\infty = 4$; $t/c = 0.05$; REF. 8, FIG. 8

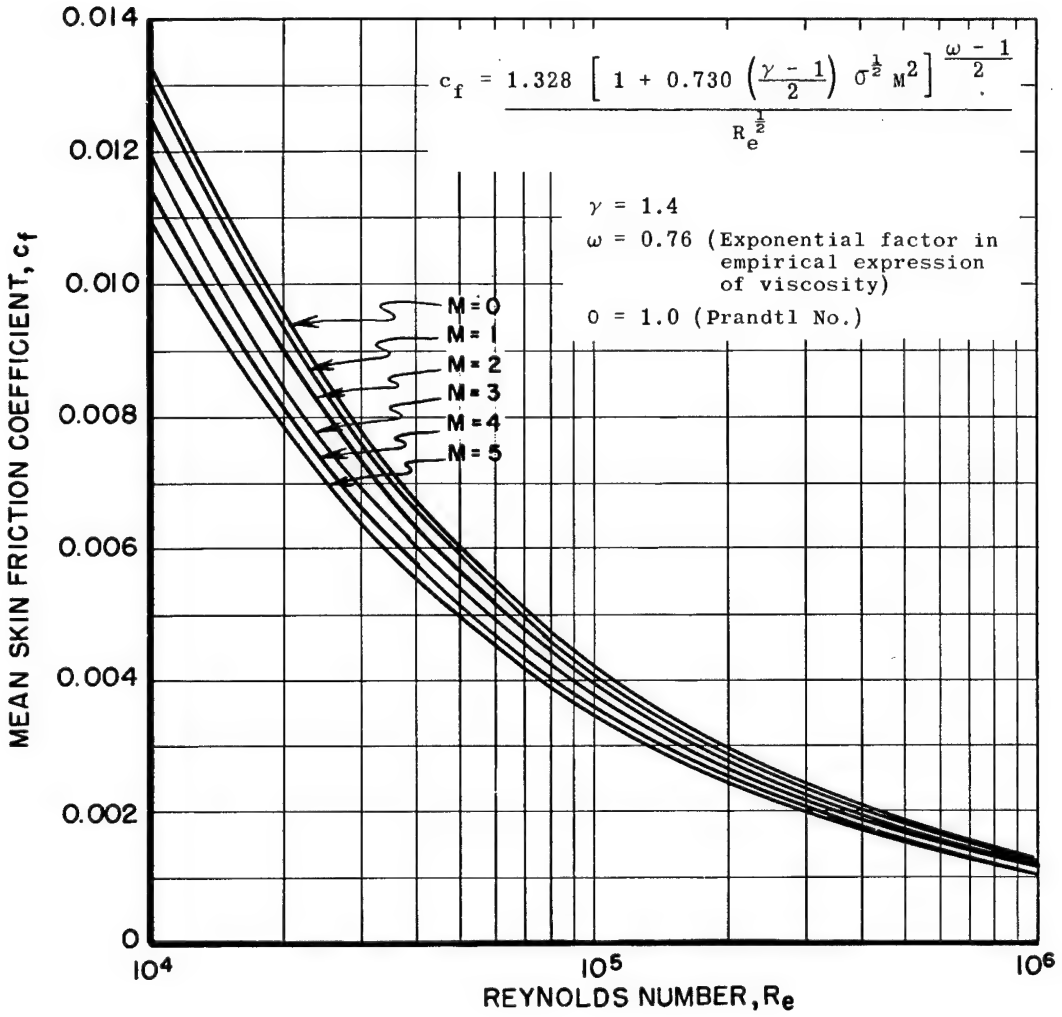

Figure 605.1-1 VARIATION OF MEAN SKIN FRICTION COEFFICIENT WITH REYNOLDS NUMBER; INSULATED FLAT PLATE - ONE SIDE ONLY; LAMINAR BOUNDARY LAYER; REF. 10

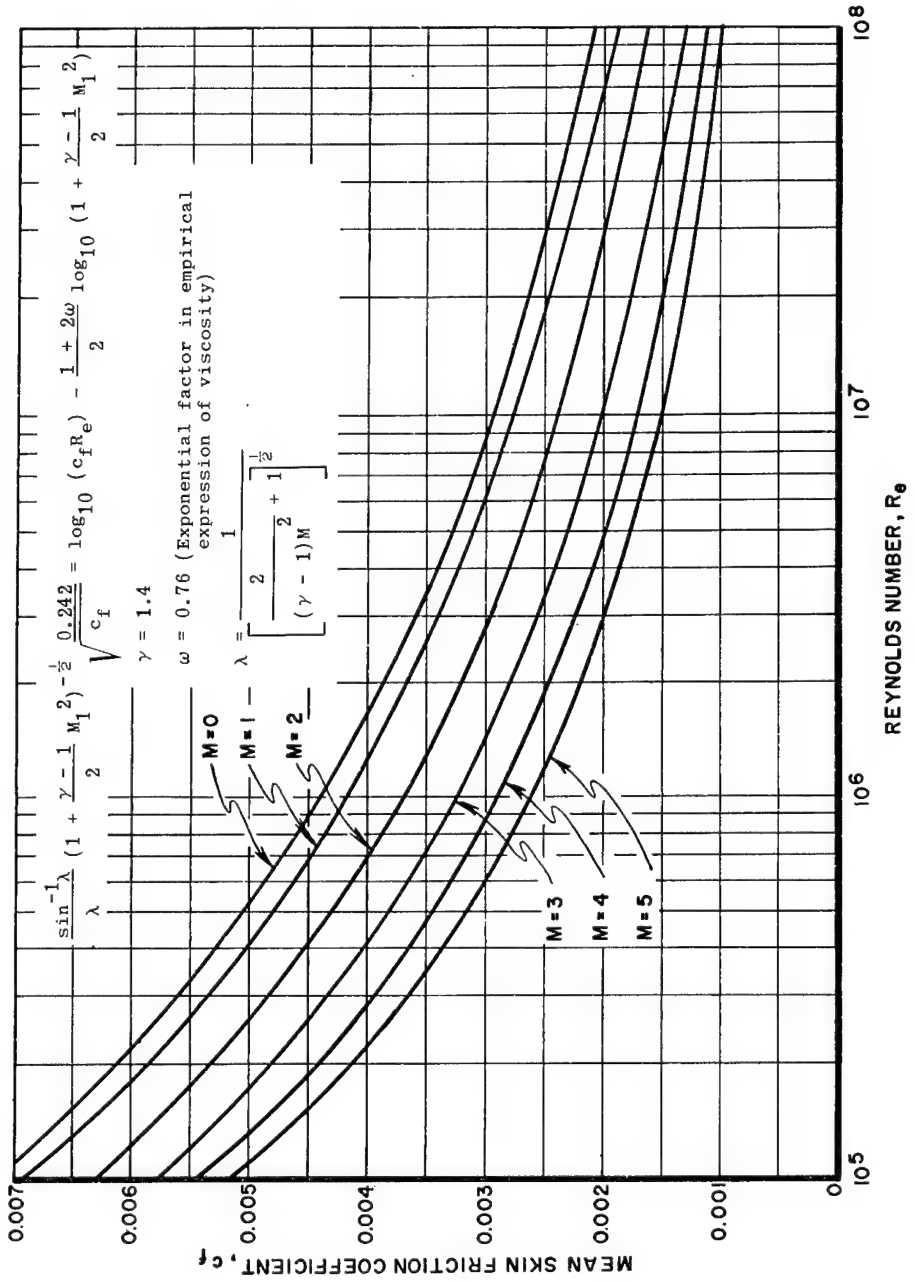

Figure 605.1-2 VARIATION OF MEAN SKIN FRICTION COEFFICIENT WITH REYNOLDS NUMBER; INSULATED FLAT PLATE - ONE SIDE ONLY; TURBULENT BOUNDARY LAYER; REF. 11

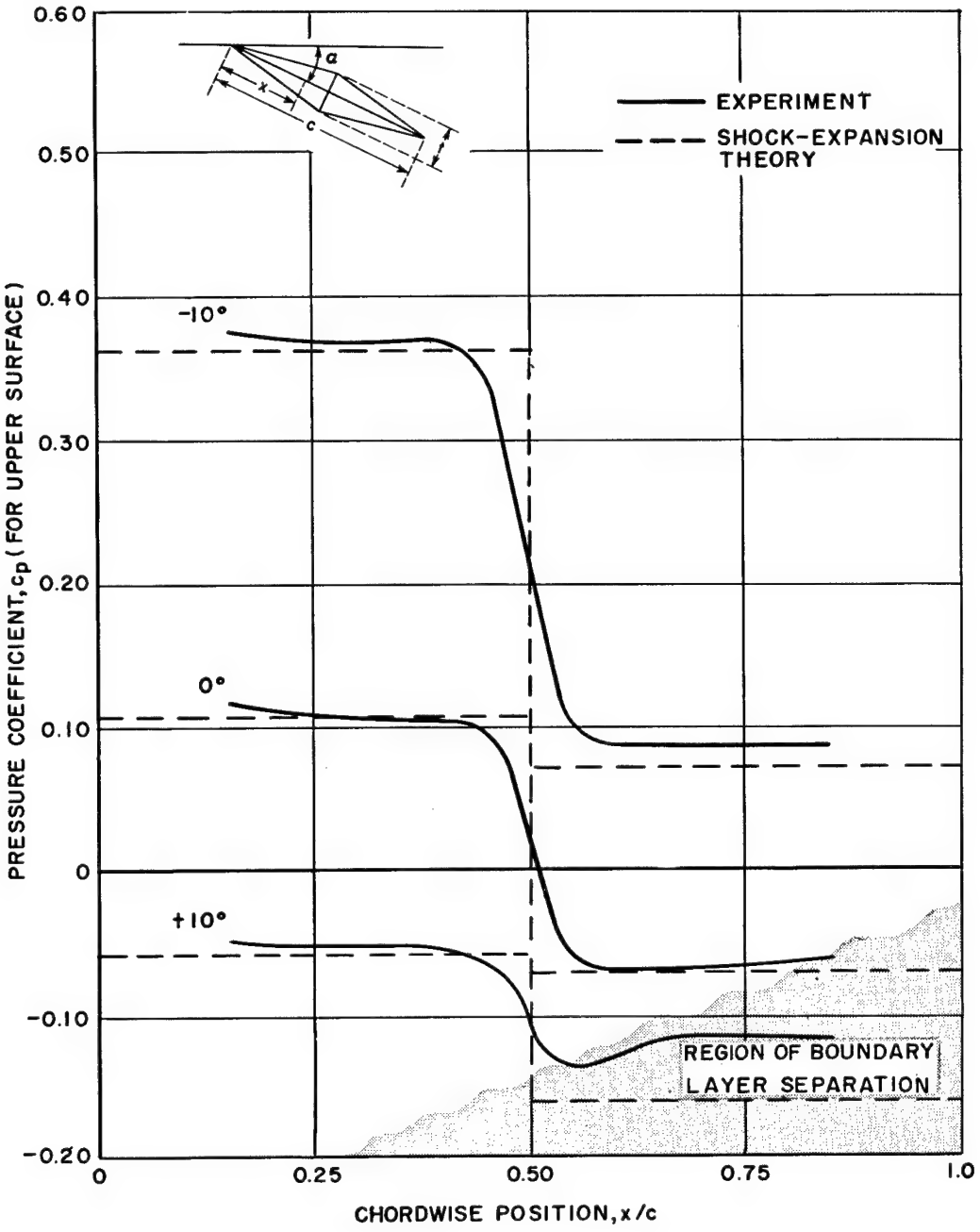

Figure 606.1-1(a) COMPARISON OF THEORY AND EXPERIMENT; CHORDWISE PRESSURE DISTRIBUTION ON UPPER SURFACE FOR A DOUBLE WEDGE AIRFOIL; $t/c = 0.10$; $M_\infty = 2.48$

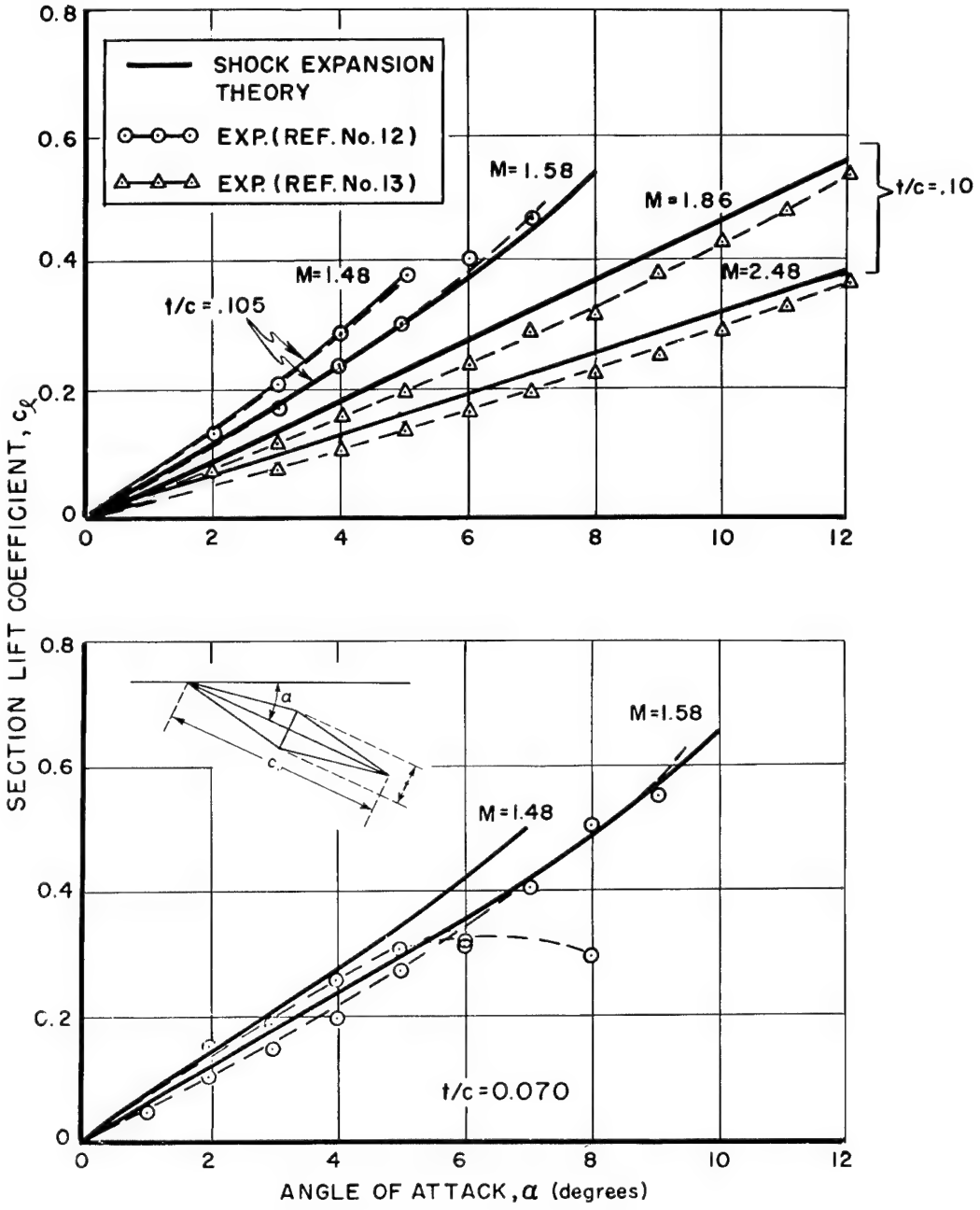

Figure 606.1-1(b) COMPARISON OF THEORY AND EXPERIMENT; VARIATION OF SECTION LIFT COEFFICIENT WITH ANGLE OF ATTACK; DOUBLE WEDGE AIRFOIL; M_∞ = 1.48, 1.58, 1.86, 2.48; t/c = 0.070, 0.105

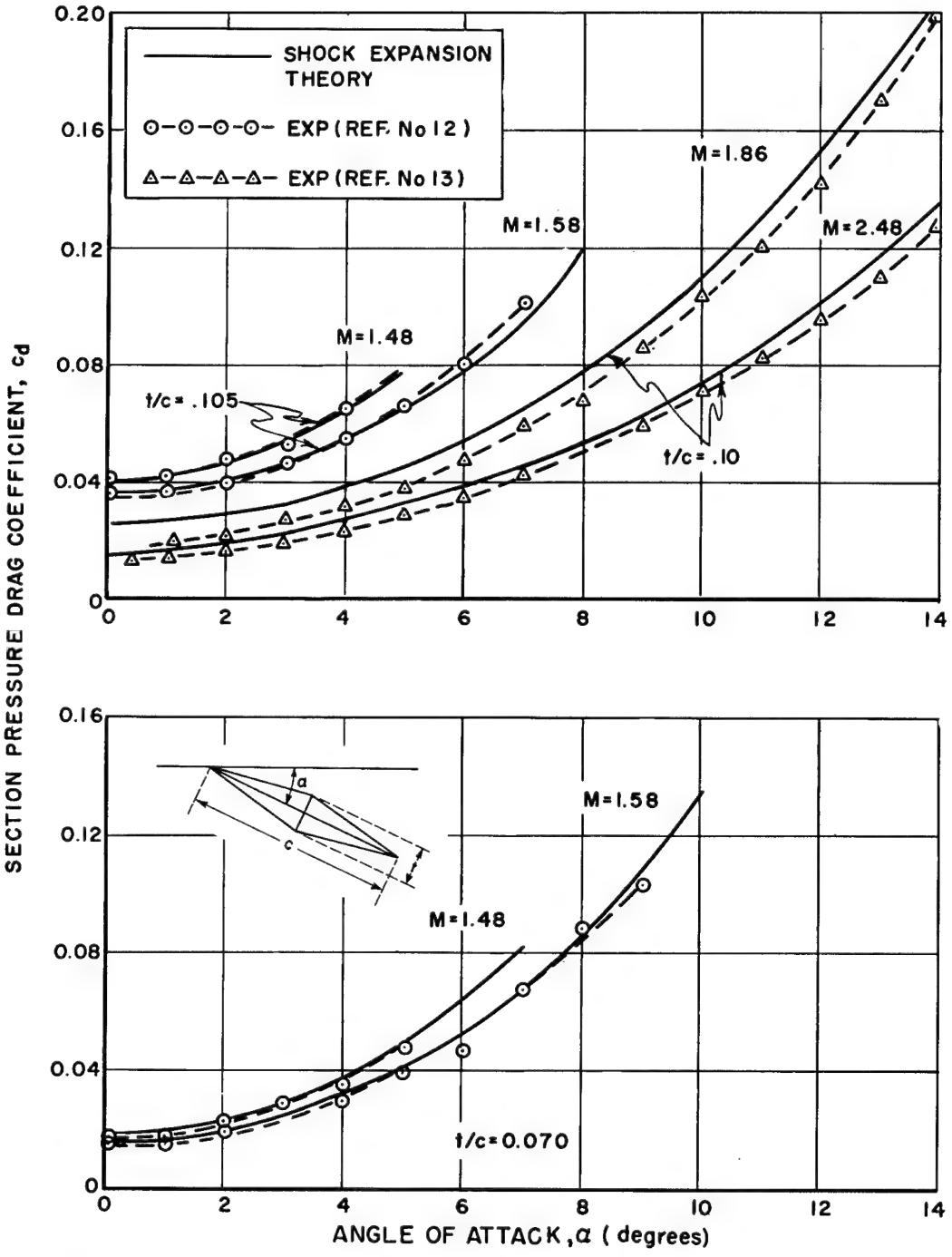

Figure 606.1-1(c) COMPARISON OF THEORY AND EXPERIMENT; VARIATION OF SECTION PRESSURE DRAG COEFFICIENT WITH ANGLE OF ATTACK; DOUBLE WEDGE AIRFOIL; M_∞ = 1.48, 1.58, 1.86, 2.48; t/c = 0.070, 0.105

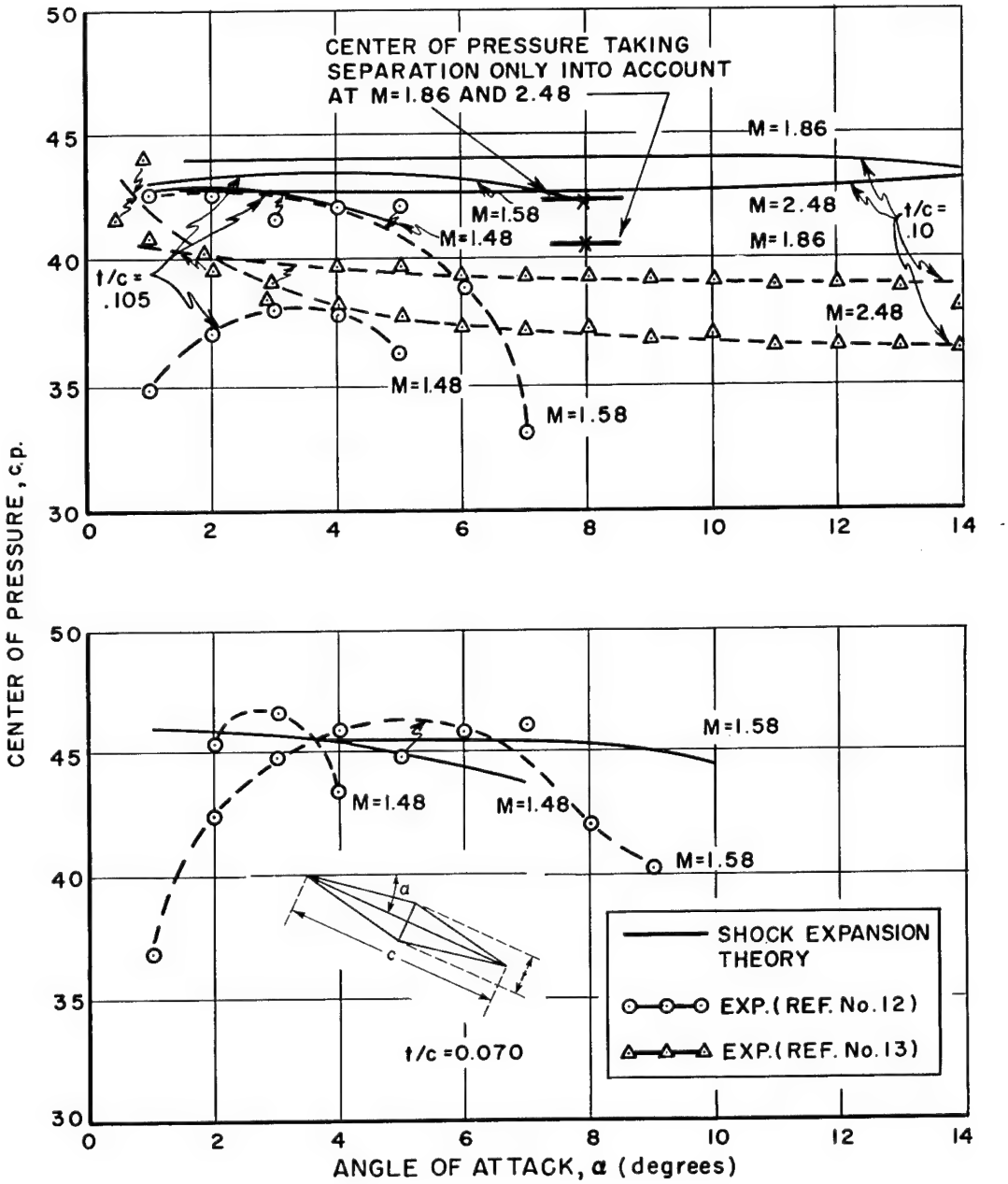

Figure 606.1-1(d) COMPARISON OF THEORY AND EXPERIMENT; VARIATION OF CENTER OF PRESSURE WITH ANGLE OF ATTACK; DOUBLE WEDGE AIRFOIL; M_∞ = 1.48, 1.58, 1.86, 2.48; t/c = 0.070, 0.105

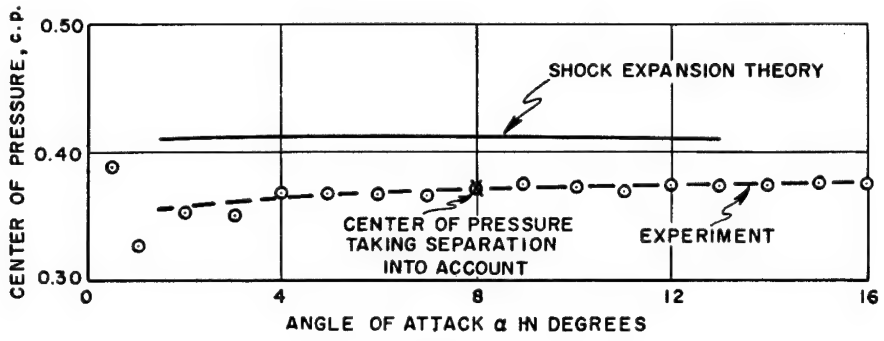

Figure 606.2-1(a) COMPARISON OF THEORY AND EXPERIMENT; CENTER OF PRESSURE FOR A BICONVEX AIRFOIL; $M_\infty = 2.48$; $t/c = 0.10$

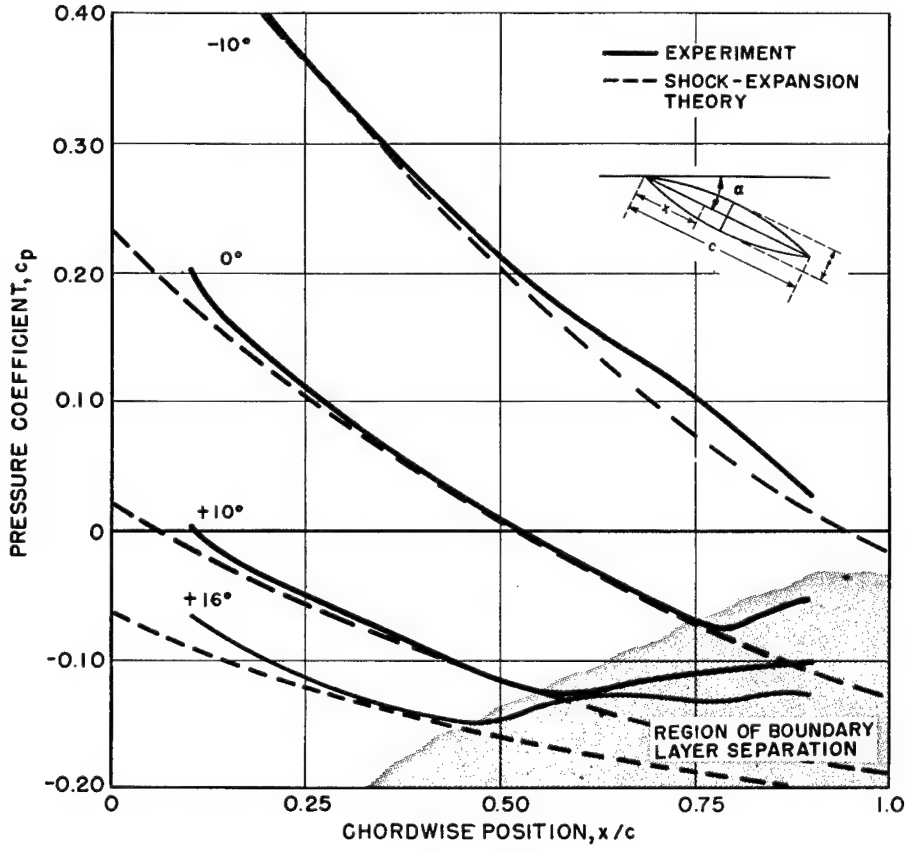

Figure 606.2-1(b) COMPARISON OF THEORY AND EXPERIMENT; CHORDWISE PRESSURE DISTRIBUTION FOR A BICONVEX AIRFOIL; $M_\infty = 2.48$; $t/c = 0.10$

447269 O - 58 - 7

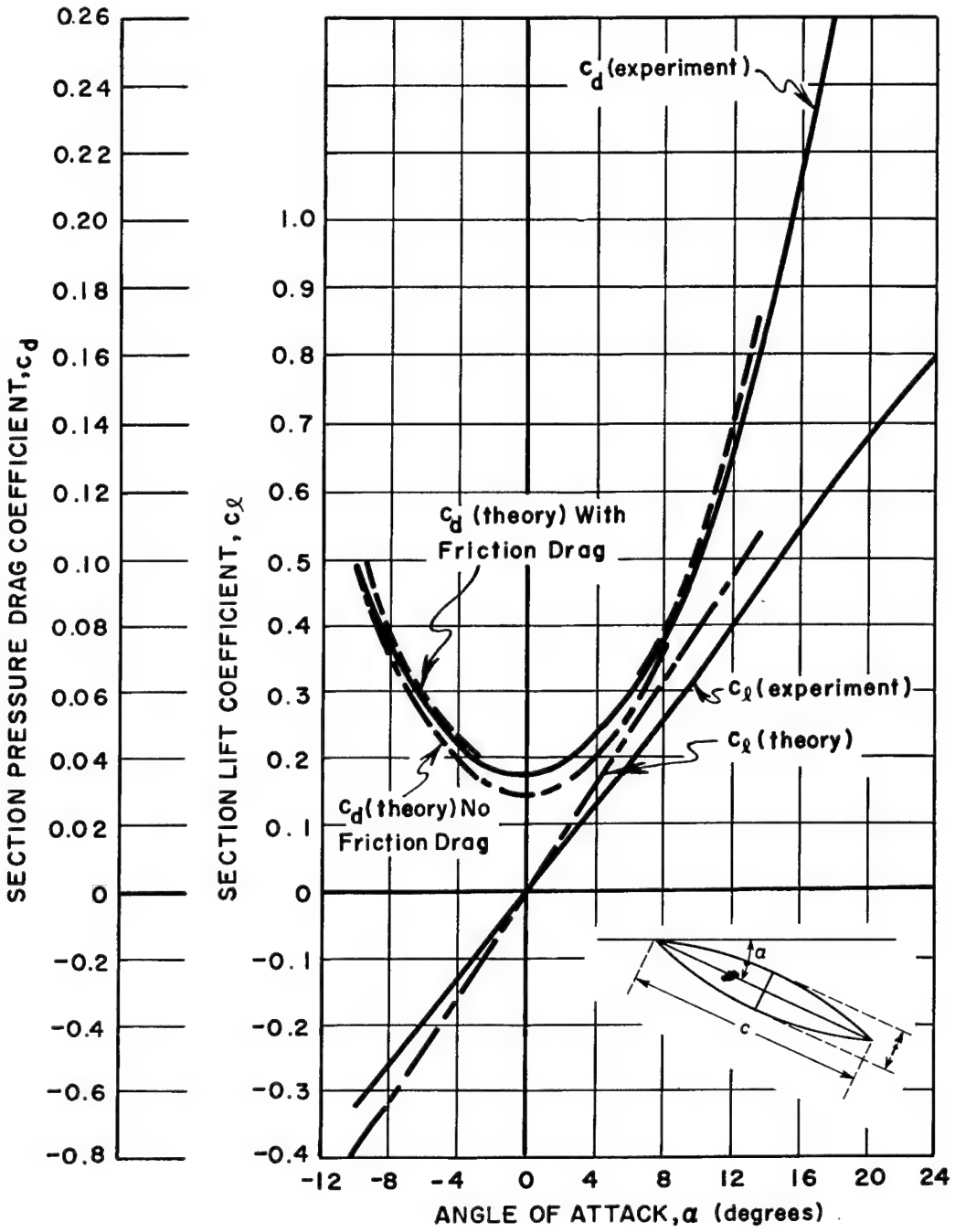

Figure 606.2-2(a) COMPARISON OF THEORY AND EXPERIMENT; VARIATION OF SECTION LIFT AND SECTION PRESSURE DRAG COEFFICIENTS WITH ANGLE OF ATTACK; BICONVEX AIRFOIL; SHOCK EXPANSION METHOD; $M_\infty = 2.13$; $t/c = 0.10$; REF. 9

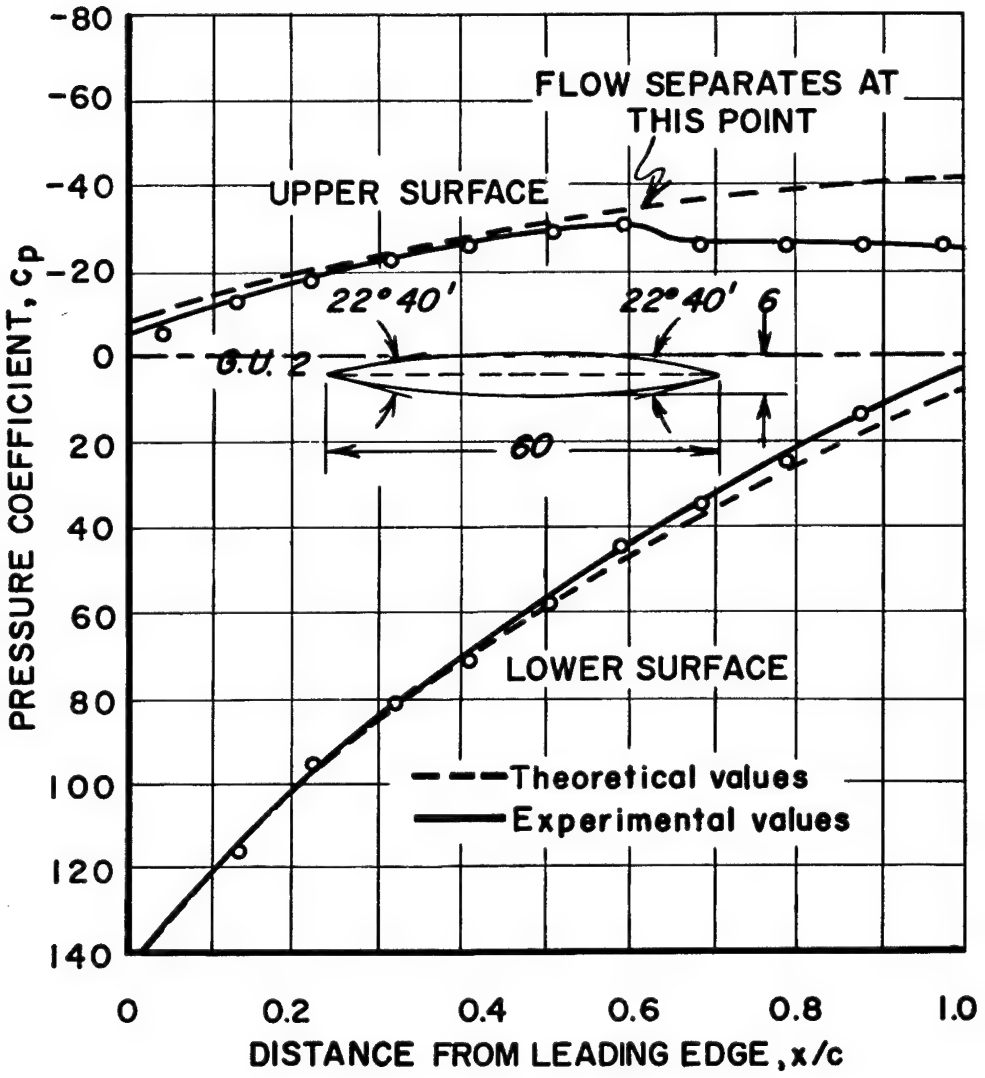

Figure 606.2-2(b) COMPARISON OF THEORY AND EXPERIMENT; CHORDWISE PRESSURE DISTRIBUTION FOR BICONVEX AIRFOIL; SHOCK EXPANSION METHOD; $M_\infty = 2.13$; $\alpha = 14°$; $R_e = 640,000$; $t/c = 0.10$; REF. 9, FIG. 13

SECTION 6 - TWO-DIMENSIONAL AIRFOILS

REFERENCES

Ref. No.	Title
1	Shapiro, A. THE DYNAMICS AND THERMODYNAMICS OF COMPRESSIBLE FLUID FLOW, Volume I. New York: The Ronald Press Co., 1953.
2	Applied Physics Laboratory, The Johns Hopkins University. "Handbook of Supersonic Aerodynamics," NAVORD Report 1488 (Volumes I and II). Washington: U. S. Government Printing Office, 1950.
3	Ackeret, J. "Air Forces on Airfoils Moving Faster than Sound," NACA Technical Memorandum 317, 1925.
4	Bonney, E. A. ENGINEERING SUPERSONIC AERODYNAMICS. New York: McGraw-Hill Book Co., 1950.
5	Ferri, A. "Two-Dimensional Potential Flow." Published in HIGH SPEED AERODYNAMICS AND JET PROPULSION, Volume VI, Section G (edited by W. R. Sears). Princeton: Princeton University Press, 1954, p. 591 ff.
6	Hilton, W. F. HIGH SPEED AERODYNAMICS. New York: Longmans, Green and Co., 1951.
7	Aeromechanics Division of the Defense Research Laboratory. "Characteristics of Two-Dimensional Wings at Supersonic Speeds," Report Number DRL-314. The Defense Research Laboratory, The University of Texas, 31 March 1953.
8	Ivey, H. Reese. "Notes on the Theoretical Characteristics of Two-Dimensional Supersonic Airfoils," NACA Technical Memorandum 1179, January 1947.
9	Ferri, A. "Experimental Results with Airfoils Tested in the High Speed Tunnel at Guidonia," NACA Technical Memorandum 946, July 1940.
10	Young, A. D. "Boundary Layers." Published in MODERN DEVELOPMENTS IN FLUID DYNAMICS - HIGH SPEED FLOW, Volume I, Chapter X (edited by L. Howarth). Oxford: The Clarendon Press, 1953.
11	Van Driest, E. R. "Turbulent Boundary Layer in Compressible Fluids," J. Aero. Sci., Volume 18 (March 1951).
12	Pindzola, Michael. "Symmetrical Double Wedge Airfoil Tests in the U.A.C. Two-Dimensional Supersonic Wind Tunnel," Meteor Report Number UAC-16. Research Department, United Aircraft Corp., January 1948.

13 Beastall, D. and Pallant, R. J. "Wind Tunnel Tests on Two-Dimensional Supersonic Aerofoils at M = 1.86 and M = 2.48," Reports and Memoranda Number 2800. Ministry of Supply, Aeronautical Research Council. London: Her Majesty's Stationery Office, July 1950.

SECTION 6 - TWO-DIMENSIONAL AIRFOILS

U. S. GOVERNMENT PRINTING OFFICE: 1958 O—447269